The chemistry of simple alcohols, amino acids and nucleic acid bases on silicon substrates

Thesis submitted in accordance with the requirements of the University of St. Andrews for the degree in Doctor of Philosophy

by Alberto López Gómez

September 2001

School of Chemistry, University of St. Andrews

ABSTRACT

The interaction between organic molecules and silicon substrates has been investigated using several surface sensitive techniques. The studies of the competitive reactions between simple alcohols and water show that only isopropanol is able to passivate the surface and inhibit further adsorption of H_2O. The reaction occurs through cleavage of OH bonds and the formation of Si-O linkages. At room temperature, the cleaved H atoms are kept at the surface through the formation of Si-H bonds. Unsaturated heterocyclic molecules like maleic anhydride react with the silicon surface through a 2+2-cycloaddition reaction and provide a well defined ordered template to achieve further film growth. Bifunctional molecules like glycine and 4-aminobenzoic acid react with the surface through the carboxylate group, leaving the amino group available for further film growth. Similarly to the alcohols, the reaction occurs through cleavage of OH bonds and formation of Si-O-C linkages. The presence of a surface modifier like Na, modifies the interaction of the carboxylate groups with the surface from unidentate to bidentate. This leads to the formation of an ordered layer with well-defined bonding sites. The study of the adsorption of uracil on Si(100)-2x1 showed that this molecule is able to form well ordered structures on the surface. The vibrational spectroscopy study indicated that only the enol tautomer of uracil is able to react with the surface.

List of publications

1. A. Lopez, T. Bitzer, T. Heller, N.V. Richardson, "Adsorption of water on alkoxy modified Si(100), Si(113) and Si(115) surfaces", *Surf. Sci.* 108-116 (2001) 473

2. A. Lopez, T. Bitzer, T. Heller, N.V. Richardson, "Adsorption of maleic anhydride on Si(100)-2x1", *Surf. Sci.* 219-226 (2001) 477

3. A. Lopez, T. Bitzer, T. Heller, N.V. Richardson, "Functional group selectivity in adsorption of 4-aminobenzoic acid on clean and Na modified Si(100)-2x1 surfaces", *Surf. Sci.* 65-72 (2001) 480

4. A. Lopez, T. Bitzer, T. Heller, N.V. Richardson, "A vibrational study of the adsorption of glycine on clean and Na modified Si(100)-2x1 surfaces", *Chem. Phys.* In press.

5. A. Lopez, T. Heller, T. Bitzer, Q. Chen, N.V. Richardson, "The influence of sodium on the adsorption of water on $SrTiO_3$ surfaces", *Surf. Sci. Lett.* In press.

6. A. Lopez, Q. Chen, N.V. Richardson, "A combined STM, HREELS and *ab initio* study of the adsorption of uracil on Si(100)-2x1", *Surf. Interf. Analy.* Submitted

Acknowledgements

I would like to thank my supervisor Prof. Neville Richardson for giving me the opportunity to study in the University of St. Andrews. I gratefully thank the financial support from the School of Chemistry. I thank specially, Dr. Thomas Bitzer and Dr. Thomas Heller for their friendship, support and enthusiasm in the time we worked together in the Department.

Gratitude is also expressed to the current members of the Surface Science group, Dr. Steve Francis, Dr. Qiao Chen, Mr. Daniel Frankel, Mr. Alexander McDowell and Mr. Tomás Rada Crespo. Thanks must also be expressed to the BESSY staff at the synchrotron line in Berlin, Germany.

I would like to also thank Prof. José Antonio Odriozola, Dr. Jorge Sambeth and Dr. José Jesús Benítez Jiménez in the Surface Science Laboratory at the Instituto de Ciencia de Materiales in Sevilla, for their support and encouragement three years ago.

Finally, my gratitude goes to my parents, sister and girlfriend for their patience, support and encouragement throughout this three years.

Declarations

I, Alberto López Gómez, hereby certify that this thesis has been written by me, that is the record of work carried out by me and that it has not been submitted in any previous application for a higher degree.

Date 25/09/01 Signature of candidate:

I was admitted as a research student in January 1999 as a candidate for the degree of PhD at the university of St. Andrews.

Date 25/09/01 Signature of candidate:

I hereby certify that the candidate has fulfilled the conditions of the Resolution and Regulation appropriate for the degree of PhD in the University of St. Andrews and that the candidate is qualified to submit this thesis in application for that degree.

Date 25/09/01 Signature of supervisor:

In submitting this thesis to the University of St. Andrews I understand that I am giving permission for it to be made available for use in accordance with the regulations of the University Library. I also understand that the title and abstract will be published and that copy of the work may be made and supplied to any bona fide library or research worker.

Date 25/09/01 Signature of candidate:

CONTENTS

CHAPTER 1.

The chemistry of silicon substrates

1.1. Introduction.

The surface chemistry of silicon has been explored in increasing detail over the last decades, especially since the invention of the scanning tunneling microscopy (STM) and the further development of the surface spectroscopy techniques. The understanding and control of silicon surfaces has been of vital importance in the manufacture of semiconductor devices (MOSFET, IGBT, GTO, etc.) since their operation is based on the electronic properties of silicon substrates. Organic molecules will play an important role in the future development of new electronic devices [1]. About 20 years ago, there was a major interest in the so-called molecular electronics [2]. The idea was to create assemblies of molecules linked together through particular functional groups to produce complex units that would operate as switches or transistors. Many ideas were developed then, although it was not possible until the discovery of the STM to obtain a complete understanding of any molecule-silicon system.

Although it is not possible to foretell where successful applications will be found, in the future, organic molecules with their tunable properties, including size, shape, chemical affinity, absorption spectrum and conductivity will create new functional possibilities. We look towards functions that current silicon technology cannot perform very well, for example, light emission, light detection and chemical sensing-all things that molecules can do very well. Molecular-scale devices remain still far away but the understanding of these systems is growing rapidly. Truly, there are many steps between attaching a molecule to a surface and creating a functional hybrid device, but the first step has already been taken in the investigations regarding the controlled adsorption of simple molecules on silicon surfaces. Ultra high vacuum (UHV) provides excellent conditions for the growth of organic layers without contamination of the sample surface.

This thesis is based on the research carried out towards the formation of an ordered organic film/silicon interface. Early investigations have demonstrated that silicon is a highly reactive substrate although inert after surface saturation [3-5]. However, in order to facilitate further film growth, additional functional groups acting as bonding sites for subsequent layers, are required. Bifunctional molecules like glycine, 4-aminobenzoic acid, phenylene diamine and unsaturated heterocyclic molecules like maleic anhydride all have the properties to become potential interface constituents. The first layer consists of molecules that react with the surface through one functional group, establishing a link between the substrate and the organic layer leaving the other functional group available for subsequent reactions. The structure and local ordering of this first layer is of crucial importance to facilitate film growth.

Two major approaches have been explored to achieve ordered monolayer structures on Si(100)-2x1. Recent investigations have shown that unsaturated organic molecules react with the silicon through a 2+2-cycloaddition reaction leading to bidentate bonded species [6-8]. This reaction mechanism involves the establishment of two linkages between the organic molecule and the silicon substrate that defines the adsorption site and the orientation of the molecules on the surface. This adsorption geometry is expected to be more ordered and well-defined than species bonded through the formation of a single silicon-molecule bond. A second approach to long range order is based in the use of a surface modifier that changes the chemical properties of Si(100)-2x1. It is widely agreed that the clean silicon surface forms very stable but rigid covalent bonds that inhibit molecular diffusion and long range order [9]. The influence of the deposition of an alkali metal template on surface chemistry has been investigated with particular emphasis in the determination of long range order after molecular adsorption.

Additionally, a part of the thesis shows results of the competitive reaction of water and simple alcohols on silicon surfaces. This research is mainly focused on the passivation of silicon surfaces and the production of surfaces that are chemically stable outside UHV conditions.

The prepared surfaces have been characterized using high resolution electron energy loss (HREELS), near edge (X-ray) absorption fine structure spectroscopy (NEXAFS), scanning tunneling microscopy (STM), low energy electron diffraction (LEED) and x-ray photoelectron spectroscopy (XPS).

1.2. The silicon surface.

Silicon has a diamond structure in which the silicon atoms are in tetrahedral coordination and bonded to four other neighbours by sp^3 hybridization. On the surface, the lattice periodicity is broken and therefore dangling bonds are there expected. The density of these dangling bonds will vary, depending on which direction of the surface normal we choose. These dangling bonds are responsible for the chemical activity of the silicon surface. In order to minimise the number of these bonds, the silicon (100) surface reorganises exhibiting under normal conditions a 2x1 reconstruction. Schlier and Farnsworth [10] first proposed the now accepted model for the silicon reconstruction from low energy diffraction (LEED) data. It is the dimer model, in which the number of dangling bonds is reduced by 50% by the creation of new bonds between the silicon atoms on the surface.

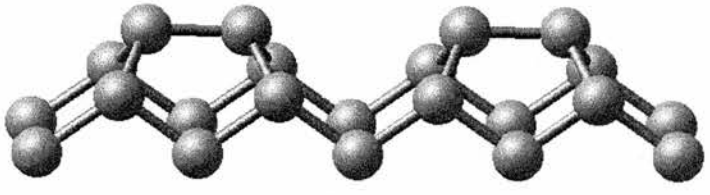

Figure 1. Si(100) surface exhibiting a 2x1 reconstruction

Prior to reconstruction, each silicon atom exhibits two dangling bonds at the surface. In the dimer model, each silicon atom bonds to a neighbouring atom along the [110] direction. The reconstruction results in the formation of rows of dimers with each silicon atom having one remaining dangling bond to be saturated. Figure 2. shows the reconstruction from the top view.

The black dots represent atoms in the surface's top most layer, while the open large (small) correspond to the second (third) layer.

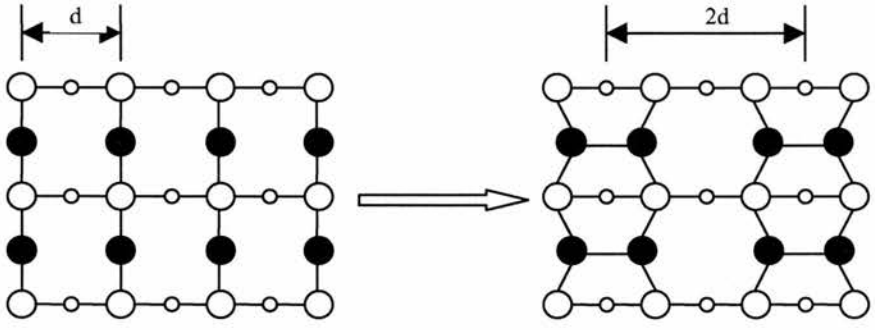

Figure 2. Top view of the dimer structure after surface reconstruction. Atoms in the unreconstructed configuration have two dangling bonds, while in the reconstructed one they have only one. Note the change in the lattice parameter along the x direction as a result of the reconstruction.

The changes in the surface reconstruction are easily viewed by low energy electron diffraction. In a non-reconstructed surface the diffraction pattern exhibits a typical 1x1 structure where the spots are separated 1/d in the k_x and k_y directions, since each atom is considered as a scattering centre. When the surface reconstructs, the 1x1 periodicity is broken and the dimers turn to be the scattering centres separated a distance 2d. Therefore, the diffraction pattern is expected to show new spots separated a distance 1/2d in the reciprocal space along the k_x direction, while the separation among spots in the k_y direction remains unchanged. Since the silicon surface is constituted of 2x1 domains rotated by 90°, the LEED pattern is the superposition of two 2x1 structures rotated by 90°. The two domains of silicon dimers are clearly visible in the STM image in fig 3.

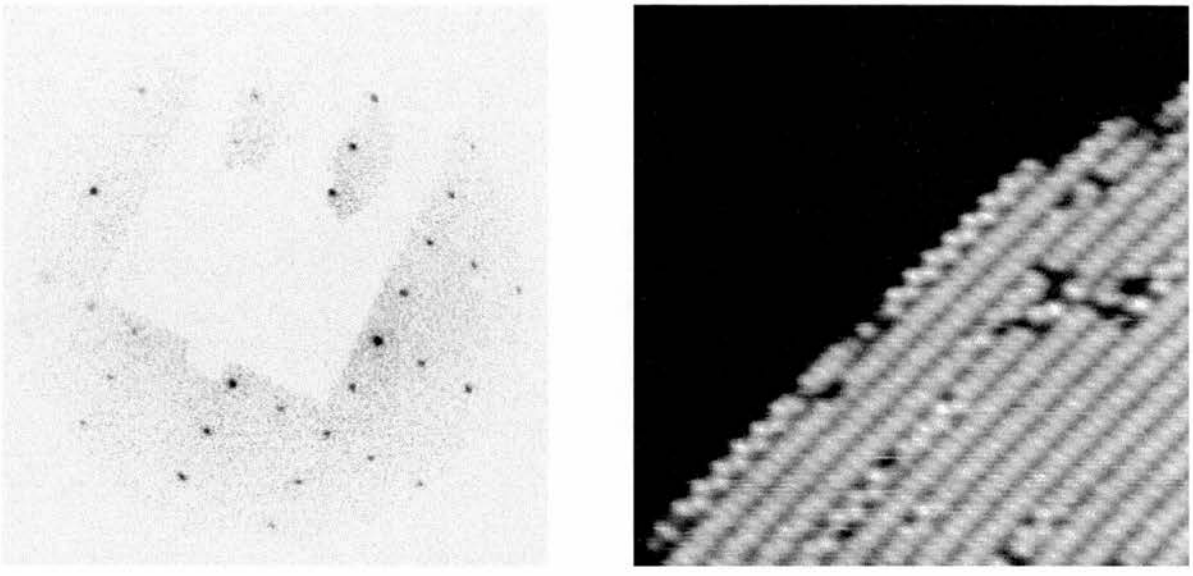

Figure 3. LEED pattern and STM image of the silicon substrate after reconstruction. The diffraction pattern can be interpreted as a superposition of two patterns coming from a 1x1 periodicity and two 2x1 periodicities rotated by 90°. The domains are clearly visible in the STM image.

Interaction between two adjacent dimers can occur for further reduction of the surface energy. Dimer buckling was proposed by Chadi and Levine, leading to an asymmetric structure on which one silicon atom moves away from the surface while the other moves towards the surface until the minimum in the surface energy is reached [11-12]. At this stage, adjacent rows of dimers buckle in opposite directions to relieve the lattice strains generated, leading to changes in the surface periodicity. The 2x1

reconstruction is preserved if all dimer buckle in the same direction, while dimers buckling in opposite directions will lead to 2x2 and 4x2 structures. The silicon dimer displays properties intermediate between those of a double bonded entity and a bi-radical. The clean silicon dimer is σ-bonded with a small π-bonding contribution. Less than optimal π-bonding occurs because the Si dangling bonds are not parallel (ideal arrangement) and therefore cannot interact strongly. The paired atoms are non-equivalent and therefore share an interaction similar to a heteronuclear bond. The up atom becomes more nearly sp^3 in character and therefore a little lower in energy and more fully occupied. The down atom becomes sp^2 like and has proportionately less local occupied state density. The degree of π-bonding varies as the dimer fluctuates. The interaction is maximum when, transiently, the dimer is symmetric (both atoms are of the same height). When the dimer is buckled the dangling bonds are no longer degenerate and π-bonding is further disfavoured. Furthermore, silicon dimers, are bistable, buckled units although at room temperatures dimers rapidly switch orientation leading to an averaged symmetric appearance in STM images [13].

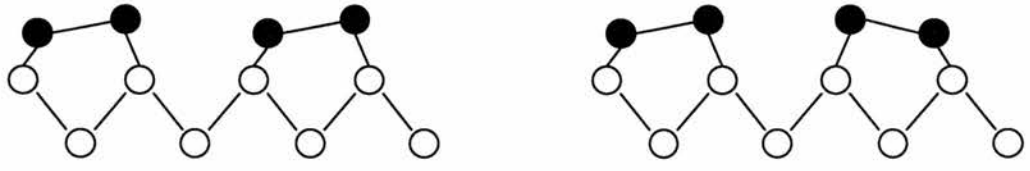

Figure 4. Side view of buckled dimers in the same and opposite directions. Note that in the case of buckling in the same direction the surface periodicity remains unaffected, while buckling in opposite directions leads to 2x2 and 4x2 structures.

1.3. Hydrogen terminated surfaces.

Hydrogen plays an important role on the passivation of silicon reconstructed surfaces. As we have seen, after reconstruction takes place, one dangling bond on each silicon surface atom is left to react with in coming molecules. The formation of the Si-H bond at the surface stabilises it by the saturation of this dangling bond. However, two different phases have been proposed for the hydrogen-terminated (100) surfaces. One is

the monohydride phase, in which the reconstruction is preserved and the hydrogen is bonded to the surface through one dangling bond per silicon left after reconstruction. The monohydride phase is formed after saturation exposure of the silicon surface to atomic hydrogen at 600 K or after high exposures at lower temperatures followed by annealing at 575K. Under these conditions only Si-H stretches could be seen in HREELS spectroscopy while sharp (2x1) spots have been reported in the LEED patterns. [14]. In the dihydride phase the silicon-silicon bonds are broken and the 2x1 reconstruction lost. Silicon atoms are bonded to two hydrogens leading to a (1x1) structure [15]. Hydrogen adsorption below the monohydride formation temperature leads to the dihydride phase and a loss of the (2x1) reconstruction.

Additionally, an unexpected structure of alternating rows of monohydride and dihydride is formed at 400K [16]. STM studies and TPD measurements have confirmed this structure [17]. This phase can arise only if Si-Si backbond breaking is accomplished. However, this is related mainly to the presence of defects or vacancies in the silicon substrate, which weaken the silicon bonds and favour the reaction with hydrogen. Schematics of these three phases can be observed in figure 5.

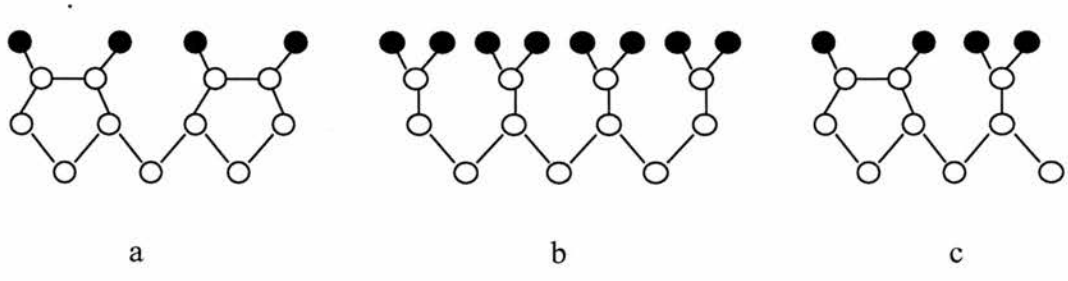

Figure 5. Hydrogen terminated Si(100) surfaces: (a) monohydride, 2x1 structure; (b) dihydride, (1x1) structure, (c) 3x1 structure.

1.4. Adsorption of oxygen.

Oxygen plays an important role in the chemistry of silicon surfaces. When working with silicon in UHV conditions, the biggest problem to deal with, is the removal of the oxide layer that is formed after reaction of the oxygen from the atmosphere with the surface. The interaction of the surface with oxygen atoms can go through two

different reactions, leading to the production of SiO or SiO_2 depending upon temperature and pressure conditions. These two processes are referred to in the literature as active and passive oxidation respectively [9]. Active oxidation is predominant at high temperatures while passive oxidation occurs mainly at high oxygen pressures. It is well established that oxygen absorbs dissociatively on the surface [18-19]. There are several positions oxygen can occupy when absorbs on silicon. The configuration of oxygen in crystalline SiO_2 is a bridging position between two silicon atoms; each silicon atom in turn is surrounded by four oxygen atoms in a tetrahedral configuration. The bridging site where oxygen is inserted into a Si-Si back bond is the preferred major adsorption site on silicon surfaces obtained from both experiment [19-20] and theoretical results [21-22]. On the other hand the dangling bonds must also be involved in the dissociation process, since hydrogen covered surfaces have been shown to be nearly inert towards O_2 [23-24]. Fig 6 shows the possible adsorption sites for oxygen on Si(100)-2x1. Initial adsorption of both molecular and atomic oxygen was found to lead to insertion of oxygen in the dimer bond (site marked 2). During this step, the 2x1 reconstruction of the silicon atoms was found to be intact since the atoms of the former dimer are pulled towards each other in the Si-O-Si bridge. At higher exposures oxygen also bonds in the remaining surface bridge sites (between the original dimer positions, site 3 in fig 6) and the two bridging sites become equivalent. Insertion of O into the bridge sites between the first and second layer (site 4 in fig 6) was predicted to occur only at elevated temperatures [25].

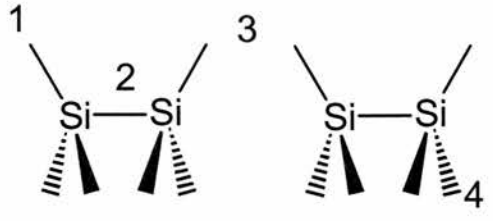

Fig 6. Possible adsorption sites for oxygen on Si(100)-2x1.

1.5. Adsorption of water.

The interaction of H_2O has been studied by several spectroscopic techniques, in order to characterize its adsorption behaviour and chemisorption processes. The most controversial issue has been the discussion of whether the adsorption occurs dissociatively or molecularly [26-28]. In molecular chemisorption, H_2O molecules react with the surface without breaking their internal molecular bonds, while in the dissociative model, OH groups and H atoms react separately with the silicon dimer, to form Si-OH and Si-H bonds respectively. HREELS and IR studies have shown however that H_2O adsorbs dissociatively on the silicon surface [29] [4]. Recently it has been reported by STM and SSIMS [30-31] that the process of chemisorption is not fully dissociative or molecular, but is dependent upon H_2O coverage. Following the adsorption of water, two different features can be seen in STM, dimers with one end dark and the other bright and dimers fully dark. On clean surfaces this is interpreted as surface defects, missing silicon atoms and missing silicon dimers respectively. Now, STM has two modes of operation on which electrons can either be tunneled from the tip into the empty surface states or from the occupied surface states into the tip. After further H_2O adsorption the images recorded by Chander et. al. [30] gave atomic resolution in both the empty and occupied modes, while for the clean surface atomic resolution was achieved only in the empty state mode. This leads to consideration of the defects observed in clean silicon as molecularly adsorbed water that leads to dissociation features when increasing the coverage.

Furthermore, only saturation of adjacent dangling bonds has been observed by STM, this means that for dissociation to occur, it must take place upon adjacent dangling bonds, although not necessarily of the same dimer. This is supported by the fact that isolated dangling bonds were very stable after saturation coverage. Interesting is to note the reported activity of these dangling bonds [30]. H and OH groups adsorbed on a particular dimer can have certain mobility towards these isolated dangling bonds until saturation is achieved.

1.6. Adsorption of hydrocarbons on silicon: [2+2] cycloaddition chemistry

The reaction of unsaturated hydrocarbons with the silicon surface, is an interesting case of interaction between two π-bonded systems. Particular attention has been paid to ethylene, acetylene, 3-pyrroline and aromatic ring compounds, which present an active behaviour towards the silicon surface [32-34]. The most accepted model for the chemisorption of these organic molecules on Si(100)-2x1 is the di-σ model [35]. In this configuration, the double bonds of the Si dimer and the double bonds of the adsorbed species are broken forming two new Si-C σ bonds. This occurs through rehybridisation from sp^2 to sp^3 of the carbon atoms in the C=C bond. Since the interacting bonds are both strongly oriented, the interaction of Si=Si dimers with the unsaturated C=C bonds effectively makes the surface Si=Si dimers act as a template for extending rotational order into the organic layer. A schematic of this adsorption model is shown in fig 7. The structure of the silicon dimer can be preserved or broken [32-36], and the main discussion is about which process is preferred.

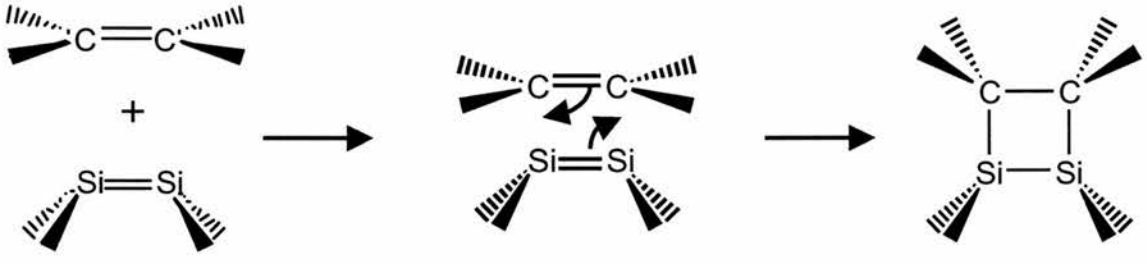

Fig 7. Schematic of the cycloaddition reaction between unsaturated C=C bonds and the Si=Si dimers.

1.6.1 Acetylene.

The study of unsaturated hydrocarbons such as acetylene (C_2H_2), is of practical importance in the understanding of the initial stages of growth of SiC films on silicon substrates. Early studies by Nishijima et. al. [37] have proposed the di-σ adsorption model described above. In this model carbon atoms are rehybridized from sp into sp^2 hybridization states and bonded to two adjacent Si atoms in the silicon dimer. This model

has been confirmed by NEXAFS results [38]. The intensity of the π^* resonance attributed to transitions from 1s to the lowest unoccupied molecular orbital (LUMO) of acetylene in the gas phase decreases dramatically after adsorption. In this adsorption geometry, the silicon 2x1 reconstruction is maintained after acetylene adsorption.

However, according to some authors, the preservation of the dimer structure after molecule adsorption would create large lattice strains that would eventually bring the molecule into a more stable state resulting in different adsorption geometry [32-36]. At low temperatures, acetylene adsorbs non-dissociatively on the Si(100)-2x1 surface. HREELS results show that, although the adsorption of acetylene occurs through rehybridisation of the carbon atoms from sp to the sp^2, the Si-Si dimer bond is cleaved after adsorption of the molecule. This adsorption model leads to the loss of the surface 2x1 reconstruction. The sp^2 rehybridisation is characterized by an electron energy loss feature observed at 1450 cm^{-1} which corresponds to the C=C stretching mode. The authors attribute the low vibrational frequency to an interaction between the dangling bonds on the Si atoms and the π orbital of the chemisorbed acetylene. Additionally exposure of the acetylene-saturated surfaces to atomic hydrogen resulted in the observation of Si-H vibrations in the vibrational spectrum.

This model has its geometrical support, because after the adsorption of acetylene silicon atoms would be 3.2Å apart, which is in between the distance in the dimerized state (2.5A) and the unreconstructed state (3.8A). As the temperature is increased decomposition occurs through cleavage of the C-H bonds and the formation of Si-H bonds [33].

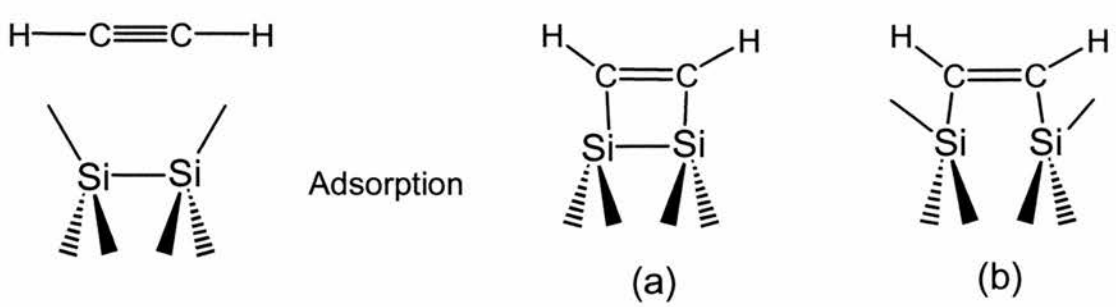

Fig 8. Schematic of the two adsorption models for acetylene on Si(100)-2x1. Adsorption occurs on both cases through rehybridisation, although the 2x1 reconstruction is lost in model (b).

1.6.2. Cyclopentene

The cycloaddition reactions can be used for the production of well-defined structures of more complicated organic layers. In the case of cyclopentene, Hamers et al [6-39] have shown that adsorption of cyclopentene on Si(100)-2x1 forms a structure ordered rotationally and translationally. This is a result of the adsorption of the cyclopentene molecule on Si(100) through the formation of a di-σ bond between the species and the Si dimer rows. A schematic of the adsorption geometry is observed below.

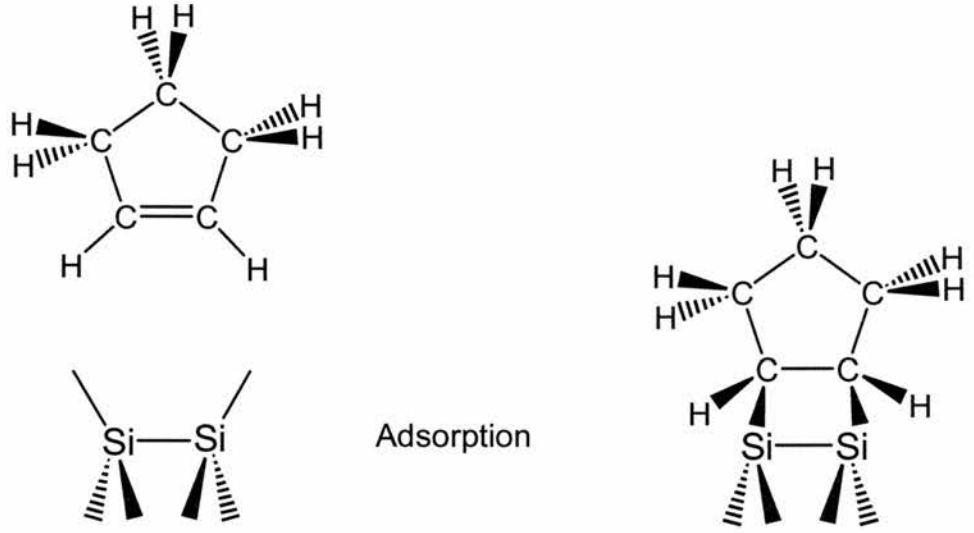

Fig 8. Di-σ bonding of cyclopentene on Si dimer. Note that the molecule is tilted to allow the cycloaddition reaction take place.

STM studies demonstrate that the molecules are aligned in rows and the species appear elongated in a direction that is the same for all molecules. Additionally, the spacing between molecules within a given row varies but is always an integral multiple of the 3.85 Å spacing between dimers in the Si(100)-2x1 surface.

The Si(100)-2x1 surface, as observed before, consists of monoatomic domains rotated by 90°. These 90° rotations in bonding direction destroy the coherence of the molecular orientation on length scales greater than the average separation between steps.

However, by using Si(100)-2x1 surfaces which are cut approximately 4° off the (100) plane, the interaction energy between steps causes the surface to adopt a configuration in which there are virtually no single height steps. Instead, the surface adopts only a bilayer structure with double height steps. An important observation is that across these double height steps the cyclopentene molecule, maintains the same rotational orientation.

1.6.3. 3-Pyrroline

The case of cyclopentene adsorbed on Si(100)-2x1 is interesting because it shows a high degree of molecular order. However, further chemical functionalisation is difficult because there is not another functional group within the ring structure to allow the controlled growth of multilayer films. The molecule 3-pyrroline is the simplest modification of the cyclopentene molecule that includes 2 functional groups.

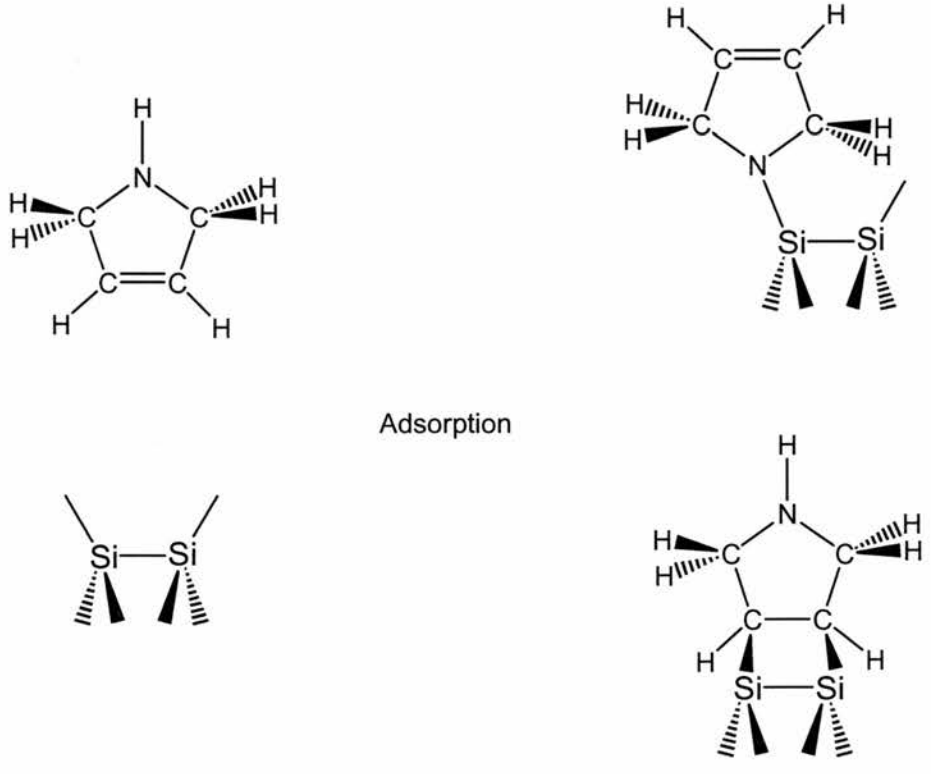

Fig 9. Schematic illustration of the two possible bonding possibilities for 3-pyrroline.

STM studies [39] show that the molecules mainly bond to Si(100)-2x1 through the cycloaddition reaction between the unsaturated C=C bond and the Si dimer. However, although the rotational and translational orders are still observed, the surface shows a second type of species with no preferential orientation. This suggests that a second type of 3-pyrroline molecule bonded to the surface through the other functional group is present at the surface.

Fig 9. Shows the two possible adsorption geometries for 3-pyrroline based on XPS and STM studies. It is important to note that both functional groups react with the substrate leading to the formation of Si-C and Si-N linkages respectively. In this case the cycloaddition reaction competes with N-H bond cleavage.

1.6.4. Norbornadiene

IR studies of the adsorption of norbornadiene were carried out to see if the methodology described above could be extended to molecules having more than one unsaturated double bond. FTIR data of norbornadiene adsorbed on Si(100)-2x1 shows no Si-H related features, but clearly resolved C-H modes [6-39]. This is an indication for adsorption of norbornadiene on Si(100)-2x1 without dissociation of hydrogen but reaction with the surface through the unsaturated C=C bond. The strong C-H mode observed at 3057 cm^{-1} characteristic of an unsaturated molecule, suggests that in at least some of the molecules, only one (or none) of the two unsaturated C=C bonds have been eliminated by bonding to the surface. The comparison of IR spectra obtained at two polarization directions shows little difference between them. This indicates that while we know that the molecule is interacting with the surface through the C=C bond, there must be more than one type of surface site at which the interaction can occur.

STM images of norbornadiene on Si(100)-2x1 show no translational or rotational ordering [40]. At lower coverages, norbornadiene molecules are seen as bright protrusions some located on top of the silicon dimers, some located between between dimer rows. Therefore, the lack of ordering can be attributed to molecular bonding in

different configurations. Fig 10 shows the possible adsorption geometries for norbornadiene on Si(100)-2x1.

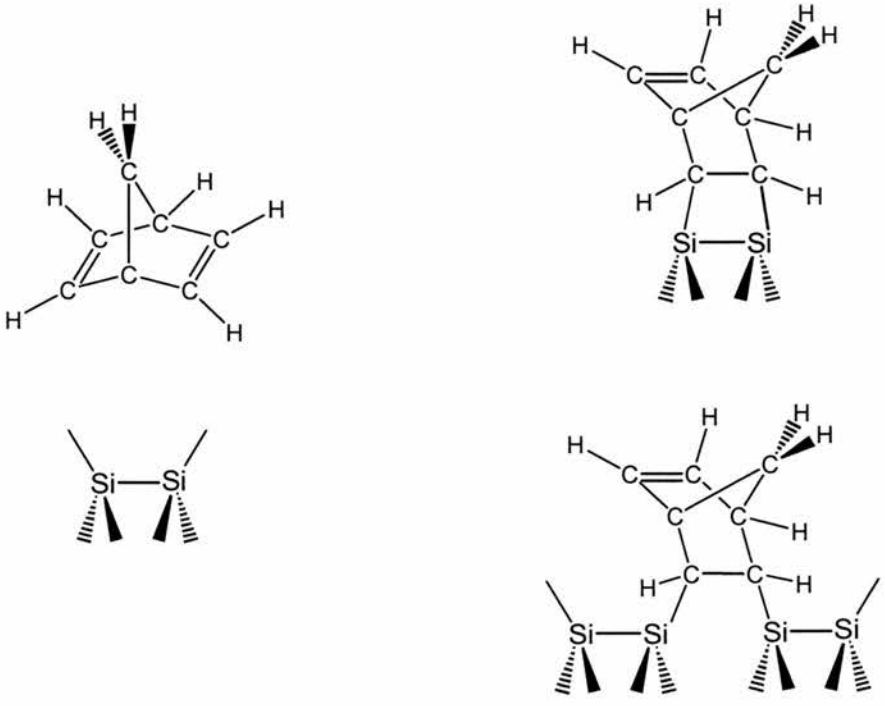

Fig 10. Possible adsorption geometries for norbornadiene on Si(100)-2x1.

1.7. Benzene:

Early studies of benzene on silicon surfaces [41], showed that the molecule chemisorbs non-dissociatively on Si(100)-2x1 preserving the surface reconstruction. It was proposed that chemisorbed benzene is di-sigma bonded to two adjacent Si atoms saturating the dangling bonds on the surface. Saturation coverage corresponded to one benzene molecule per four silicon atoms, which gives one adsorbate for two silicon dimers. Later studies [42] have proposed two possible σ-bonded structures for the chemisorption, which correspond to the 1,3- and 1,4 cyclohexadiene analogs. *Ab initio* calculations have reported similar stabilities for these structures and a strong controversy

has arisen about the bonding model [35]. In the 1,4- cyclohexadiene like structure (also referred as "butterfly" picture b in Fig. 6.), there are two C=C bonds and two sp^3 hybridized carbon atoms which form the Si-C bonds. The molecule sits parallel to the surface on one single dimer row. The 1-3 cyclohexadiene like structure presents the ring, tilted respect to the surface and also bonded to one single dimer row (picture c in Fig 6.). Finally, Gokhale et al. [43] have proposed a model in which the aromatic ring is bonded between two silicon dimers in a tetra-σ structure (referred to as "pedestal" picture a in Figure 11.). Figure 11. shows a schematic of these three configurations for benzene adsorption on Si(100)-2x1.

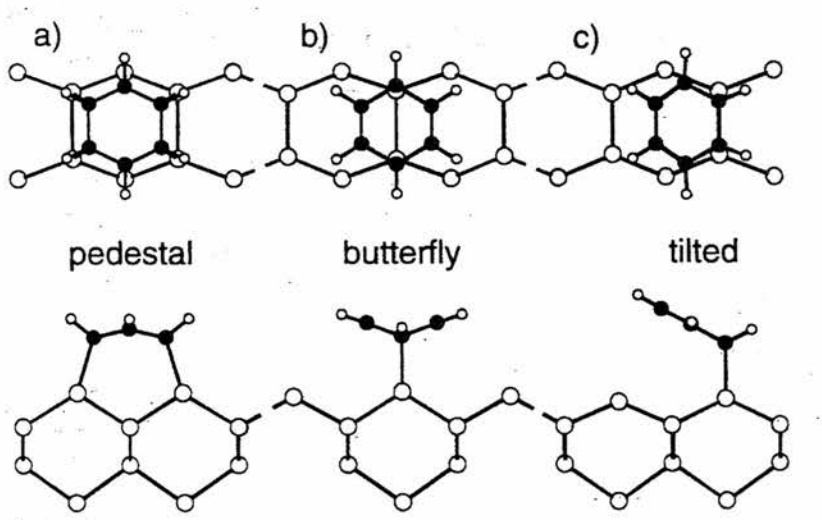

Figure 11. Side and top views of three models proposed for the adsorption of benzene on Si(100)-2x1.

Several attempts have been made to try to distinguish between these three structures using several spectroscopic techniques. Kong et al. [42] have assigned a model for the chemisorption from NEXAFS experiments in which the splitting of the C(1s)->π^* transition peak of the spectrum, is taken as a proof of the breakdown of the conjugation of the ring due to the bond to silicon. However the conjugation of the ring is broken in all three models proposed, (rehybridisation of the orbitals to form the σ structure with the silicon dimer) and splitting of the referred NEXAFS peak can be predicted for the three models from symmetry considerations [44].

These experimental results have stimulated theoretical attempts to calculate the energies for the three σ structures in order to provide a better description of the adsorption. These studies employ a semiempirical method to describe the electronic structure and calculate the molecular orbital energy, which can then be compared to the results obtained by NEXAFS. Semiempirical and basic principles calculations have been carried out by U. Birkenheuer et al. [45] finding the pedestal configuration to be more stable under semiempirical considerations, while under "basic principles" approach, the "butterfly" structure became energetically more favoured. To solve this uncertainty, the vibrational features have also been calculated, showing differences between the butterfly and pedestal structures. The most important is a vibrational feature (1635 cm^{-1}) related to the C=C bond that is predicted and present in the butterfly configuration but missing in the pedestal.

1.8. Adsorption of benzoic acid and aniline

Benzoic acid and aniline, each consist of a phenyl ring but differ in the functional group, COOH and NH_2 respectively. Vibrational studies of the adsorption of these molecules on Si(100)-2x1 have been carried out by Bitzer et al [46] showing that benzoic and aniline adsorb dissociatively on Si(100)-2x1 at room temperature. The reconstruction of the silicon surface remains unchanged, however, the LEED pattern showed weakened diffraction spots on a bright electron background indicating a disordered surface structure. In both spectra Si-H stretching modes are seen, indicating Si-H species present at the surface. Additionally the observation of distinctive Si-O, C-O (Si-N and C-N) vibrational features show that the chemisorption of benzoic acid (aniline) on clean Si(100)-2x1 occurs through H cleavage at the functional groups, followed by the formation of Si-O-CO-R (Si-NH-R) linkages. The displaced hydrogen atom bonds to one of the neighbouring silicon atoms of a dimer. In the case of aniline, the observation of a small feature at 3390 cm^{-1}, assigned to a N-H stretching mode, demonstrates that only a single atom is dissociated from the amino group. Both resulting aromatic species are unidentate coordinated on the silicon surface. The coordinations suggested are further supported by the observation of the carbonyl band and the N-H stretch for benzoate and

the aniline respectively. A model for the adsorption of benzoic and aniline on Si(100)-2x1 is shown in fig 12.

The formation of benzoate and aniline on Si(100)-2x1 in a bidentate bridging coordination cannot be achieved by annealing the sample to high temperatures. In the case of the benzoate molecule, annealing the sample to 570 K results in the disappearance of the C-H stretching modes which indicates the complete thermal-induced dissociation of the molecule. This process is accompanied by a desorption of the phenyl ring leaving the carboxylate group on the surface. The change in the intensity of the carboxylate group-related vibrations shows that the coordination of the CO_2 group has been altered. A higher thermal stability has been observed for aniline on Si(100)-2x1. The observation of the C-H and N-H vibrational modes after annealing to 740 K indicates that the dissociation process of in this case involves both the aromatic ring and the amino group.

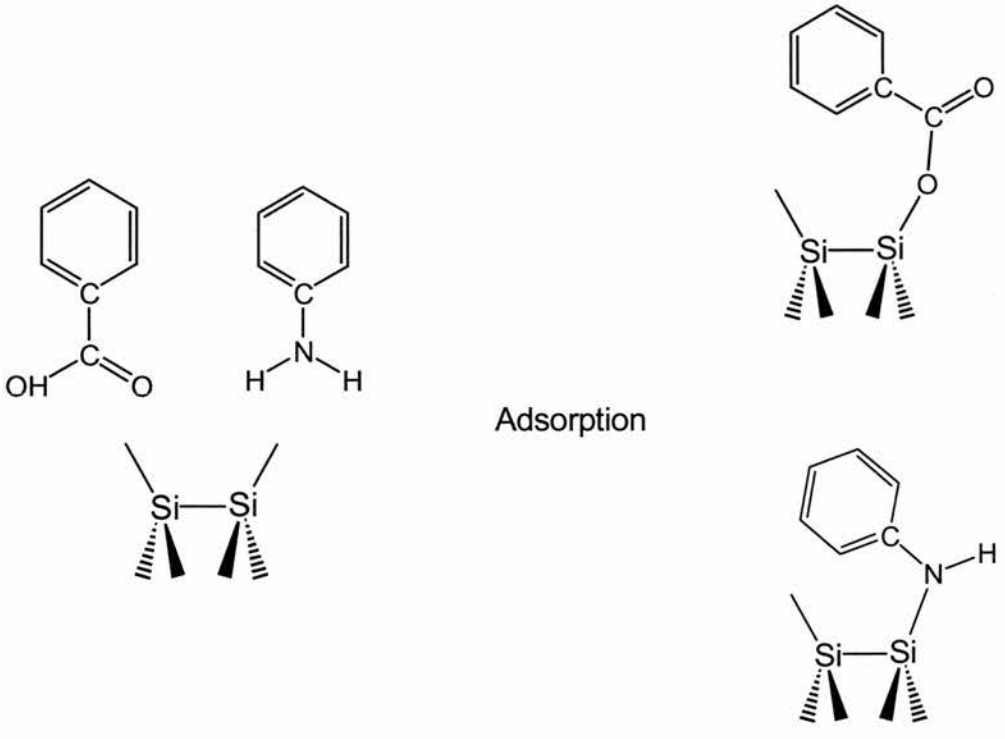

Fig 12. Schematics of the adsorption of benzoic acid and aniline on clean Si(100)-2x1. Note that the carbonyl bond is preserved in the benzoate/Si(100) system. In both cases, the adsorption process leads to unidentate species at the surface.

1.9. Coadsorption of alkali metals on Si(100)-2x1: Na

The interaction of alkali metals with Si(100)-2x1 has been widely studied during the last years both experimentally [47-49] and theoretically [50-52]. The surface sensitive techniques have aided a better understanding of the chemistry occurring at the alkali metal/semiconductor interface. The first model based on photoelectron diffraction (PED) results [49] suggested two adsorption sites, the pedestal and cave bridge, respectively for the adsorption of alkali metals on Si(100)-2x1. These results are supported by *ab initio* total energy calculations, which show that the most stable geometry results in the formation of the so-called double-layer model with two preferential adsorption sites [50]. On the other hand, Tochihara and Wei et. al. have proposed a model supported by LEED data in which the alkali metal atoms were found to be adsorbed on a single adsorption site, the pedestal, and forming one dimensional alkali metal linear chains [47-48].

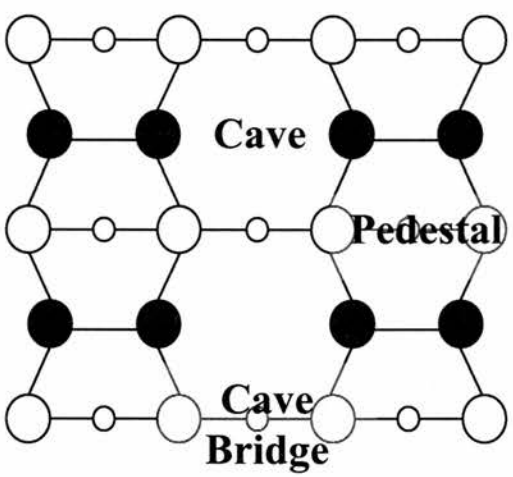

Fig 13. Schematic of the reconstructed Si(100)-2x1 surface with the possible adsorption sites for Na atoms.

Recent STM measurements agree with the formation of these linear structures on Si(100)-2x1 but differ in the adsorption site for the alkali atom. For the monolayer K/Si(100)-2x1 surface it was shown that K atoms form one-dimensional linear chains distant 7.68 Å and parallel to the silicon dimer rows along the <110> direction where the K atoms are predominantly found in the cave site. [53].

More detailed studies using PEXAFS have been carried out to understand the local environment of the alkali metals adsorbed on the Si(100)-2x1 surface. This technique is a variation of the surface EXAFS. It is now well established that the PEXAFS technique probes the short-range order of atoms in the topmost atomic layer on the surface. The very high surface sensitivity of this method is due to the small escape length (≈5 Å) of primary electrons in the kinetic energy range of the PEXAFS data. Additionally, polarisation dependent PEXAFS enables bond lengths as well as their orientation relative to the surface plane to be probed. The Na 2p PEXAFS data [54] showed that Na-Si distance is the same at low and monolayer coverages and close to the sum of the Na and Si covalent radii. These results support the model of covalent bonding between the Na and Si atoms proposed earlier by core-level and valence-band photoemission studies [55]. The measured Na-Si and Si-Si distances indicate that Na is adsorbed primarily on the cave site. This finding is in very good agreement with the fact that Na atoms are covalently bonded to the silicon atoms, which makes the cave the most favoured adsorption site. There is no evidence of Na-Na distance perpendicular to the <110> direction consistent with any double layer models. Ab initio total energy molecular calculations [56] support the cave site adsorption geometry. Additionally, the studies indicated that the coadsorbed alkali metals do not induce major changes in the surface reconstruction.

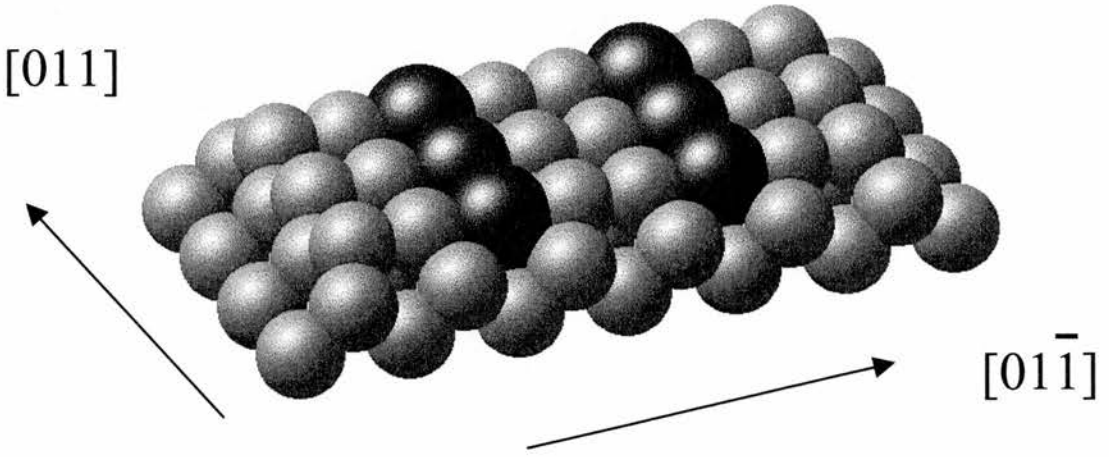

Fig 14. Schematic of coadsorbed Na atoms on Si(100)-2x1.

1.10. References

[1] M. Sokolowski, E. Umbach. Vacuum Solutions 21 (1999) 15-18

[2] F.L. Carter. Journal of Vacuum Science & Technology B 1 (1983) 959-968

[3] F. Stucki, J. Anderson, G.J. Lapeyre, H.H. Farrell. Surface Science 143 (1984) 84-92

[4] H. Ibach, H. Wagner, D. Bruchmann. Solid State Communications 42 (1982) 457-459

[5] D. Schmeisser, F.J. Himpsel, G. Hollinger. Physical Review B-Condensed Matter 27 (1983) 7813-7816

[6] J.S. Hovis, H. Liu, R.J. Hamers. Surface Science 404 (1998) 1-7

[7] J.S. Hovis, S. Lee, H.B. Liu, R.J. Hamers. Journal of Vacuum Science & Technology B 15 (1997) 1153-1158

[8] J.S. Hovis, R.J. Hamers. Journal of Physical Chemistry B 101 (1997) 9581-9585

[9] H.N. Waltenburg, J.T. Yates. Chemical Reviews 95 (1995) 1589-1673

[10] R.E. Schlier, H.E. Farnsworth. Journal of Chemical Physics 30 (1959) 917-924

[11] D.J. Chadi. Journal of Physical Chemistry 34 (1979) 90-107

[12] J.D. Levine. Surface Science 43 (1973) 43-47

[13] R.J. Hamers, Y.J. Wang. Chemical Reviews 96 (1996) 1261-1290

[14] C.C. Cheng, J.T. Yates. Physical Review B 43 (1991) 4041-4045

[15] K. Oura *et al.* Physical Review B 41 (1990) 1200-1203

[16] M.S. Wrighton, A.B. Ellis, D.L. Wolczanski, Morse D.L. Journal of the American Chemical Society 98 (1976) 2774

[17] J.J. Boland. Surface Science 261 (1992) 17-28

[18] X.M. Zheng, P.V. Smith. Surface Science 232 (1990) 6-16

[19] U. Hofer, P. Morgen, W. Wurth, E. Umbach. Physical Review B 40 (1989) 1130-1145

[20] J.P. Pelz, R.H. Koch. Physical Review B 42 (1990) 3761-3764

[21] B. Schubert, P. Avouris, R. Hoffmann. Journal of Chemical Physics 98 (1993) 7593-7605

[22] B. Schubert, P. Avouris, R. Hoffmann. Journal of Chemical Physics 98 (1993) 7606-7612

[23] J. Westermann, H. Nienhaus, W. Monch. Surface Science 311 (1994) 101-106

[24] H. Bu, J.W. Rabalais. Surface Science 301 (1994) 285-294

[25] P.V. Smith, A. Wander. Surface Science 219 (1989) 77-87

[26] D. Schmeisser. Surface Science 137 (1984) 197-210

[27] W. Ranke, D. Schmeisser. Surface Science 149 (1985) 485-499

[28] P.A. Thiel, T.E. Madey. Surface Science Reports 7 (1987) 211-385

[29] Y.J. Chabal, S.B. Christman. Physical Review B 29 (1984) 6974-6976

[30] M. Chander, Y.Z. Li, J.C. Patrin, J.H. Weaver. Physical Review B 48 (1993) 2493-2499

[31] X.L. Zhou, C.R. Flores, J.M. White. Applied Surface Science 62 (1992) 223-237

[32] C. Huang, W. Widdra, X.S. Wang, W.H. Weinberg. Journal of Vacuum Science & Technology a-Vacuum Surfaces and Films 11 (1993) 2250-2254

[33] C. Huang, W. Widdra, W.H. Weinberg. Surface Science 315 (1994) L953-L958

[34] F. Rochet *et al.* Physical Review B-Condensed Matter 58 (1998) 11029-11042

[35] R.A. Wolkow. Annual Review of Physical Chemistry 50 (1999) 413-441

[36] P.A. Taylor *et al.* Journal of the American Chemical Society 114 (1992) 6754-6760

[37] M. Nishijima, J. Yoshinobu, H. Tsuda, M. Onchi. Surface Science 192 (1987) 383-397

[38] F. Matsui *et al.* Surface Science 401 (1998) L413-L419

[39] R.J. Hamers, J.S. Hovis, S. Lee, H.B. Liu, J. Shan. Journal of Physical Chemistry B 101 (1997) 1489-1492

[40] J.S. Hovis, H. Liu, R.J. Hamers. Applied Physics a-Materials Science & Processing 66 (1998) S553-S557

[41] Y. Taguchi, M. Fujisawa, T. Takaoka, T. Okada, M. Nishijima. Journal of Chemical Physics 95 (1991) 6870-6876

[42] M.J. Kong *et al.* Journal of Physical Chemistry B 104 (2000) 3000-3007

[43] S. Gokhale *et al.* Journal of Chemical Physics 108 (1998) 5554-5564

[44] A. Lopez, T. Bitzer. Private discussion (1999)

[45] U. Birkenheuer, U. Gutdeutsch, N. Rosch. Surface Science 409 (1998) 213-228

[46] T. Bitzer, T. Alkunshalie, N.V. Richardson. Surface Science 368 (1996) 202-207

[47] H. Tochihara. Surface Science 126 (1983) 523-528

[48] C.M. Wei, H. Huang, S.Y. Tong, G.S. Glander, M.B. Webb. Physical Review B 42 (1990) 11284-11287

[49] T. Abukawa, S. Kono. Surface Science 214 (1989) 141-148

[50] I.P. Batra. Physical Review B 39 (1989) 3919-3922

[51] K. Kobayashi, Y. Morikawa, K. Terakura, S. Blugel. Physical Review B 45 (1992) 3469-3484

[52] B.L. Zhang, C.T. Chan, K.M. Ho. Physical Review B 44 (1991) 8210-8213

[53] P. Soukiassian, J.A. Kubby, P. Mangat, Z. Hurych, K.M. Schirm. Physical Review B 46 (1992) 13471-13479

[54] S.T. Kim, P. Soukiassian, L. Barbier, S. Kapoor, Z. Hurych. Physical Review B 44 (1991) 5622-5628

[55] P. Soukiassian, M.H. Bakshi, Z. Hurych, T.M. Gentle. Surface Science 221 (1989) L759-L768

[56] P.S. Mangat *et al.* Physical Review B 47 (1993) 16311-16321

CHAPTER 2.

Experimental and *ab initio* methods

2.1. NEXAFS

2.1.1. Introduction:

In the study of chemisorbed molecules on surfaces, X-ray absorption has played an important role in the determination of the internal molecular structure of the adsorbed species. In particular, the so-called NEXAFS technique (near edge x-ray absorption fine structure), has been used to determine specific bonds and molecular bond-lengths of molecules adsorbed on substrates [1-6]. By comparison of spectra from free and chemisorbed molecules, NEXAFS has shown which molecular orbitals are involved in the chemisorption and how these are oriented relative to the substrate. Compared to gas phase spectroscopy, x-ray absorption of chemisorbed molecules presents two major problems. First, the atomic density on a typical surface is in the range of 10^{15} atoms/cm^2 and therefore this is a typical density of adsorbed molecules on the surface. Second, the signal from the molecular layer is superimposed on the background signal from the substrate. The combination of these two problems makes this technique suitable only if powerful x-ray sources are used.

The x-ray absorption cross section σ_x of an atom or molecule is defined as the number of electrons excited per unit time divided by the number of incident photons per unit time and unit area. The absorption cross section for N_2 [7] is 10^{-18} cm^2/molecule and assuming a monolayer of nitrogen adsorbed on the substrate (10^{15} molecules/cm^2 , this gives 10^3 photons needed to create one absorption event. If each one of these absorption events releases a photoelectron, which is detected within a solid angle and under certain conditions, an efficiency factor must be taken into account. Assuming this to be 10^{-3}, that is, one out of one thousand photoelectrons produced is detected, in order to obtain reasonable statistics, a flux of 10^9 photons per second is required. Additionally, highly monochromatized x-rays need to be used in order to produce the expected excitations.

Only highly collimated synchrotron sources provide sufficient intensity and energy resolution to accomplish these experiments.

2.2.2. NEXAFS theory:

We want to measure a signal that is proportional to the absorption cross section σ_x and can give us information about the molecular orbitals from the excitation of inner electron states. The number of photons absorbed by the molecular layer in the limit of small adsorbate concentrations can be expressed as:

$$N_{abs}=I_0A_0\sigma_x(h\nu)\rho$$

Where I_0 is the incident photon flux density, A_0 is the area exposed to the beam, ρ the atomic area density and $\sigma_x(h\nu)$ the absorption cross section. The number of absorbed photons is proportional to the absorption cross section or the number of photoelectrons emitted and holes produced. However, several processes can occur during x-ray absorption. The absorbed photon releases the photoelectron and the hole left behind can be filled by electrons from outer shells either radiatively by emission of fluorescent photons, or non-radiatively by the emission of an Auger electron. This is better explained in Figure 1.

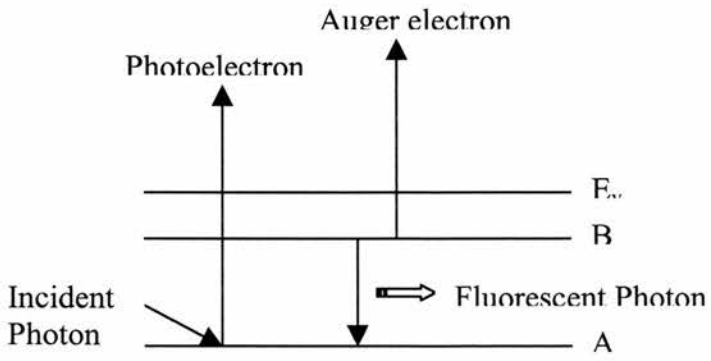

Figure 1. In this diagram are displayed the processes that can occur after x-ray absorption by an atom. The photon absorption results in the emission of a photoelectron and the creation of a core hole. The hole can be filled by an electron from an outer shell and initiating the emission of an Auger electron and/or a photon.

In order to measure the absorption cross section, a direct measurement of the photoelectrons emitted after the photon absorption is not viable because the features below the ionisation potential would be lost, since only electrons which can escape into the vacuum are detected. This is the origin of the step function observed at the absorption edge. This fact suggests that only the detection of Auger electrons or fluorescent photons associated with secondary processes can provide information about the empty molecular orbitals that lie below and above the vacuum level. Figure 2. shows that electrons from the atomic level 1s can be excited directly into the vacuum giving rise to the step function.

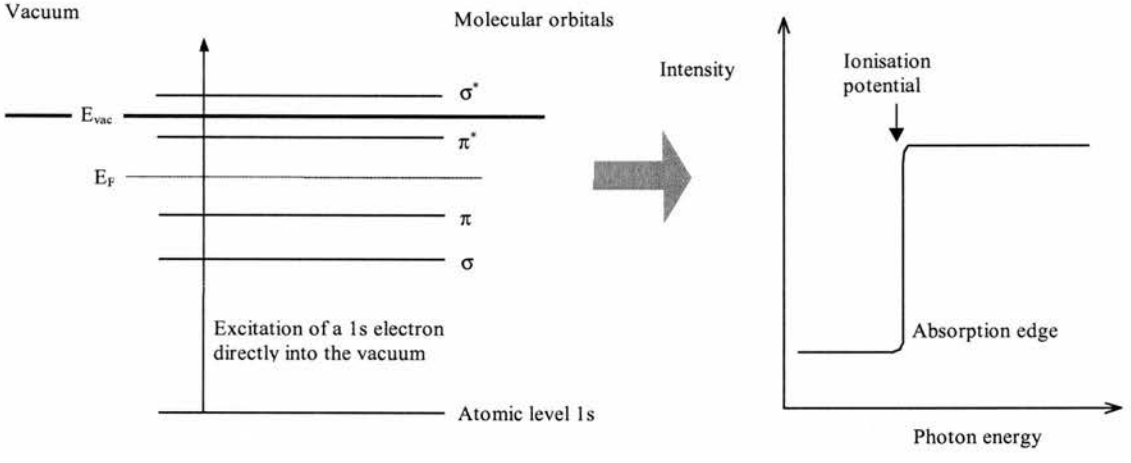

Figure 2. This figure shows the spectrum obtained if photoelectrons were detected after the x-ray absorption process. With increasing photon energy the ionisation potential is reached and electrons from the 1s atomic level have energy to reach the vacuum giving rise to the observed step function.

Figure 3. shows the absorption fine structure if electrons are excited from the 1s atomic orbital into upper and lower unoccupied molecular orbitals. If such transitions occur, (in fact they are resonant transitions since the energy scale is quantified) core electrons can fill the holes created, and consequently Auger electrons can be emitted towards the detector.

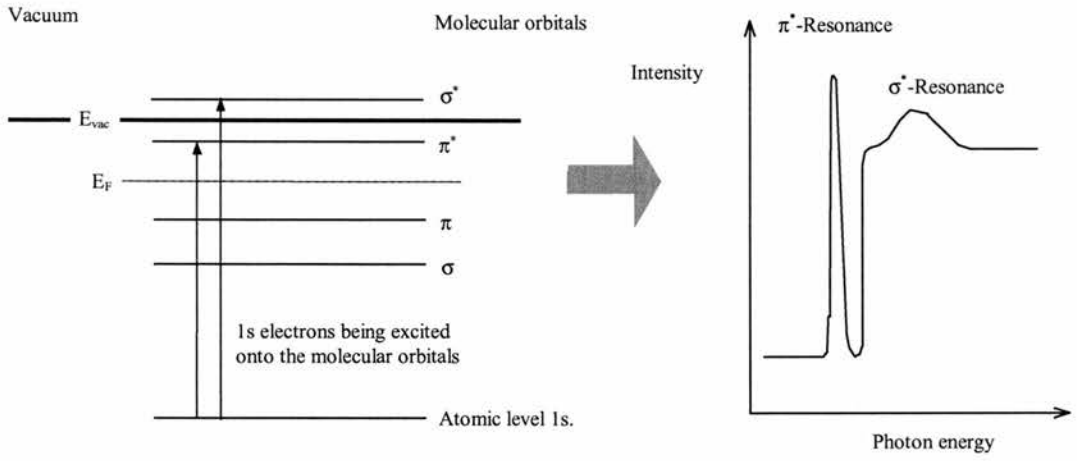

Figure 3. This figure shows the expected spectra if Auger electrons are detected. The transition from the 1s atomic level to the π molecular orbital creates a hole that can be filled with electrons from outer levels. An Auger electron from a core level can reach the detector in these conditions and give rise to the peak observed. Since the transition 1s->π* is resonant and well defined this process generates the emission of detected Auger electrons.

The NEXAFS structure arises from the dependency of the absorption cross section with photon energy. By collecting secondary electrons the absorption fine structure can be resolved near the absorption edge.

It is important to note that all these processes are taking place simultaneously and Auger electrons and photoelectrons are being emitted indifferently from the sample. Several detection modes can be used to obtain a signal from the electrons being emitted from the sample. In total electron yield (TEY) detection mode, all electrons with different kinetic energies are collected and the signal is formed mainly by low energy electrons from the "inelastic tail". Although the number of counts is large, the relative signal to noise ratio is low because inelastic scattered electrons contribute to the signal. In partial electron yield (PEY) a grid at a negative potential is placed at the channeltron entrance. This allows only electrons with a kinetic energy above a threshold to reach the detector and the background coming from electrons excited directly into the vacuum is reduced. By suitable choice of this retarding voltage, photoemission peaks can be avoided in the NEXAFS spectrum, which simplifies the analysis process. The last detection technique is selective electron yield (SEY) in which only the electrons in a

determined kinetic energy window are allowed to enter the channeltron. This is done using hemispherical potential plates whose voltage can be adjusted to select a precise kinetic energy. In this way the energy window monitored can be further adjusted to avoid peaks coming from excitations of core levels.

The measured NEXAFS signal depends also on the conditions of the storage ring which affect the intensity of the incident X-rays. In order to correct anomalies introduced by variations of the source, a reference grid monitor is used. This method uses a gold grid placed at the exit of the monochromator to follow possible variations of the x-ray source. Normalisation is carried out through division of the electron yield signal by this gold reference signal, and the ratio is taken as the NEXAFS spectrum of the sample. Since the gold grid is near the dosing chamber, adsorption of contaminants can not be avoided and this gives rise to absorption peaks in the signal that make the tracking of beam current difficult.

Two additional methods are used to minimise unwanted signals coming from the substrate or contaminants physisorbed on the surface.

-Division by clean sample spectrum. In this type of correction, an initial NEXAFS spectrum of the substrate must be obtained. The ratio between the exposed surface spectrum and the clean one gives the corrected signal. This method does not correct any instabilities of the x-ray source and longer acquisition times may be needed.

-Subtraction of the clean sample spectrum. This method is employed mainly to remove contamination peaks on the recorded spectra, although it does not correct the source variations during acquisition.

2.2.3. Angular dependence of NEXAFS resonances.

One of the most important applications of the NEXAFS spectroscopy is the determination of the molecular orientations of the chemisorbed species on substrates. This is based on the dependence of the resonance's intensity with angular orientation of

the substrate relative to the synchrotron light. The x-rays emitted by the storage ring are polarised so that the electric vector **e** has a strong component parallel to the plane of the synchrotron. Since the molecule is adsorbed on the surface and has a relative orientation towards the light source, the rotation of the substrate rotates the molecule and its molecular orbitals and therefore the orientation of these towards the photon beam is changed. As stated previously the π^* and σ^* resonances can be described in terms of molecular orbitals as dipole transitions from the atomic state 1s to the p component of the π^* and σ^* final states. The change in the intensity of these resonances is proportional to the oscillator strength and the x-ray absorption cross section for each molecule. For explicit calculation of the resonance intensity we have to estimate the mean value of the momentum when the transition occurs between the 1s core level to the molecular orbital. This magnitude squared is proportional to the number of electrons absorbed and this to the number of Auger electrons emitted, which in ultimate terms give rise to the signal recorded. Quantum mechanics give an expression for the intensity of the resonances based on initial and final state wavefunctions.

$$I_{if} \propto \left| \langle f | e \cdot p | i \rangle \right|^2 \qquad \mathbf{1}$$

where considering the polarisation of the electric vector turns to,

$$I \propto P \left| \langle f | e'' \cdot p | i \rangle \right|^2 + (1-P) \left| \langle f | e^{\perp} \cdot p | i \rangle \right|^2 \qquad \mathbf{2}$$

in which i is the initial state (core level 1s) and f the final state (p component of the molecular orbital π), and P is the polarisation factor defined as:

$$P = \frac{|E''|^2}{|E''|^2 + |E^{\perp}|^2} \qquad \mathbf{3}$$

where $E^{//}$ and $E^{\perp}$ are the electric field components parallel and perpendicular to the incidence plane respectively.

The angular dependence of the NEXAFS spectra is determined by the spatial orientation of the orbital, as can be interpreted from equations (1) and (2). In a classical physics description, this would be interpreted as an excitation occurring only if the polarisation vector and electric vector are parallel. The orientation of the molecular

orbital can be described in terms of "vector" final states or "plane" final states depending upon the direction of each molecular orbital relative to the substrate. As an example, let us take the benzene molecule adsorbed on silicon in which the π^* orbitals lie perpendicular to the surface, while the σ orbitals sit in the plane parallel to the substrate and perpendicular to each other. In this case the vector description would be used for the π orbitals and the plane interpretation would be used for the σ orbitals, since two orthogonal vectors define a plane. We will only derive the mathematical description for the "vector" case, since analogue expression can be derived for the "plane" situation.

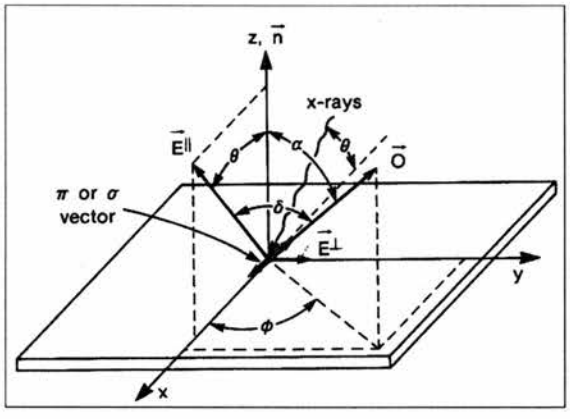

Figure 5. This figure shows the incidence geometry for the vector case. The incident x-rays come in the x-z plane and the weak component of the electric field $E^{\perp}$ lies parallel to the surface. The O vector defines the orientation of the orbital represented by a vector.

Following mathematical calculations to estimate the matrix elements from equations (1) and (2) and using the corresponding eigenfunctions, it can be demonstrated that the resonance intensity in the vector description can be expressed as a function of incidence, tilt and azimuthal angles as (see figure 5):

$$I_v'' = Cos^2\theta\, Cos^2\alpha + Sin^2\alpha\, Sin^2\theta\, Cos^2\phi + 2Sin\alpha\, Cos\alpha\, Sin\theta\, Cos\theta\, Cos\phi \qquad \mathbf{4}$$

$$I_v^{\perp} = Sin^2\phi\, Sin^2\alpha \qquad \mathbf{5}$$

where $I_v^{//}$ and $I_v^{\perp}$ are the resonance intensities in the vector description.

It is important to note that to obtain the integrated intensity emitted by the surface, it is necessary to average the azimuthal angle and integrate over all possible values of ϕ. For twofold or higher substrate symmetry, the terms with Cos ϕ in equations [4] and [5] average to zero since every molecule has its mirror equivalent. Therefore the equations in these case become,

$$I_v'' = Cos^2\theta\, Cos^2\alpha + Sin^2\alpha\, Sin^2\theta\, Cos^2\phi \qquad \mathbf{6}$$

and

$$I_v^{\perp} = Sin^2\phi\, Sin^2\alpha \qquad \mathbf{7}$$

for the vector representation. Note that for a tilt angle of α=45° and the resonance vector parallel to $E^{//}$ (ϕ=0°) the resonance intensity is independent of the incident angle θ.

For threefold axis symmetry, the term $Cos^2\phi$ averages to ½ since three molecule orientations are equivalent , therefore the expressions become,

$$I_v'' = Cos^2\theta\, Cos^2\alpha + \frac{1}{2} Sin^2\alpha\, Sin^2\theta = \frac{1}{3}[1 + \frac{1}{2}(3Cos^2\theta - 1)(3Cos^2\alpha - 1)] \qquad \mathbf{8}$$

and

$$I_v^{\perp} = \frac{1}{2} Sin^2\alpha \qquad \mathbf{9}$$

An important prediction from these equations is that for a certain incidence angle called "magic angle" the resonance intensity does not depend on molecular orientation. This angle happens to be 54.7° and no distinction can be established between an ordered surface and a disordered one if the spectra are being recorded at this incidence angle.

2.2. HREELS .

2.2.1. Introduction.

High-resolution electron energy loss spectroscopy is a powerful technique used in the characterisation of adsorbed molecules on crystal substrates [8-14]. A beam of monochromatised electrons is used to excite the molecule normal modes and obtain structural information from the vibrational analysis. Since the molecular vibrations lie within the 10^{-1}-10^{-3} eV range, low kinetic energy (6eV) electrons are used to probe these excitations. This can be understood as an interaction between the incoming electrons and a surface dipole, which slows down the reflected electrons and leads to an energy loss spectrum [15]. The experimental sources for the HREELS (High-resolution electron energy loss spectroscopy) are rather similar in most spectrometers used for surface analysis purposes.

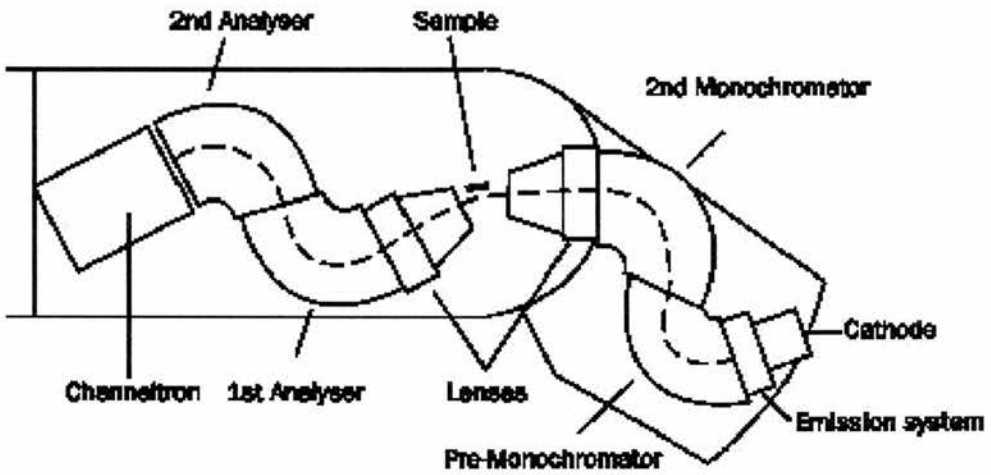

Figure 6. Experimental setup of an electron energy loss experiment. Electrons coming from the filament pass through the monochromator, strike the sample and the energy of the scattered electrons is measured by the analyser. The result is the energy loss spectrum.

The electron source is generally a hot filament, which emits electrons through thermoionic emission. These electrons are injected by an electrostatic lens into an energy monochromator that is normally built of plates and hemispherical sectors kept and different potentials. Once the beam is monochromatic, it is projected towards the

surface, normally at 45-degree incidence angle. Electrons scattered by the surface are analysed by an electron-energy analyser, which consists of different plates kept at different potentials to avoid energy dispersion of the beam. Figure 6 shows a schematic of the monochromator and analyser experimental setups.

An important feature in this type of spectroscopy is the beam's resolution, which is defined as the spectral distribution of the incident electrons. The aim is to analyse the sample with the most monochromatic beam, (narrow spectral distribution) in order to resolve loss features very close in the energy spectrum. This is achieved by proper monochromatization of the incident electron and scattered beams. The monochromator works in such a way that only those electrons with certain energy can go through, when different potentials are applied to the set of plates and hemispheres. The highest resolution reported to date is around 1 meV although most of the studies are carried out in the 4-8 meV resolution range. In certain surfaces, like silicon, the resolution is limited by the surface itself, and further increase in the spectrometer performance gives no better results. In the case of silicon the limited resolution is due to plasmon excitations, which produce the broadening of the energy loss peaks [16].

2.2.2 HREELS theory.

The interaction of electrons with surfaces that lead to molecular vibrational excitations in HREELS can be classified in three different types, although no precise boundaries can be traced between them since all processes occur dynamic and simultaneously [7-15].

2.2.2.1. Dipole scattering.

In the discussion of the inelastic scattering of electrons by adsorbed molecules, dipole scattering can be considered as a long ranged interaction mechanism. Adsorbed molecules behave like potential dipoles that can be excited through oscillating electric fields. Incoming electrons are moving charged particles that modulate an electric field

around their environment in a time dependent basis. As the electron approaches the surface, an adsorbed molecule "sees" the electron's electric field and the electric field caused by the redistribution of charge in the solid. As can be easily understood, the surface dipole couples with the time dependent electric field and the dipolar momentum changes from P_0 in the unperturbed state, to $P_0+p\cdot e^{-i\omega t}$ in the excited state. The initial dipolar momentum P_0 comes from the charge distribution in the crystal's unit cell, while the final one is related to the excitement of a normal mode of frequency ω and has dynamic character, coming from the time dependency. Now, as for the inelastic scattering of x-rays, the cross section contains a dependency on the scalar product between k_I-k_f and the polarisation of the normal mode of vibration, where k_I and k_f are the wavevectors of the incident and scattered beams respectively. In the case of the specular direction, ($\theta_i = \theta_f = 45°$), k_I-k_f is perpendicular to the surface, so therefore in this configuration the contribution to the cross section of normal modes parallel to the surface vanishes. The surface dipole selection rule, gives an indication for the intensity of the features in a vibrational spectrum. In cases where the dynamic electric dipole are oriented parallel to the surface they are completely screened and not observed in the EELS spectrum. On the other hand, an enhancement is observed for vibrations with a dynamic dipole moment oriented perpendicular to the surface.

The most important feature of dipole scattering is that it enhances the small momentum transfer processes. This is because, the momentum transfer in vibrational excitations is small compared to the momentum the electron has when approaching the surface.

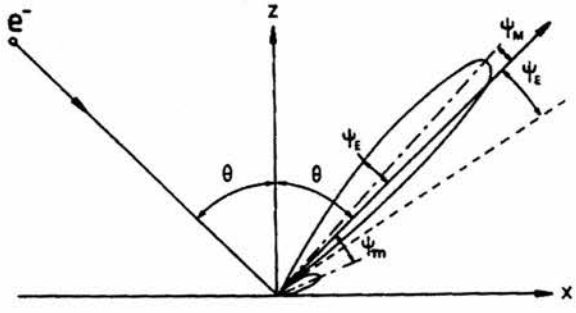

Figure 7. Schematic of the distribution of elastic and inelastically scattered electrons by a surface.

The inelastic dipole scattering is followed by elastic backscattering from the substrate, which provides the momentum transfer to reflect the electron towards the detector. Therefore the intensity of the observed loss features is concentrated near the specular direction. Inelastically scattered electrons with a small change in the momentum (usually $\Delta k=0.05$ Å^{-1} for an electron approaching the surface with 2 eV kinetic energy) are confined in lobes near the specular direction. Elastically scattered electrons give rise to the known diffraction spots in LEED and the observed elastic peak in HREELS, typically several orders of magnitude greater than the loss features. Figure 7. shows the distribution of dipole scattered electrons by a surface in the specular direction.

It is important to note that vibrational motions of adsorbed molecules do not only produce dipolar scattering, but any perturbation that involves charge fluctuations is capable of scattering electrons inelastically. A useful magnitude to calculate is the scattering efficiency S per unit energy dhω and unit solid angle dΩ, denoted as $d^2S/dh\omega d\Omega$. This quantity gives the probability that an electron is scattered from the initial state into a final state that lies within the solid angle dΩ and energy range dhω. Integration of this expression over the solid angle subtended by the entrance slit of the analyser will give the probability of electrons entering the detector after being dipole scattered. It can be demonstrated that this magnitude is proportional to the so-called loss function, expressed as

$$\frac{dS}{dh\omega} \propto \mathrm{Im}\left[-1/(1+\varepsilon(\omega))\right]$$

where $\varepsilon(\omega)$ is the substrate's dielectric function, which can be described in terms of free carriers contributions [15]. The loss function can be expressed as a function of the background dielectric constant ε_∞, the plasma frequency ω_{sp} and the relaxation time $\tau(\omega)$ as,

$$\mathrm{Im}\left[-1/(1+\varepsilon(\omega))\right]=\frac{\omega\omega_{sp}^{2}}{(1+\varepsilon_{\infty})\tau(\omega)}\left[(\omega_{sp}^{2}-\omega^{2})^{2}+\omega^{2}/\tau^{2}(\omega)\right]^{-1}$$

Figure 8. shows a plot of this function for electrons scattered by the silicon surface at room temperature. Note that for highly doped samples the function has a maximum around ω_{sp} while the feature broadens for low doping levels.

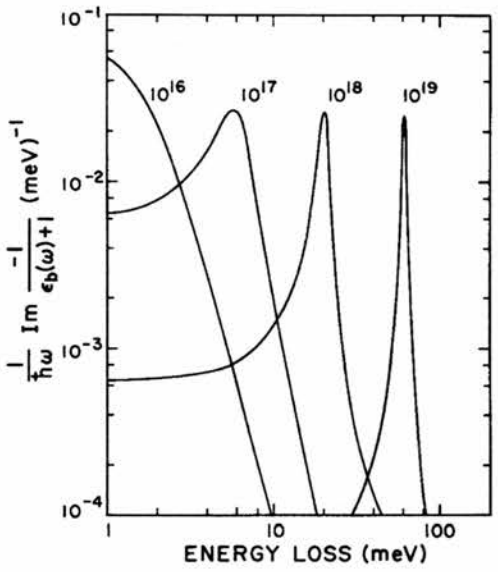

Figure 10. Schematic of the dependence of the loss function with the doping level for silicon semiconductors.

For low doped semiconductors, $\tau(\omega)$ is larger than for highly doped semiconductors, therefore the term $(\omega_{sp}^{2}-\omega^{2})^{2}$ is predominant in the previous equation which can be rewritten as,

$$\mathrm{Im}\left[-1/(1+\varepsilon(\omega)\right]\cong\frac{\pi}{2(1+\varepsilon_{\infty})}\delta(h\omega-h\omega_{sp})$$

Integrating equation 10 along all energies and the mentioned solid angle gives,

$$S = \int dh\omega \frac{dS}{dh\omega} = \frac{\pi}{a_0 k_I \cos\theta_I} \frac{1}{(1+\varepsilon_\infty)}$$

which is close to unity under the conditions of the electron energy loss experiments.

This means that the probability of electrons scattered within a wide energy range is significant, resulting in a broadening of the energy distribution of electrons reflected from the semiconductor surface. For this reason, to carry vibrational spectroscopy at semiconductor surfaces a consideration of the sample's doping level is required in order to achieve reasonable resolution.

2.2.2.2. Impact scattering.

So far, in the description of the interaction between the electron beam and the adsorbed molecule, it has only been considered the scattering of electrons at small deflections angles. We are now focusing on electrons reflected from the surface outside the mentioned "dipolar lobe", which have been scattered under the impact scattering regime. Elementary excitations can also be induced through a much short-range interaction between the probe electron and atoms in the surface. In the case of molecular adsorbates, vibrational excitations occur through the scattering of the electron by the ion cores of the molecule. Impact scattering cross sections typically show an oscillatory behaviour that comes from the coherent interferential processes occurring during the interaction. As a result of these, overtone excitations are favoured and features lying away from the elastic peak can be easily identified since the background signal is much reduced.

The specular direction has no enhanced importance in impact scattering, and this characteristic is used to distinguish from dipole and non-dipole active modes in energy loss spectroscopy.

2.2.2.3. Resonance ion scattering:

Resonance scattering occurs when the probe electron is captured by the molecule and this is brought to an excited state to form a transient negative ion and remitted towards the detector. The capture of an electron by the molecule alters the molecular potential, inducing changes in the adsorbed molecule's resonances compared to the gas phase.

-Resonance lifetime: The interaction of the negative ion with the surface may change the tunneling rate for capture and emission by modifying the potential barrier that confines the captured electron.

-Resonance energy: Again, the deformation of the molecular potential shifts the energy levels leading to a shift of the resonance.

-Angular distribution of scattered electrons: The surface orients the molecule giving a characteristic angular emission profile. This angular distributions reflect changes in the resonance symmetry upon charge modifications.

-Resonance decay channels: The surface changes the ratio between competing resonances. For example a reduction of the lifetime alters the relative probabilities of exciting a sequence of vibrational overtones. Coupling of the molecule with the surface, gives rise to a new range of available frequencies such as the vibration of the whole molecule against the surface.

2.3. Low energy electron diffraction (LEED)

Low energy electron diffraction (LEED) uses low kinetic energy electrons (10-100 eV) to probe the surface periodicity. These electrons are directed towards the sample by an electron gun (in this case, at normal incidence). The electrons diffracted by the surface are detected by the fluorescence they cause on a phosphor screen that is placed in front of the sample. The diffraction of electrons occurs because of the periodic arrangement of atoms in the surface. In the case of the silicon (100) surface, the structure is such that the dimers formed along (011) directions after the surface reconstruction become the scattering centres giving rise to the 2x1 reconstruction.

The diffraction pattern gives information about the size of the unit cell while the background intensity is reflects the extent of disorder and number of defects at the surface. It is important to note that LEED is sensible to long range order and only areas with a certain periodicity contribute to the sharp diffraction spots. A schematic of the LEED experimental setup is shown in fig 11 below.

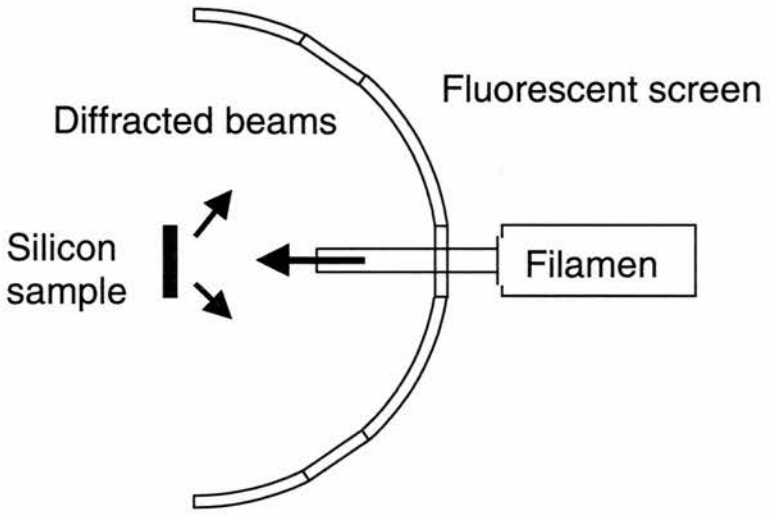

Fig 11. Schematic of the LEED experimental setup.

In the case of Si(100)-2x1 LEED is particularly useful in the determination of the surface reconstruction after adsorption of organic molecules.

2.4. X-ray photoelectron spectroscopy (XPS)

In X-ray photoelectron spectroscopy (XPS), monoenergetic soft X-rays bombard the sample causing electrons from atomic core and valence levels to be ejected. The identification of species present at the surface can be made directly from the kinetic energies of these ejected photoelectrons. The kinetic energy K_e of these photoelectrons is approximately given by the expression,

$$Ke = h\upsilon - Be$$

where hυ is the energy of the incident photons and B_e is the binding energy of the electrons in a core level. Additional processes can occur in an XPS experiment. The incident photons can also excite electrons from other core levels into unoccupied orbitals or directly into the vaccum. These would result in a number of photoelectrons with kinetic energies given by,

$$Ke = h\upsilon - Be - E1$$

and

$$Ke = h\upsilon - Be - E2$$

to reach the detector and give rise to two additional peaks. The first equation refers to a shake up and E1 is the energy difference between a core level and the unoccupied orbital in which the electron is excited into. The second equation describes a shake off being E2 the energy of this second core level. In the first case the second excited electron stays in the atom while in the second case it is ejected and is able to reach the detector.

On a finer scale, it is also possible to identify the chemical state of elements from the shift in the kinetic energy. In the case of metals atoms bonded to high electronegativity atoms, the measured kinetic energy shifts to lower values compared to the pure element. This effect is known as chemical shift and is due to valence charge being transferred from the metal to the electronegative atom, resulting in a stronger electrostatic interaction between the core levels and the nucleus of the metal [17-18].

The relative concentrations of elements can be determined from the measured photoelectron intensities, although it is necessary to correct for analyser transmission and ionisation cross sections using known samples.

2.5. Scanning tunneling microscopy (STM) .

The power of STM in surface chemistry lies in its ability to resolve the electronic states of surfaces and adsorbed species both energetically and spatially. Based in the

quantum mechanical interpretation of atomic structures, the electron density is not confined by the surface atoms but extends into the vacuum according to their wave function. If a metal tip is brought close to the surface, the overlap of wave functions between tip and sample allows a tunneling current to flow when voltage is applied between the tip and the sample. The interference between the tip and surface electronic states forms a topographic view of the surface structure in real space. The STM image shows the symmetry and the shape of the surface periodicity, the size and shape of domains as well as details of the molecular structure of adsorbates on surfaces.

The most notable example of STM in relation to semiconductor surfaces was the local reconstruction of Si(111)-7x7 shown by Binnig et. al. [19].

2.6. Ab initio methods

2.6.1. Introduction

The application of quantum-mechanical principles to chemical problems can assist in the determination of magnitudes that are not obtainable through experimental techniques. Additionally, the understanding of chemical bonding, spectral phenomena, molecular reactivities, and various other fundamental chemical problems rests heavily on our knowledge of the detailed quantum behaviour of electrons in atoms and molecules. Electrons in quantum-mechanical systems are described by wave functions which are solutions of the Schrodinger equation,

$$\overline{H}\varphi = E\varphi$$

where $\overline{H}$ is a mathematical operator called a Hamiltonian, and E and φ are the eigenvalues and eigenfunctions respectively which satisfy the equation. The Hamiltonian operator corresponds to the Hamiltonian function in classical mechanics and it can be understood as the total energy of the system expressed in terms of coordinates and conjugate momenta. These variables refer to the position and momentum of electrons and nuclei in an atom or molecule. Since the energy range in quantum mechanics is

quantized, the energy can only take discrete values given by E. The Schrödinger equation can be analytically solved only in the case of hydrogen. In the case of more complex elements and polyatomic molecules it is necessary to use approximations in order to obtain the wave functions that describe the electronic states of these systems. The basic approximation in quantum chemistry is the so-called Born-Oppenheimer approximation. In this approximation the wave functions corresponding to electrons and nuclei in a molecule are separated and the eigenfunction solution of the Schrödinger equation can be written as,

$$\varphi(q_i, q_\alpha) = \varphi_{elec}(q_i; q_\alpha)\varphi_N(q_\alpha)$$

The Born-Oppenheimer approximation introduces little error for the ground electronic states of diatomic molecules. Corrections for excited electronic states are larger than in the ground state, but still are usually small compared with errors introduced by the approximations used to solve the electronic Schrodinger equation of a many electron molecule.

2.6.2. Hartree-Fock theory

Molecular quantum-mechanical methods are classified as either *ab initio* or semiempirical. Semiempirical methods use a simpler Hamiltonian than the correct molecular Hamiltonian and use parameters whose values are adjusted to fit experimental data or the results of *ab initio* calculations. An example of a semiempirical method is the Hückel MO treatment of conjugated hydrocarbons [20], which uses a one electron Hamiltonian and takes the bond integrals as adjustable parameters rather than quantities to be calculated theoretically. In contrast *ab initio* calculations uses the correct Hamiltonian and does not use experimental data other than the values of the fundamental physical constants. For atoms or molecules with a large number of electrons, the best approach to finding a good wave function lies in first calculating an approximate wave function using the Hartree procedure. This method is the basis for the use of atomic and molecular orbitals in many electron systems.

The Hamiltonian operator for an n-electron system can be written as,

$$\overline{H} = -\frac{\hbar^2}{2m_e}\sum_{i=1}^{n}\nabla_i^2 - \sum_{i=1}^{n}\frac{Ze^2}{r_i} + \sum_{i=1}^{n-1}\sum_{j=i+1}^{n}\frac{e^2}{r_{ij}}$$

The first sum contains the kinetic operators for the n electrons. The second is the potential energy for the attractions between the electrons and the nucleus of charge Ze. The last sum is the potential energy of the interelectronic repulsions. A first approach to solve the Schrodinger equation in the many electron system would be to neglect the electronic repulsion sum, in which case the equation would separate into n-one electron hydrogen like equations. Although the approximate wave function is quite useful, it is lacking in quantitative accuracy. The next step is to use a variation function that has the same form as the approximate wave function but it is not restricted to hydrogenlike or any other particular form of orbitals,

$$\varphi = g_1(r_1,\theta_1,\phi_1)g_2(r_2,\theta_2,\phi_2)\cdots g_n(r_n,\theta_n,\phi_n)$$

The aim is now to determine the functions g_1, g_2, g_n that minimise the system energy, which in the quantum mechanics formalism is written as,

$$E = \frac{\int \varphi^* \overline{H}\varphi d\tau}{\int \varphi^* \varphi d\tau}$$

The procedure for calculating these g_I was developed by Douglas Hartree and is called the Hartree self-consistent field method (SCF). Initially we guess a product wave function as described by the expression above. We solve the one-electron Schrödinger equation for electron 1 assuming instantaneous interactions between this electron and the other electrons. This will give us an improved orbital for electron 1. We proceed in a similar manner with all remaining electrons until we have a set of improved orbitals for

all n electrons. Then we go back to electron 1 and repeat the process. We continue to calculate improved orbitals until there is no further change from one iteration to the next. The final set of orbitals gives the Hartree self-consistent field wave function.

In the above discussion we have not paid attention to the spin of the electrons and the Pauli principle. The true wave functions should include the spin explicitly and should be antisymmetric to interchange of electrons. This introduces a new term in the Hamiltonian described above which is referred to as exchange interaction and is the result of the Fermion nature of the electrons. The SCF calculation that uses antisymmetrized orbitals is called a Hartree-Fock calculation. The method to solve the Hartree-Fock differential equations introduces the so-called basis functions, which represent the Hartree-Fock orbitals as linear combinations of a complete set of known functions.

The GAUSSIAN 98 software used for the *ab initio* calculations presented in this thesis use Gaussian-type functions for the atomic orbitals in a linear combination of atomic orbitals. In a 3-21G basis set, each inner-shell atomic orbital is represented by a single gaussian-type function that is a linear combination of three primitive gaussians. For each valence shell atomic orbital there are two basis functions, one of which is a gaussian-type function that is a linear combination of two gaussian primitive functions and one which is a single primitive gaussian. By using these gaussian-type functions as a combination of primitive gaussians, the number of variables can be reduced which gives large savings in computational time [20]. The energy of the system in this approximation can be expressed as,

$$E_{HF} = E_{NN} + E_{eN} + E_{ee} + E_{ex}$$

where the items correspond to the classical coulomb interaction between nuclei, electron-nuclei, electron-electron and exchange interaction respectively.

The energies calculated by the Hartree-Fock method differ from experimentally obtained values by typically 1% . The origin of this discrepancy lie in the way the Hartree-Fock SCF wave function takes into account the interactions between electrons.

Since electrons repel each other, they tend to keep out of each other's way. In the case of helium, if one electron is close to the nucleus at a given instant, it is energetically more favourable for the other electron to be far from the nucleus at that instant. This indicates that the motions of electrons are correlated and it is necessary to introduce this correlation into the wave function. The Hartree-Fock wave function does have some electron correlation built in, as the function satisfies the antisymmetric requirements of the Pauli principle.

2.6.3. Density functional theory

The density functional theory (DFT) method is an attempt to obtain information about electronic properties not through the calculation of the wave functions but through the electron probability density $\rho(x,y,z)$. In 1964 Hohenberg and Kohn proved that the ground state molecular energy, wave function, and all other molecular electronic properties are uniquely determined by the electron probability density $\rho(x,y,z)$ [21]. The formalism says that the ground state energy E_0 is a functional of $\rho(x,y,z)$ and can be expressed as $E_0=E_0[\rho(x,y,z)]$. The functional relation associates a number with the function ρ, and therefore by knowing the ground state electron density it is possible to calculate all the ground state electron properties. However, the determination of this electron density requires the calculation of the wave functions obtainable through the Hartree-Fock SCF method (note that in strict HF calculations the electron density was obtained *after* calculating the wave functions φ). The current density functional theory methods have been developed in conjuction with Hartree-Fock calculations to construct the electron density matrix with Hartree-Fock wave functions. The DFT includes all exchange and correlation effects although, the main problem is the determination of the correct functional $E_x[\rho(x,y,z)]$ and $E_c[\rho(x,y,z)]$ respectively for different molecules.

If ρ varies slowly with position it can be shown that the exchange functional $E_x[\rho(x,y,z)]$ can be written as,

$$E_x[\rho] = \int \rho(x,y,z)\varepsilon_x(\rho)dxdydz$$

where the integral is over all space and ε_x is the exchange energy per electron in a homogeneous electron gas with electron density ρ. However in a molecule, the positive charge is not uniformly distributed but located only at the nuclei. Therefore, ρ varies rapidly in a molecule and the expression above is an approximation called local density approximation (LDA). An improved version of this LDA is called local spin density approximation (LSDA) and it uses different densities ρ^{α} and ρ^{β} for electrons with different spins [21]. A further non-local gradient correction to this functional was introduced by the Becke 88 functional [22].

In the case of correlation functionals, Vosko, Wilk and Nusair developed the VWN functional [23] based on local density correlations in the uniform electron gas. A further development of this functional is the LYP, which corrects the non-local correlations [24].

The cluster calculations described in this thesis have been carried out using the B3LYP functional, which has frequently given best results in molecular geometry optimizations and vibrational frequency computations [25-26]. This functional includes a combination of two corrections, the Becke 88 and the LYP, which are in this case described by three parameters, A, B, C. The use of parameterised functionals results in significant reduction of computational time.

2.7. References

[1] J.L. Solomon, R.J. Madix, J. Stohr. Surface Science 255 (1991) 12-30

[2] A. Golzhauser *et al.* Surface Science 334 (1995) 235-247

[3] Taborski J., Vaterlein P., Dietz H., Zimmermann U., Umbach E. Journal of Electron Spectroscopy and Related Phenomena 75 (1995) 129-147

[4] M.J. Kone, A.V. Teplyakov, J.G. Lyubovitsky, S.F. Bent. Surface Science 411 (1998) 286-293

[5] T. Okajima *et al.* Journal of Physical Chemistry a 102 (1998) 7093-7099

[6] G. Polzonetti *et al.* Journal of Electron Spectroscopy and Related Phenomena 99 (1999) 175-187

[7] R.E. Palmer, P.J. Rous. Reviews of Modern Physics 64 (1992) 383-440

[8] T. Tsuruoka *et al.* Surface Science 428 (1999) 257-261

[9] H. Ikeda *et al.* Applied Surface Science 117 (1997) 109-113

[10] B.G. Frederick, Q. Chen, F.M. Leibsle, S.S. Dhesi, N.V. Richardson. Surface Science 394 (1997) 26-46

[11] B.G. Frederick *et al.* Surface Science 394 (1997) 1-25

[12] Y. Nakagawa, M. Higashi, H. Ikeda, S. Zaima, Y. Yasuda. Applied Surface Science 132 (1998) 192-196

[13] C. Gregoire, L.M. Yu, F. Bodino, M. Tronc, J.J. Pireaux. Journal of Electron Spectroscopy and Related Phenomena 99 (1999) 67-82

[14] W.P. Mckenna, G. Apai. Journal of Physical Chemistry 96 (1992) 5902-5907

[15] H. Ibach, D.H. Mills. Electron Energy Loss Spectroscopy and Surface Vibrations. Academic Press Inc. (1982)

[16] H. Ibach, H. Wagner, D. Bruchmann. Solid State Communications 42 (1982) 457-459

[17] C.R. Brundle, C.A. Evans, S. Wilson. Encyclopedia of Materials Characterization, Butterworth-Heinemann (1992) 282-292

[18] K. Siegbahn, L. Karlsson. Photoelectron Spectroscopy, Springer, Berlin (1982)

[19] G. Binnig, H. Rorher, C. Gerber, E. Weibel. Physical Review Letters 49 (1983) 120

[20] Levine I. N. Quantum Chemistry-4th ed. Prentice Hall, Inc. New Jersey (1991) 549-579

[21] T. Hohenberg, W. Kohn. Physical Review 136 (1964) B864

[22] A.D. Becke. Physical Review A 38 (1988) 3098

[23] S.H. Vosko, L. Wilk, Nusair M. Canadian Journal of Physics 58 (1980) 1200

[24] C. Lee, W. Yang, R.G. Parr. Physical Review B 37 (1988) 785

[25] H. Lampert, W. Mikenda, A. Karpfen. Journal of Physical Chemistry 101 (1997) 2254

[26] R. Konecny, D.J. Doren. Surface Science 417 (1998) 169-188

CHAPTER 3.

The adsorption of maleic anhydride on Si(100)-2x1

3.1. Introduction:

The increasing use of organic films in a great number of technological applications has motivated several investigations regarding the coupling of organic molecules with semiconductor substrates [1]. The ability of these molecules to modify the chemical, physical and electronic properties of the interface makes them interesting for a wide range of technological applications. The silicon surface is of special interest in the microelectronics industry and great progress has been achieved in fields like thin film displays, lithography and molecular electronics. Further investigations on nano-structuring of electronic devices and sensor technology, demand a more complete understanding of the chemistry of organic molecules on silicon substrates.

Recent investigations have shown that highly ordered organic monolayer films can be formed on Si(100) [1-4]. The adsorbed molecules, if appropriately functionalised, can subsequently be used as controlled bonding sites for linking other organic substituents [2]. STM studies, have shown that bonding of cyclopentene on Si(100)-2x1 results in a highly ordered monolayer, which ordering can be extended to multilayer films [4]. Since the molecule bonds to the surface through a di-σ configuration, via a 2+2 cycloaddition, a strong covalent Si-C bond with its consequent directional character is formed, and the chemisorbed molecules are oriented with respect to the silicon dimers. Further orientation of the overlayers can be achieved by interadsorbate interactions and molecular packing.

3.2 The molecular layer deposition technique:

An improved control of the film growth is provided by the use of molecular layer deposition (MLD). In this technique, which is schematically shown in Fig 1, the selective and sequential reaction of functional groups is exploited. In a first step, a molecule A is

chemisorbed on the substrate until saturation is achieved. Excess molecules are desorbed by heating the substrate since the interaction between molecules A is weak relative to the chemical bond formed between molecule A and the substrate. In the next step, molecule B is dosed on the substrate and chemically couples to molecule A. Afterwards, the surface might be exposed to molecule C. By repeating this process, a polymer film with an {A-B-C-} structure can be produced. This technique also, in principle, allows one to tailor the optoelectronic and dielectric properties of a polymer film by the introduction of other molecules with appropriate functionalities in the polymer chain.

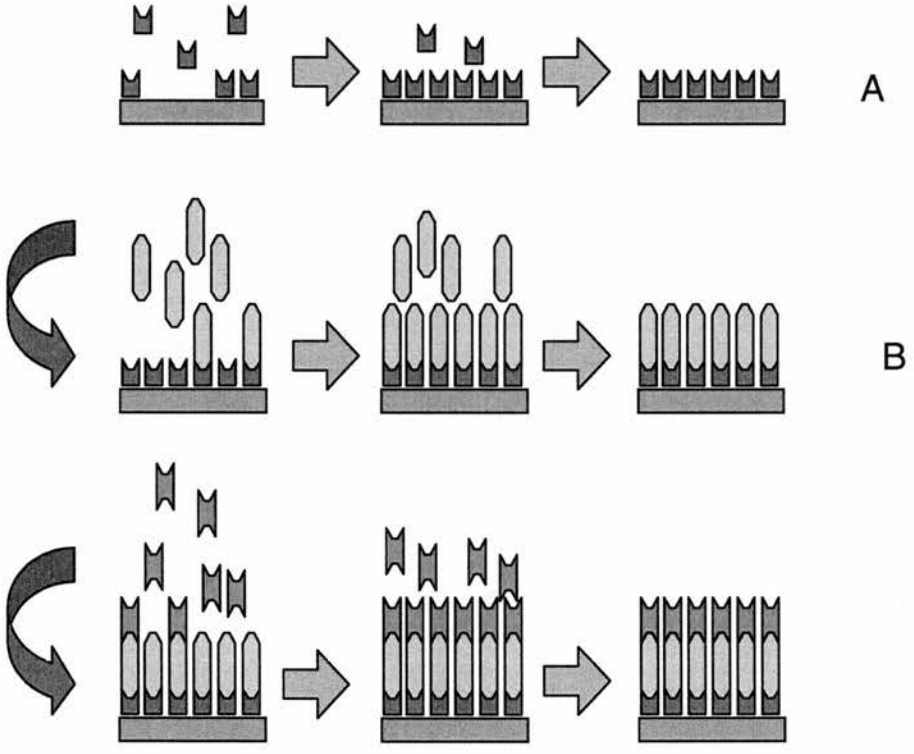

Fig 1. Schematic of the molecular layer deposition (MLD) technique.

Bitzer et. al.[5] have recently achieved the growth of thin polymide films on Si(100)-2x1 using the molecular layer deposition technique. The authors report the controlled growth of an alternating structure of phenylene diamine (NH_2-C_6H_4-NH_2) (PDA), and pyromellitic dianhydride (C_2O_3-C_6H_2-C_2O_3) (PMDA) layers. The sequential formation of this polymide can be seen in Fig 2. First, the Si(100)-2x1 surface was functionalised by the adsorption of **maleic anhydride** at room temperature which has

been proposed to chemisorb through the olefin bond [1]. Then, in step 2 phenylene diamine (PDA) couples to the chemisorbed maleic anhydride species through an anhydride ring opening reaction. In step 3, pyromellitic dianhydride (PMDA) reacts with the amino functionalised surface.

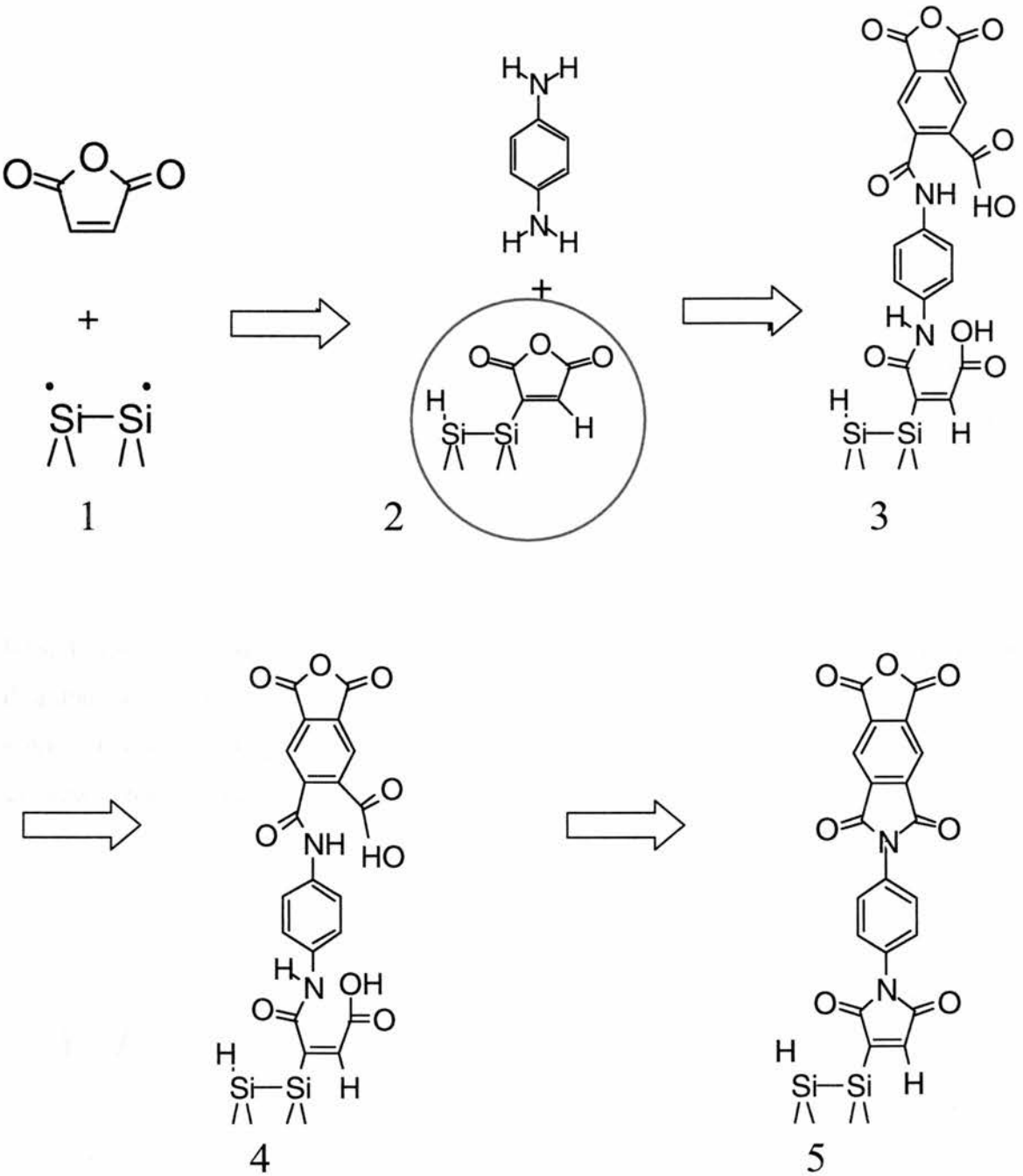

Fig. 2. Growth of polymide films on Si(100)-2x1 using maleic anhydride as film/substrate interface.

Further film growth is accomplished by the sequential exposure to PDA and PMDA, respectively. Imidisation of the film is achieved in step 5 by curing at 400° C . However, the film integrity depends crucially on the structure of the maleic anhydride film/Si(100)-2x1 interface.

In order to characterise this interface, we have studied the adsorption of maleic anhydride on Si(100)-2x1 using XPS, LEED, NEXAFS, HREELS and STM. *Ab initio* calculations have been carried out to assist the interpretation of the NEXAFS data. We observe that at low coverages the adsorption occurs mainly through cycloaddition of the C=C bond to the dangling bonds of Si-Si dimers, analogous to the behaviour of ethene, cyclopentene, pyrroline, etc [3-4-6-9]. The Si-Si dimer bonds are not cleaved in the chemisorption, process as the continued observation of a 2x1 pattern in low energy electron diffraction (LEED) shows. In the NEXAFS spectra, the absence of a π^* resonance associated with the C=C bond, confirms the rehybridisation of the carbon atoms in the olefin bond. The angular dependence of the resonance intensity indicates a molecular plane inclination of 48° relative to the substrate plane. At higher dosages, chemisorbed maleic anhydride species, are bonded to the Si surface atoms via a single Si-C linkage with retention of the C=C double bond. In this case, the dissociated hydrogen bonds to one of the neighbouring Si dimer atoms.

3.3 Experimental:

The experiments were carried out in three different UHV chambers with a base pressure in the low 10^{-10} mbar regime. The NEXAFS experiments were performed at the HE-TGM2 beam line at BESSY I (Berlin, Germany). The spectra were recorded at monolayer and multilayer coverages. Multilayer formation was achieved by condensing maleic anhydride on the l-N_2 cooled manipulator shaft made of copper. The multilayer spectra were recorded at the magic incidence angle ($\theta=55^\circ$), while the monolayer spectra were recorded at 30° and 90° incidence angles.

The NEXAFS data has been normalised by dividing the transmission spectra of clean Si(100)-2x1 and fitting the part before the absorption features by a straight line, taking this as zero and assuming as unity the signal far beyond the σ resonances. Correction of the storage ring current has been performed using a gold grid monitor at the entrance of the UHV chamber. The photon energy was calibrated using the carbon K-edge on the peak at 284.7 eV of contaminant carbon adsorbed on the gold grid.

The HREELS spectra were recorded at 8 eV kinetic energy of incident electrons and in the specular direction ($\theta_i=\theta_f=45°$). The spectrometer (VSW-HIB 1000) was tuned to 35 cm^{-1} in the straight through position. Samples sized 17 x 6 mm^2 cut from n-type Si (100) wafers with a resistivity of 500 Ωcm were mounted on a sample carrier with Ta clips. In order to facilitate resistive heating of the samples for oxide removal, these were coated with a thin platinum layer at the back. Oxide removal was confirmed after heating to approximately 1200 K and observing the oxide desorption peak. The cleanliness of Si(100)-2x1 was confirmed in both, HREELS and NEXAFS, by the absence of oxide or contaminant features. XPS spectra of multilayers of maleic anhydride were recorded at liquid nitrogen temperatures with a pass energy of 20 eV using a hemispherical analyser. The energy scale was calibrated using the carbon contamination peak at 284 eV. The peak positions were used to determine the energy of the C1s atomic levels and assist in the interpretation of the NEXAFS data.

STM experiments were carried out in an ultra high vacuum system (base pressure $<10^{-10}$ mbar) equipped with an Omicron STM. Tungsten tips used in the STM analysis were prepared by an electrochemical etching technique. Samples were cut from wafers (P doped) polished on both sides with a resistivity of 1-3 Ωcm. Clean Si(100)-2x1 was prepared by heating the silicon crystal to 1400 K. The pressure did not exceed $2x10^{-10}$ mbar during oxide removal. The filled state STM images were taken at a tunneling current of 0.2 nA and a sample bias of –2.0V. The experiments were carried at room temperature.

Maleic Anhydride (Aldrich 99% purity) was admitted into UHV through a leak valve. Prior to the experiments, maleic anhydride was purified by several cycles of sublimation and pumping.

3.4. Results:

3.4.1. HREELS results.

Following the exposure of Si(100)-2x1 to 2L maleic anhydride, sharp 2x1 spots could still be observed in the low energy electron diffraction (LEED) pattern. Although coincidentally maleic anhydride might give rise to a 2x1 overlayer on Si(100), the retention of the 2x1 LEED pattern is taken as indicating the preservation of the surface reconstruction.

The HREELS spectra of maleic anhydride adsorbed on Si(100)-2x1 have been recorded at low and high coverages. Fig. 3 shows the on-specular HREELS spectra of Si(100)-2x1 exposed to (a) 2 L and (b) 10 L of maleic anhydride at room temperature. All the features observed in the vibrational spectra have been assigned by comparison with our *ab initio* calculations which will be described in detail in section 3.4.4. Table 1. shows the frequency assignment of the observed features by comparison with our *ab initio* calculations. In the lower spectrum the features at 2990 cm^{-1} and 3070 cm^{-1} can be attributed to ν_{as} (C-H) and ν_s (C-H) stretching modes of sp^3 hybridised carbon atoms respectively. The loss peaks at 1619 cm^{-1} and 1775 cm^{-1} are related to the ν(C=C) and the ν_s(C=O) stretching modes respectively. The β(C-H) bending vibrations give rise to the features observed at 1313 cm^{-1}, 1212 cm^{-1} and 1080 cm^{-1} respectively. The anhydride ring modes gives rise to the peaks observed at 960 cm^{-1} and 614 cm^{-1} respectively. Additional β(CH) bending vibrations can be observed at 790 cm^{-1} and 480 cm^{-1} respectively. The features at 1080 cm^{-1} and 790 cm^{-1} are attributed to out of plane (C-H) vibrations. At a dosage of 10 L maleic anhydride (curve b), new features appear in the spectrum. The strong intensity at 3147 cm^{-1} is attributed to a ν_{as} (C-H) stretching mode of sp^2 hybridised carbon atoms. The ν(SiH) stretch is now observable at 2128 cm^{-1}.

At low coverages, fig 3 (a), maleic anhydride chemisorbs on Si(100)-2x1, primarily through a rehybridisation from sp^2 to sp^3 of the carbon atoms in the olefin bond. Bonding of maleic anhydride to the silicon dimers via a [2+2]-cycloaddition reaction is consistent with the absence of a ν(SiH) stretching mode at 2128 cm^{-1}. However, the ν (C=C) observed at 1619 cm^{-1} indicates that a minority of species are bonded through cleavage of the hydrogen bond. Increasing the dosage, fig 3 (b), results in an increased ν(C=C) intensity and the appearance of a distinctive Si-H stretching mode at 2128 cm^{-1}. These suggest an increase in the number of molecules bonded through a single Si-C linkage with retention of the C=C bond after C-H cleavage.

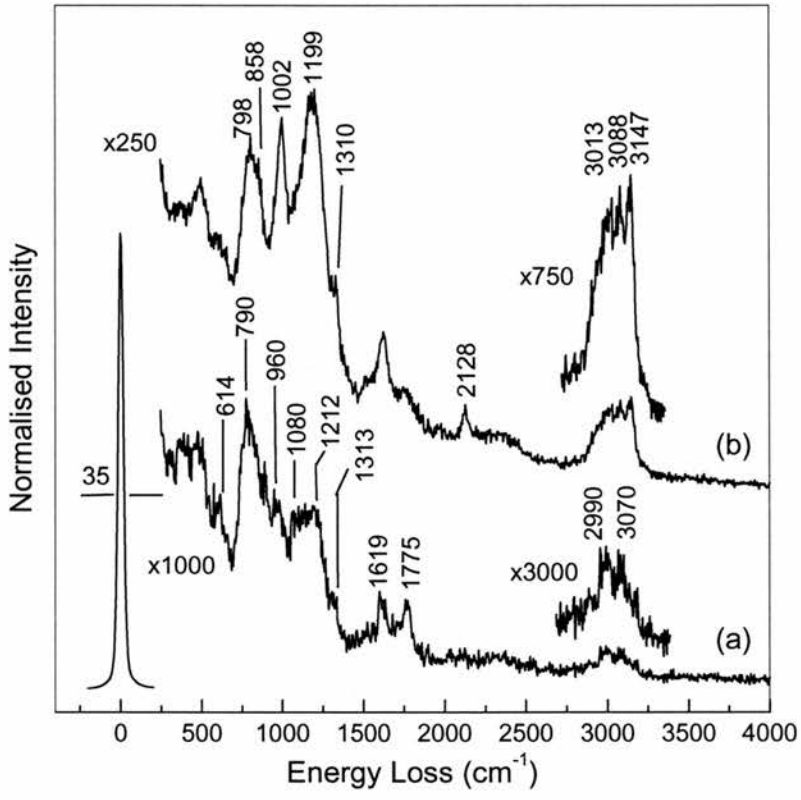

Fig 3. HREELS spectra of Si(100)-2x1 exposed to (a) 2 L and (b) 10 L maleic anhydride.

In this adsorption geometry, the carbon atoms in the olefin bond retain their sp^2 hybridisation. The band observed at 3147 cm^{-1}, characteristic for sp^2 hybridised carbon atoms, supports this adsorption model. It is expected that the cleaved hydrogen atom

most likely saturates the adjacent dimer, giving rise to the Si-H stretching vibration at 2128 cm^{-1}.

GAUSSIAN 98 (cm^{-1})	2L Maleic anhydride	10L Maleic anhydride	Assignment
	HREELS (cm^{-1})		
-	-	3147	ν_s(C-H)
3010	3070	3088	ν_s(C-H)
2995	2990	3013	ν_{as}(C-H)
2040	-	2128	ν(Si-H)
1757	1775	1760	ν_s(C=O)
1694	-	-	ν_{as}(C=O)
-	1619	1620	ν(C=C)
1295	1313	1310	β(C-H)
1253	1212	1200	β(C-H)
1076	1080	1098	β(C-H)
985	960	1002	Ring(C-C)
844	-	858	Ring (C-O)
763	790	798	β(C-H)
608	614	614	Ring (C-O)
514	480	495	β(C-H)

Table 1. Frequency assignments of calculated modes in the spectra of Si(100)-2x1 exposed to 2 L maleic anhydride.

3.4.2. NEXAFS results.

Fig 4 shows the C 1s NEXAFS spectra of Si(100)-2x1 exposed to 2L of maleic anhydride recorded at 30° (a) and 90° (b) incidence angles, and multilayers of maleic anhydride (c). The multilayer results are presented in table 2, together with assignments based on our *ab initio* calculations of an isolated molecule. The transitions are also displayed in fig 8. In the multilayer case, the sharp π^* resonance observed at 284.0 eV, is assigned to transitions from the C1s level in the olefin bond, into the lowest unoccupied molecular orbital (LUMO). The resonance observed at 287.8 eV in spectrum (c) has contributions from transitions from the C1s levels in the olefin bond into the LUMO+1, and transitions from the C1s level of the carbon atoms in the anhydride ring into the

LUMO (see figure 8). The assignment of all the π-related features observed in the NEXAFS spectrum is given in table 2.

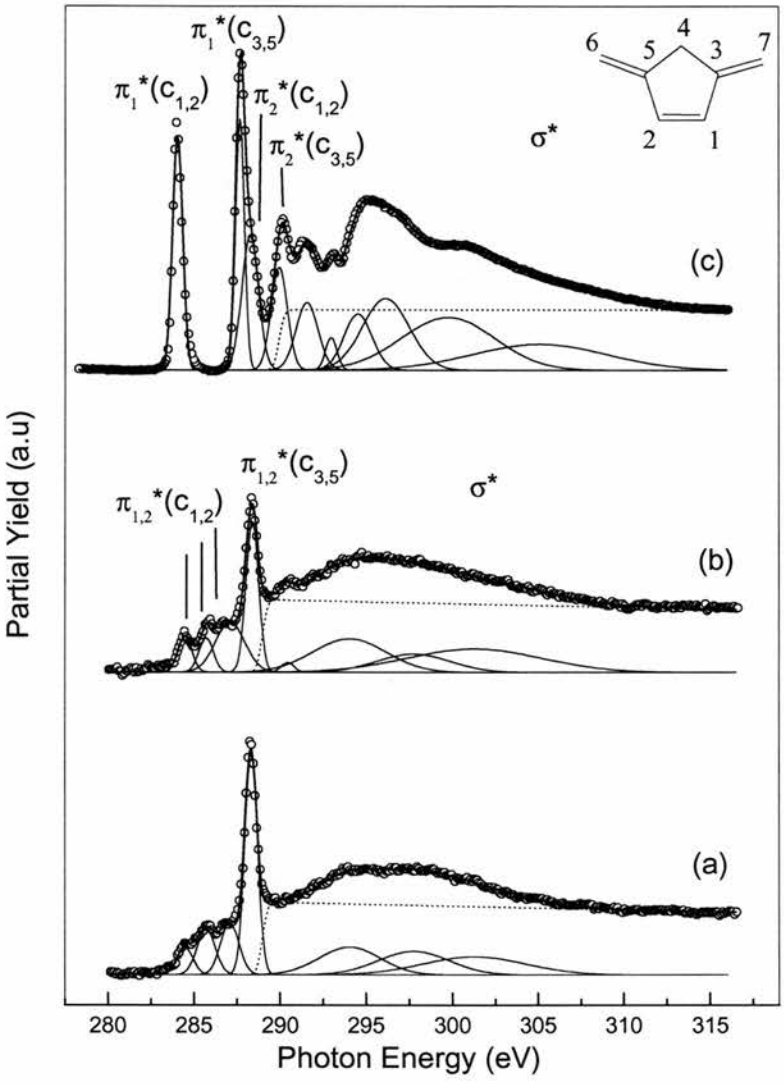

Fig 4. C 1s NEXAFS spectra of multilayers maleic anhydride (c) and monolayer recorded at 30° (a) and 90° (b) incidence angles.

The sharp π* resonance observed at 284.0 eV in spectrum (c) is absent in the spectra (a) and (b). Additionally, these spectra show an intense π* resonance at 288.3 eV. By comparison with our *ab initio* results, we attribute this feature to transitions from the C1s (C=O) levels into the LUMO (see fig 8). In the lower energy range of spectra (a) and (b), low intensity features are present at 284.4 eV, 285.7eV and 287.0 eV. According to our calculations, we tentatively assign these resonances to transitions from the C1s (C-Si)

levels into the first unoccupied molecular orbitals of the chemisorbed species. An analysis of the intensities of the π^* resonance at 288.3 eV gives an intensity ratio of 0.67 for normal to grazing incidence angles. From this ratio we calculate a polar tilt angle α between the molecular plane and the surface plane of 48°±3°. Fig 5 shows the comparative O1s NEXAFS spectra of Si(100)-2x1 exposed to 2L of maleic anhydride recorded at (a) 30° and (b) 90° incidence angles, and (c) multilayers of maleic anhydride. Assignments of the major features observed in the spectrum are given in table 2. The intensity ratio for normal and grazing incidence is 0.86, which gives a polar tilt angle of 51°±3°.

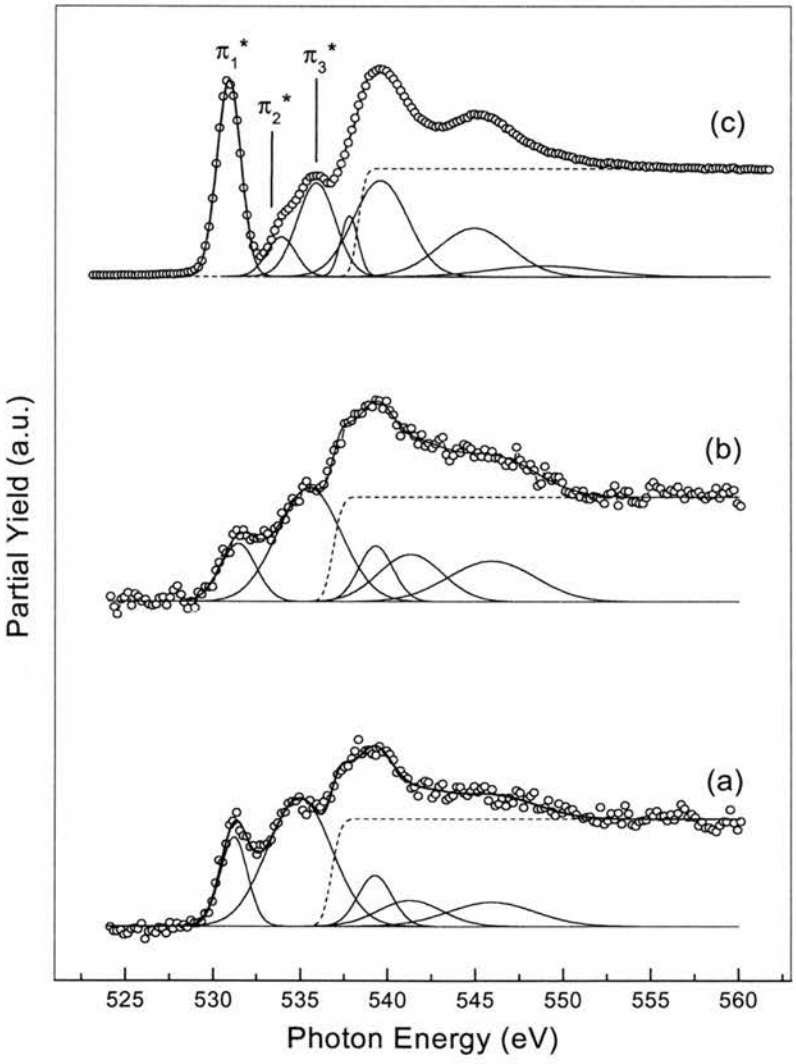

Fig 5. O 1s NEXAFS spectra of multilayers maleic anhydride (c) and monolayer recorded at 30° (a) and 90° (b) incidence angles.

The assignments of the features observed in the C1s and O1s NEXAFS spectra are given in table 2. The values displayed are referred to the lowest transition, which in the case of the C1s spectra is the C1s(C=C)->π^*_1 transition.

	Multilayers transitions	Using GAUSSIAN	Observed in NEXAFS
Carbon Edge	$\pi^*_1(C_{1,2})$	0.0	0.0
	$\pi^*_1(C_{3,5})$	3.7	3.7
	$\pi^*_2(C_{1,2})$	3.8	3.7
	$\pi^*_2(C_{3,5})$	7.5	7.6
	$\pi^*_3(C_{1,2})$	4.6	4.2
	$\pi^*_3(C_{3,5})$	8.3	9.0
Oxygen Edge	$\pi^*_1(O_{6,7})$	0.0	0.0
	$\pi^*_2(O_{6,7})$	3.7	3.7
	$\pi^*_3(O_{6,7})$	4.6	5.0

Table 2. Relative energies of C1s and O1s to π^* transitions of multilayer maleic anhydride.

3.4.3. XPS results.

The relative position of the C1s levels of multilayers maleic anhydride has been studied using XPS. Figure 6 shows the XPS spectrum of multilayers maleic anhydride.

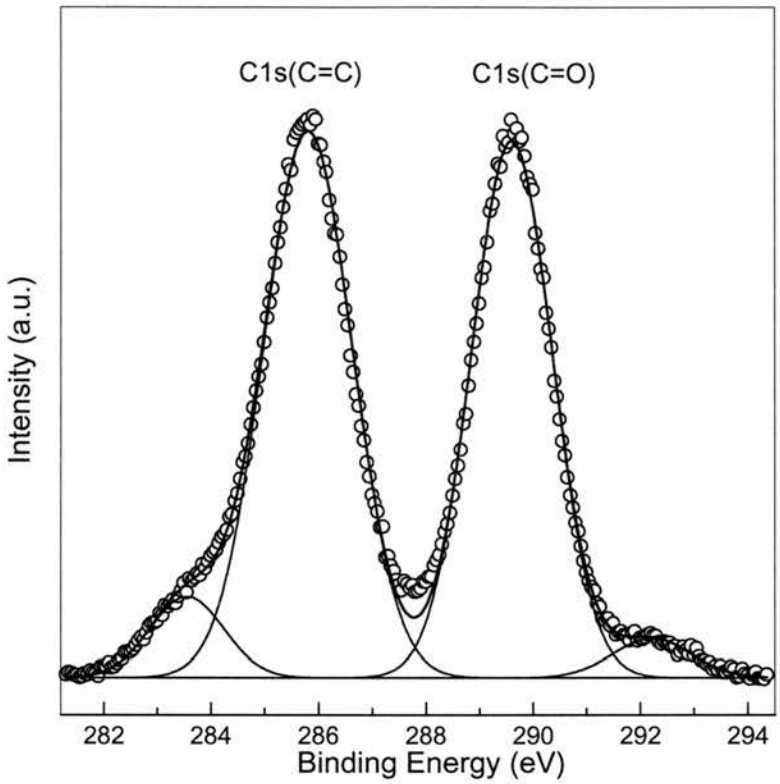

Fig 6. XPS of multilayers maleic anhydride condensed on the manipulator shaft.

The determination of the C1s(C=C) and C1s(C=O) levels has been essential for the understanding of the NEXAFS spectra. The XPS spectrum shows two photoemission peaks at 285.7 eV and 289.6 eV, which are attributed to olefin and carbonyl bonds C 1s levels respectively. Note that the energy separation is crucial for the interpretation of NEXAFS data since electrons are excited from both atomic orbitals into unoccupied π^* levels.

3.4.4. Ab initio calculations:

Ab initio methods have been used to model the unoccupied molecular orbitals and simulate the vibrational spectrum to assist the interpretation of the NEXAFS and

HREELS data. The cluster calculations have been performed using the GAUSSIAN 98 software [10] under the *b3lyp* functional and 6-31G basis set. Initially, we have calculated the geometry and frequencies of undisturbed maleic anhydride in order to validate the used approximations. The geometry optimisation predicts a molecular structure, which is in good agreement with the reported data in the literature [11-14]. By comparison with previously published vibrational spectra of undisturbed maleic anhydride [12-13], all calculated frequencies have been scaled by a factor of 0.96. In a reasonable approximation the multilayer regime can be considered as free molecules since the intermolecular forces are sufficiently weak to introduce only a minor perturbation in the electronic and vibrational structure. The monolayer regime was modelled as one maleic anhydride molecule interacting with a silicon cluster as described in fig 7.

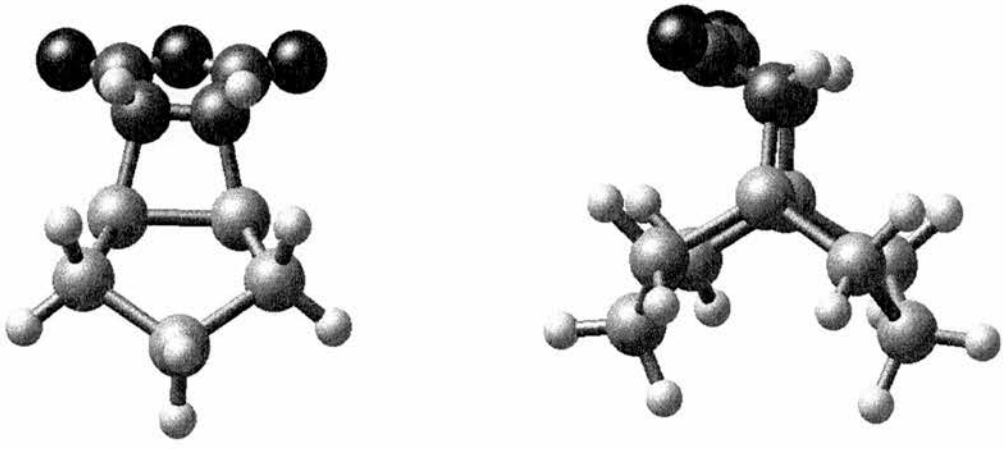

Fig 7. Side views of the optimised maleic anhydride/Si(100)-2x1 cluster.

The optimisation procedure was carried out in two stages. Firstly, a Si_8H_{12} cluster consisting of eight-silicon atoms with all bonds saturated with hydrogens was fully optimised. Secondly, the maleic anhydride molecule was adsorbed on the dimer and the geometry of the silicon/hydrogen cluster was frozen during the optimisation. In justification for the use of a symmetric dimer cluster it is important to note that, although the experimental observation of buckling dimers on clean Si(100)-2x1 has been widely reported in the literature [15] this has not been observed even for the hydrogen terminated surface [16]. Therefore, in principle, there is no reason to assume asymmetric dimers in

the presence on maleic anhydride [17]. The geometry optimisation predicts a polar tilt angle of 30° relative to the surface plane (see fig 7). Following the geometry optimisation, the vibrational frequencies were calculated via computation of the force constants. Table 1. showed the calculated frequencies in comparison with those obtained from the vibrational spectra of Si(100)-2x1 exposed to 2 L and 10 L maleic anhydride respectively.

Fig 8. shows the π^* orbitals, their symmetries and relative energies, in the ground state of the free molecule (multilayer), and cluster (monolayer) as determined by the GAUSSIAN 98 calculations. Additionally, the expected transitions from C1s and O1s levels to empty π^* levels are shown. The splitting of the carbon 1s levels has been obtained from shown XPS data.

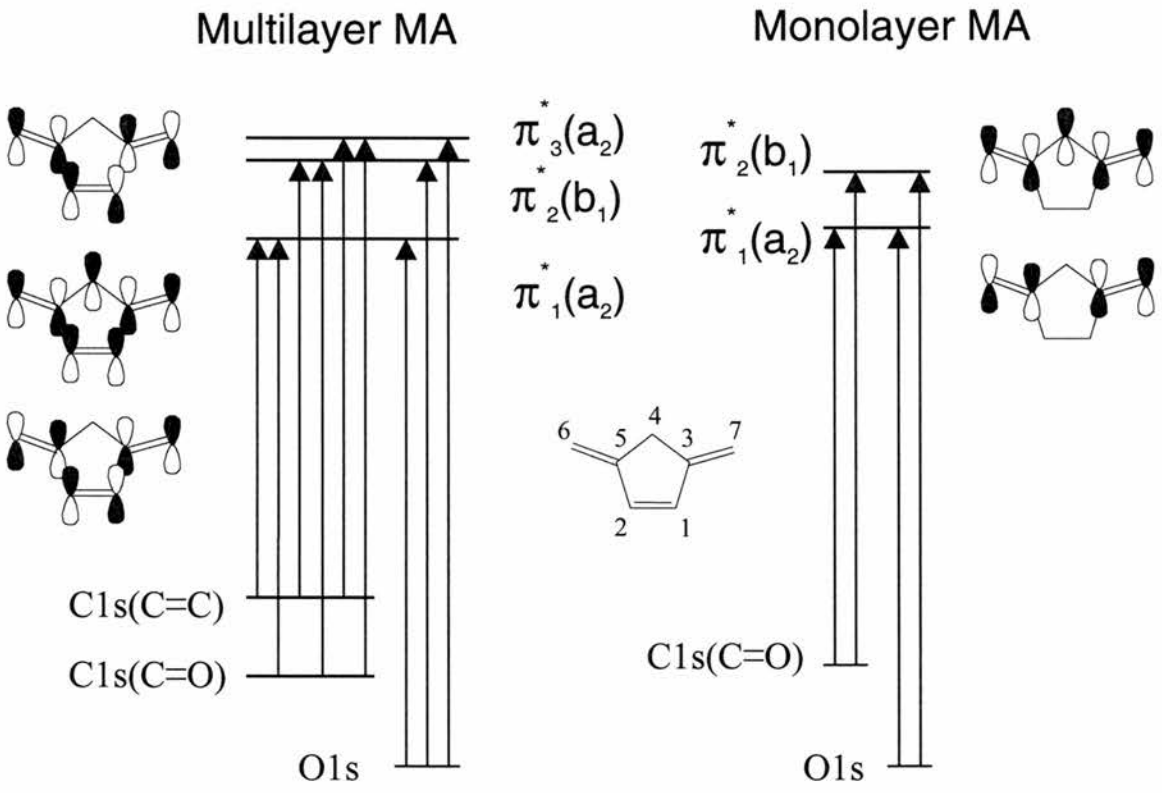

Fig 8. Schematic of allowed transitions from C1s and O1s atomic levels into unoccupied molecular orbitals according to the ab initio results. The contributions from atomic p_z atomic orbitals to the π^* levels is also shown. The figure displays the situation in the monolayer and multilayer regimes.

In the multilayer case, the LUMO was found to have a contribution from all the atoms in the anhydride ring. On the other hand, the LUMO of the cluster has a strong contribution from the Si dimer atoms, although this contribution is weaker in the upper molecular orbitals. In addition, the transitions shown for the cluster are exclusively from C1s and O1s levels into unoccupied maleic anhydride molecular orbitals, having no contribution from Si atoms. It should be noted that the olefin bond C1s atomic levels are absent in the chemisorbed species. According to the calculations, the molecular orbitals shown have contributions from carbon and oxygen atoms in the (C=O) bond. Note that transitions from the C1s (C-Si) levels into those unoccupied molecular orbitals are forbidden since these orbitals have no overlap with the C1s levels of C-Si bonds.

3.4.5. Scanning tunneling microscopy (STM)

In this section, we present STM studies of the initial adsorption of maleic anhydride on Si(100)-2x1. In particular, we are interested in the identification of maleic anhydride adsorption sites at low and high coverages and the local rearrangements of silicon dimers after adsorption.

Fig 9 shows the filled state image of 0.03 L maleic anhydride chemisorbed on Si(100)-2x1. The two domains of symmetric silicon dimers rotated 90° are clearly visible separated by one single height atomic step. Note the zig zag rows of asymmetric dimers at the step edges and around the surface defects. This is mainly due to pinning of the silicon dimer by defects that "freezes" the asymmetric structure and spreads along dimer rows. The maleic anhydride molecules appear as bright objects located mainly *between* dimer rows. This adsorption site for maleic anhydride molecules is also predominant at higher coverages. Fig 10 shows the STM image of clean Si(100)-2x1 exposed to 0.12 ML maleic anhydride. It is clearly observed that more 98% of maleic anhydride molecules adsorbed on inter-dimer sites. Again, the image shows the lack of preferential adsorption of maleic anhydride on defect sites.

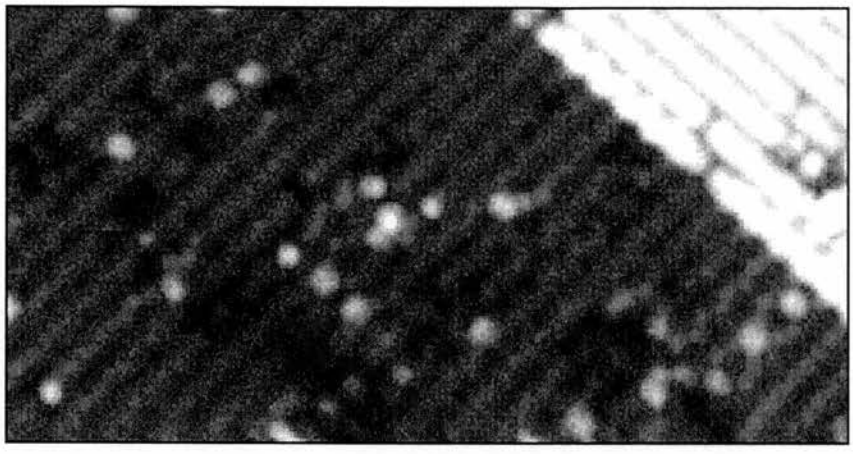

Fig 9. Filled state STM image of maleic anhydride adsorbed on Si(100)-2x1. Maleic anhydride molecules are seen as bright protrusions. The brighter area in the top-right corner corresponds to the elevated adjacent silicon terrace.

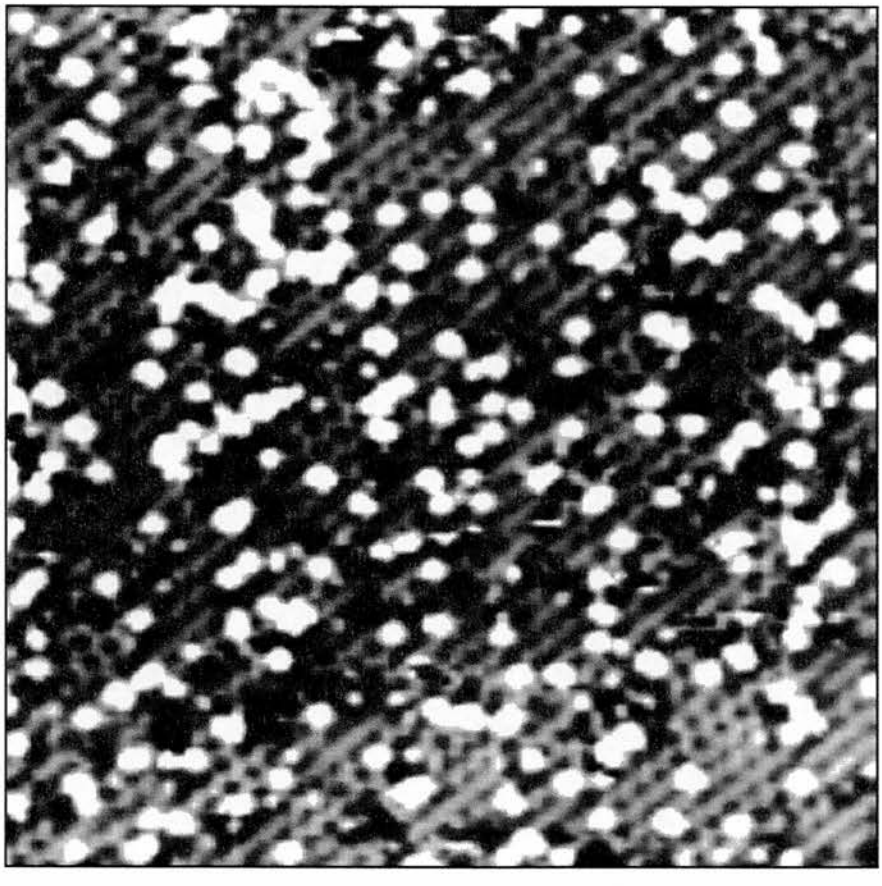

Fig 10. STM image of Si(100)-2x1 exposed to 0.12 ML maleic anhydride. The image is 250 Å x 250 Å. Tunneling current 0.2 nA. Sample bias –1.8 V.

Details of the adsorbed molecules are shown in fig 11 and fig 12 (a) and (b). In figs 11 the STM image shows that all molecules are located between dimer rows and that this leads to a local rearrangement of the silicon dimers. Also, note that in the proximity of the adsorption sites, zig-zag shaped asymmetric dimers are present. In this case it is the maleic anhydride molecule that pins the dimer after adsorption on Si(100)-2x1 resulting in the structure observed. The analysis of the image indicates the lack of a preferential adsorption of the molecules at the surface defects and an induced local c(4x2) local reconstruction of silicon dimers after maleic anhydride adsorption in the areas of otherwise clean silicon.

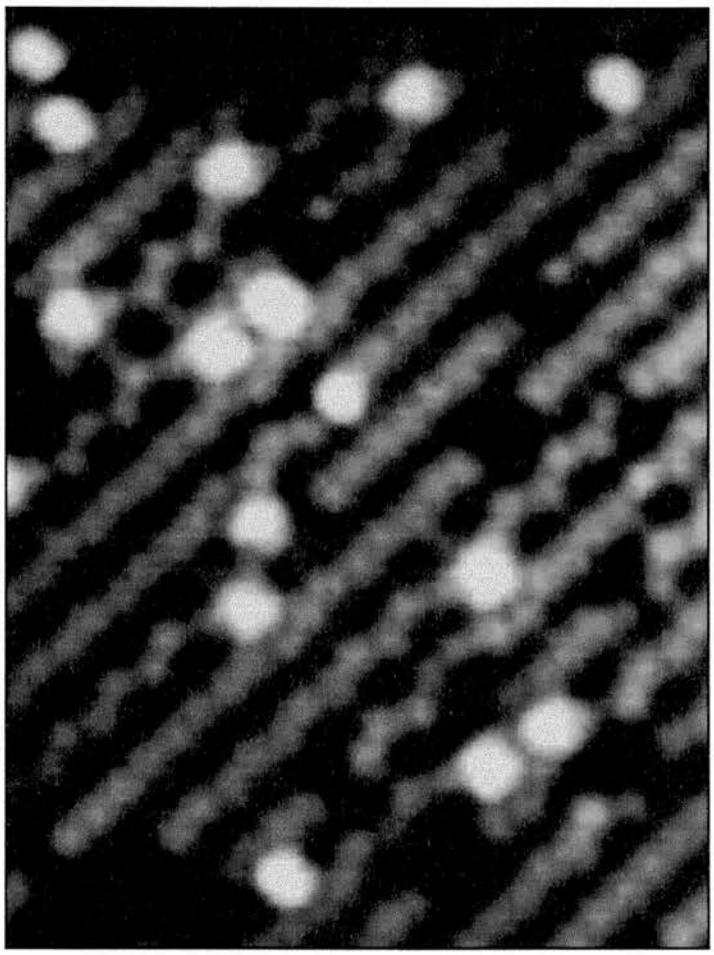

Fig 11. Details of adsorbed maleic anhydride on Si(100)-2x1. Note the rearrangement of the silicon dimers after the adsorption. The image is (79 Å x 106 Å). Tunneling current 0.2 nA. Sample bias -2.3 V.

Fig 12 shows the filled and empty state images of maleic anhydride adsorbed on Si(100)-2x1. Maleic anhydride molecules have been drawn to scale on the image to show that the adsorption site between dimer rows is suitable based on steric considerations. The radical differences between filled and empty state images must reflect the spatial distribution and symmetry of the relevant occupied and unoccupied molecular orbitals. The occupied molecular orbital must be, from the filled state image, antisymmetric since the image shows a nodal plane parallel to the dimer rows. On the other hand the unoccupied molecular orbital must be symmetric which is on good agreement with the prediction from our ab initio calculations (see fig 8). However, a complete understanding of the orbitals involved requires a more detailed modelling of the surface.

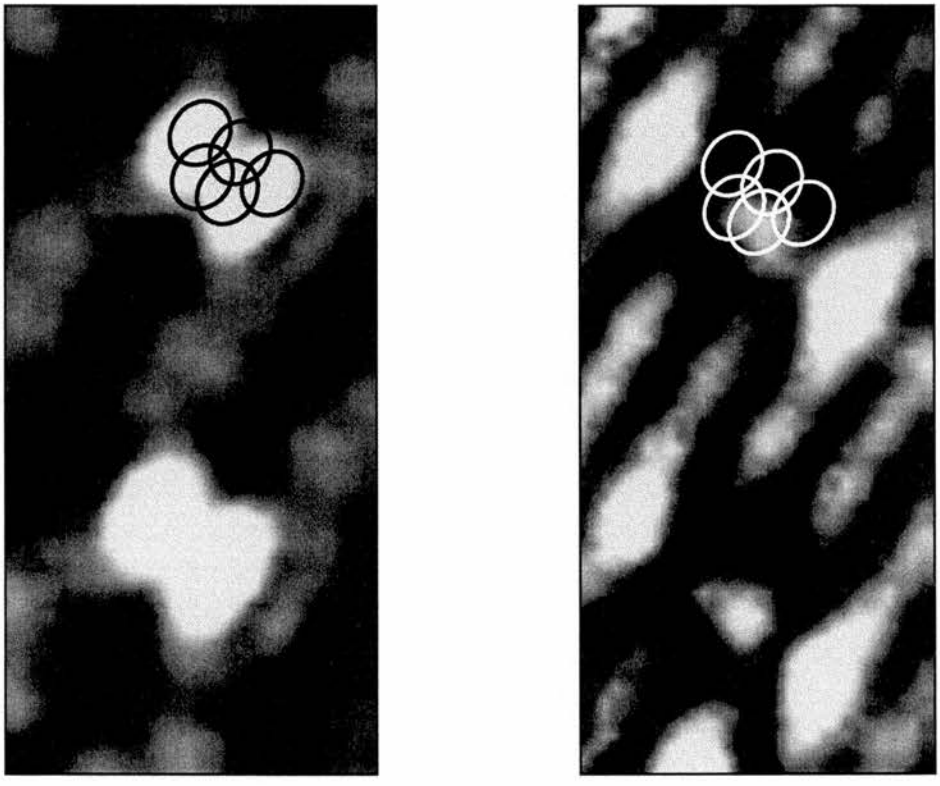

Fig 12. (a) filled and (b) empty state STM images of maleic anhydride adsorbed on Si(100)-2x1. The schematic of maleic anhydride drawn to scale is also shown on both images. The images are 18Åx37Å and were taken at a tunneling current of 0.18 nA and sample bias of (a) –1.7 V and (b) 1.5 V.

3.5. Discussion of structural models.

HREELS results show that bonding of maleic anhydride to the silicon substrate occurs at low coverages through cycloaddition to the C=C bond. At low coverages, the observation of ν_{as}(C-H) and ν_s(C-H) stretching modes at 2990 and 3070 cm^{-1} respectively, indicate that a rehybridisation of carbon atoms in the olefin bond from sp^2 to sp^3 has occurred. However, a vibrational mode at 1619 cm^{-1} due to a ν(C=C) stretch is clearly present though weak, indicating that a minority of species may bond through C-H bond cleavage. At a dosage of 10 L maleic anhydride, the strong intensity at 3147 cm^{-1} points to a significant concentration of maleic anhydride species with intact C=C double bonds on the surface. Here, the ν(Si-H) stretching mode can be seen at 2128 cm^{-1}. In both spectra, the preservation of the anhydride group can be concluded from the observation of the ring modes at 614 cm^{-1} and 960 cm^{-1} respectively. The reaction of maleic anhydride with the Si dimer through the C=O bond, would lead to the observation of a Si-O stretch which is not present in the vibrational spectra. It should be noted that the observation of the C-H vibrational modes is mainly due to impact scattering processes. In the 10L-dosage spectrum, the increase in the intensity of the C-H band is an indication for an increase in the coverage. We attribute this observed change in the bonding geometry to steric considerations. Approaching saturation coverage the number of dimers available for cycloaddition is reduced and the monodentate adsorption geometry becomes more favoured.

The NEXAFS data is consistent with these EELS results. The feature assigned to transitions from the C 1s levels in the olefin bond into the lowest unoccupied molecular orbital (π^*(C=C)) of the isolated molecule disappears upon chemisorption. The remaining strong feature in the monolayer is assigned to transitions from the C 1s levels in the carbonyl carbons into the π^*(C=O) molecular orbital. According to the *ab initio* study, new empty molecular orbitals with strong contribution from the Si atoms are formed. These give rise to the low intensity features observed in the NEXAFS spectra below the (C=O) resonance. The molecular plane tilt obtained from the polarisation dependence of the O1s NEXAFS spectrum (51°±3°) is in good agreement with that

obtained from the C 1s spectrum (48°±3°). However, a slight discrepancy arises between these and the tilt predicted by the *ab initio* method (30°). We expect maleic anhydride molecules bonded to the substrate in a di-σ configuration, to form an ordered layer that gives the observed resonance polar dependence. However the monodentate species present at the surface have, in principle, random orientation. Therefore the disagreement between the *ab initio* and experimental results may be a consequence of the influence of the minority species on the spectra. A schematic of the maleic anhydride bonded in the two adsorption geometries is given in fig 13.

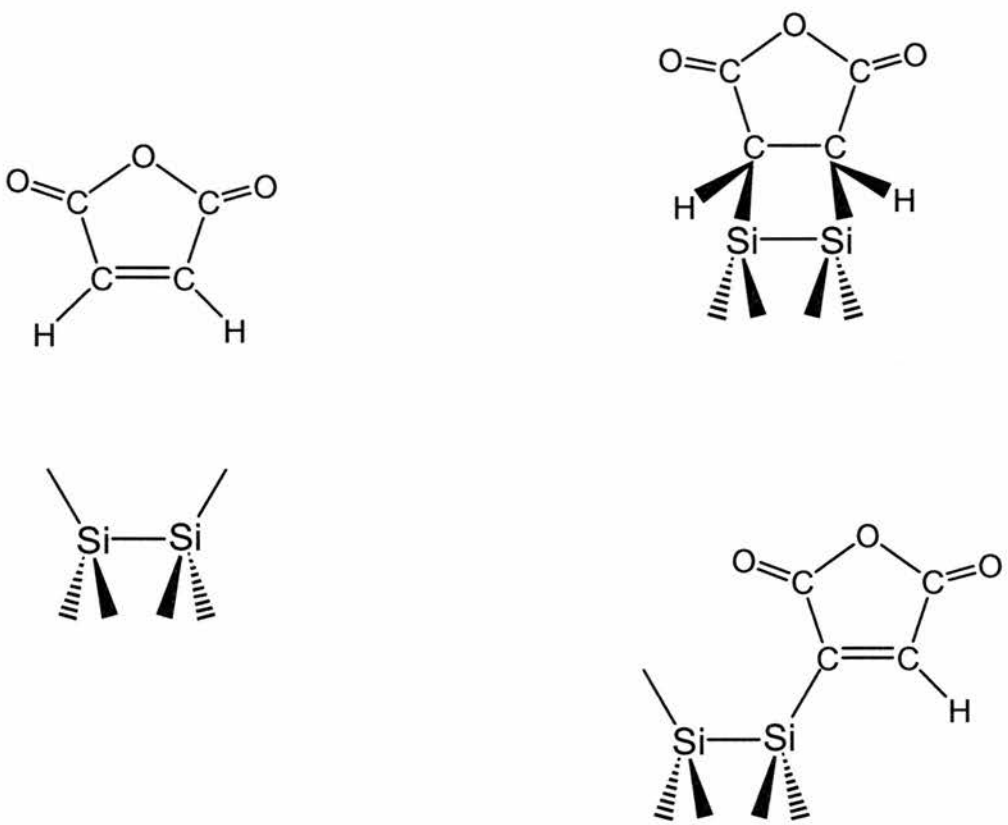

Fig 13. Two adsorption geometries based on NEXAFS and HREELS results

So far it has been assumed that maleic anhydride bonds primarily on top of the dimer. The *ab initio* calculations described above describe well the tilt angle, the molecular orbital structure and the vibrational spectrum observed in NEXAFS and

HREELS respectively. However, the STM results show clearly that at low coverages, maleic anhydride chemisorbs at room temperature almost exclusively on inter-row adsorption sites which is in contrast to previous observations of hydrocarbons on Si(100)-2x1. The detailed modelling of maleic anhydride adsorbed on inter dimer sites requires the consideration of at least three dimers. This has an impact in the number of atoms and therefore variables to compute in order to perform any geometry optimization. The computability of such a cluster is limited by the computer capacity and we have only been able to optimize this cluster at a semiempirical AM1 level. This optimization shows that by steric considerations it is necessary that Si atoms involved in the adsorption process move towards the maleic anhydride molecule. This causes the lengthening of Si dimer bonds although the 2x1 reconstruction is preserved after the molecule adsorption. Fig 14 shows the schematic of maleic anhydride molecules adsorbed on inter-dimer sites in a buckled surface.

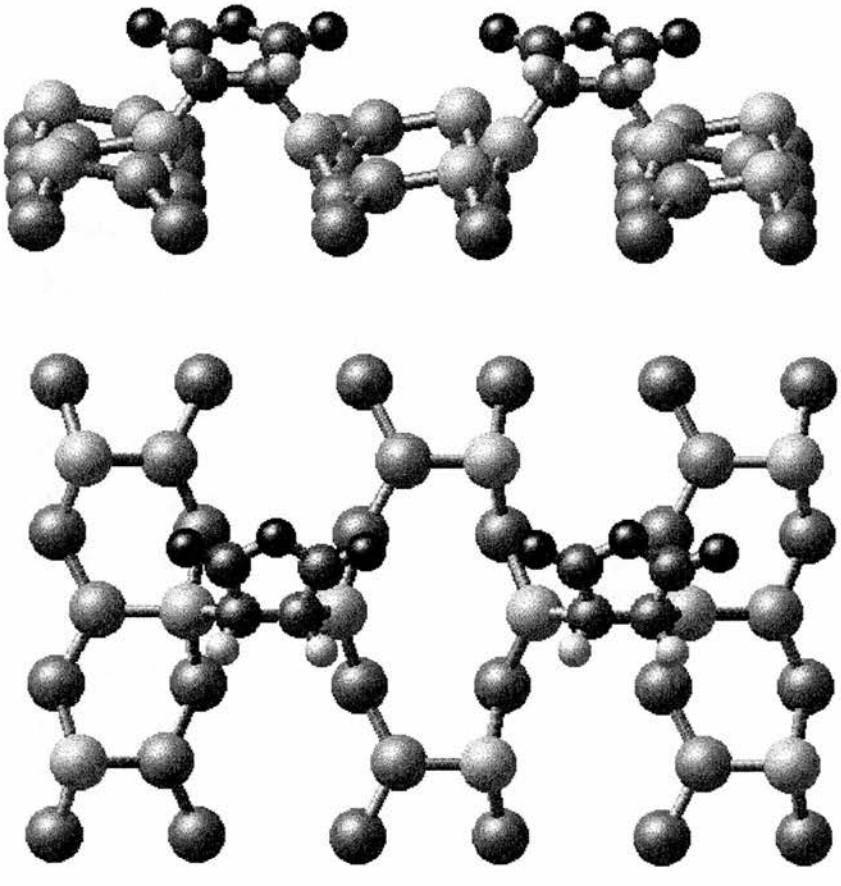

Fig 14. Side and top views of maleic anhydride adsorbed on a buckled Si(100)-2x1 surface.

The position of the atoms was not fully optimized, however the chemisorption of maleic anhydride in this geometry leads to a less strained Si-C-C-Si linkage than in the case of adsorption on the intra-dimer position. Fig 14 shows that with the adsorption of a second maleic anhydride molecule on a neighbouring site, the Si-dimer bond between the adsorbed hydrocarbons weakens and the silicon atoms relax towards the organic molecules. The weakening of silicon dimer bonds after cycloaddition reaction has been suggested in early STM work and predicted by *ab initio* calculations [6] [18]. At higher maleic anhydride coverages, silicon atoms in the Si-C-C-Si linkage may form a new strained Si-Si dimer bond that would resemble a Si dimer structure. Single bonded maleic anhydride species with the double C=C bond preserved are not observed in the STM images shown. This chemisorption involves the cleavage of one silicon-hydrogen bond and the bonding of hydrogen to one of the adjacent dimers.

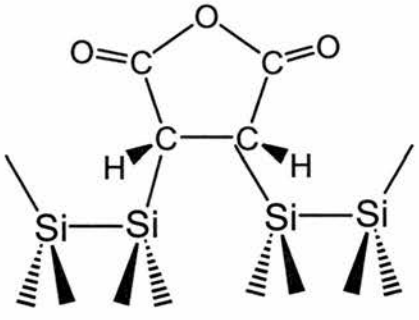

Fig 15. Adsorption of maleic anhydride on inter-dimer sites as observed by STM.

3.6. Conclusions

The adsorption of maleic anhydride on clean Si(100)-2x1 has been studied using HREELS, NEXAFS, XPS, ab initio calculations and STM. NEXAFS measurements reveal that the chemisorbed species are tilted 30° from the surface plane. The analysis of HREELS results shows that the adsorption of maleic anhydride on Si(100)-2x1 through ring opening is unlikely to occur and at low coverage the chemisorption occurs mainly through rehybridisation of the carbon atom in the olefin bond. Additionally, a second

type of species bonded through cleavage of the hydrogen bond are present at higher coverages.

However from these experimental results only, it is not possible to obtain information of the precise adsorption site of the molecules at the surface. The STM experiments show clearly that the molecules preferentially adsorb between dimer rows. Fig 12 shows the different adsorption geometries for maleic anhydride Si(100)-2x1 and the proposed models based on the results obtained from HREELS, NEXAFS and STM respectively.

3.7. References

[1] R.A. Wolkow. Annual Review of Physical Chemistry 50 (1999) 413-441

[2] T. Bitzer, N.V. Richardson. Applied Physics Letters 71 (1997) 662-664

[3] J.S. Hovis, H. Liu, R.J. Hamers. Surface Science 404 (1998) 1-7

[4] R.J. Hamers, J.S. Hovis, S. Lee, H.B. Liu, J. Shan. Journal of Physical Chemistry B 101 (1997) 1489-1492

[5] T. Bitzer, N.V. Richardson. Applied Physics Letters 71 (1997) 1890-1892

[6] A.J. Mayne *et al.* Surface Science 284 (1993) 247-256

[7] J.S. Hovis, R.J. Hamers. Journal of Physical Chemistry B 102 (1998) 687-692

[8] J.S. Hovis, R.J. Hamers. Journal of Physical Chemistry B 101 (1997) 9581-9585

[9] J.S. Hovis, H. Liu, R.J. Hamers. Applied Physics a-Materials Science & Processing 66 (1998) S553-S557

[10] M.J. Frisch *et al.* GAUSSIAN 98, Gaussian, Inc., Pittsburgh, PA (1998)

[11] H. Froitzheim, U. Kohler, H. Lammering. Surface Science 149 (1985) 537-557

[12] P. Mirone, P. Chiorboli. Spectrochimica Acta 18 (1962) 1425-1432

[13] C. Lauro, S. Califano, G. Adembri. Journal of Molecular Structure 2 (1968) 173-192

[14] C. Xu, D.W. Goodman. Langmuir 12 (1996) 1807-1816

[15] H.N. Waltenburg, J.T. Yates. Chemical Reviews 95 (1995) 1589-1673

[16] G.A.D. Briggs, A.J. Fisher. Surface Science Reports 33 (1999) 3-81

[17] R.J. Hamers, Y.J. Wang. Chemical Reviews 96 (1996) 1261-1290

[18] A.J. Fisher, P.E. Blochl, G.A.D. Briggs. Surface Science 374 (1997) 298

Acknowledgements

I would like to specially thank Dr. Thomas Bitzer and Mr. Tomás Rada Crespo for their help in the acquisition of the STM images.

CHAPTER 4.

The influence of Na on the adsorption of glycine on Si(100)-2x1

4.1. Introduction:

In order to understand and thereby control the interface between organic molecules and inorganic substrates and the further development of thin organic films, it is important to study model systems in some detail. The structure and local order of the layer acting as interface between the organic film and the substrate is influential in determining the growth process and this may be susceptible to the influence of a surface modifier. The study of the bonding geometry of model species such as simple amino acids can assist in the interpretation of more complex systems including aspects of biochemically active thin films.

The adsorption behaviour of several species, containing either a carboxylic acid group or an amino group, on Si(100)-2x1 has been studied previously. Molecules whose primary functionality is a carboxylic acid, such as benzoic acid, adsorb by cleavage of the O-H bond and its replacement by a single covalent O-Si bond [1]. The displaced hydrogen typically remains attached to the surface as Si-H. Similarly, amines such as aniline attach via a Si-N linkage following cleavage of a N-H bond and again the hydrogen is retained as Si-H [1]. In the case of 4-aminobenzoic acid [2], bonding through the carboxylic acid group is preferred in a manner analogous to the adsorption of benzoic acid [3]. In all three examples the strong covalent Si-N and Si-O bonds inhibits diffusion and subsequent ordering of the adsorbate. Earlier HREELS studies [3-4] have shown that the deposition of a Na template on Si(100)-2x1 dramatically modifies the chemistry at the surface. The deposited alkali metal atoms modify the strong covalent character of the silicon substrate leading to a more "metallic" behaviour of the surface. In the case of 4-aminobenzoic acid on Na/Si(100)-2x1 [2] the species were bonded to the substrate through the carboxylate group in bidentate coordination leaving the amino group unperturbed leading to an amino terminated surface.

In this study, we concentrate on the adsorption of glycine and its deuterated analogue, d_5-glycine on clean Si(100)-2x1 and Na/Si(100)-2x1. This allows us to compare the behaviour of this simple amino acid with the aromatic 4-aminobenzoic acid studied earlier [2]. HREELS has been used to study the chemistry at the surface after the adsorption of the species. *Ab initio* calculations using GAUSSIAN 98 [5] have been performed to assist in the interpretation the vibrational spectra. A comparative study of glycine and its deuterated form enables us to assign the vibrational features unambiguously. Section 4.2 describes the experimental arrangements. HREELS results of glycine and its deuterated form are described in section 4.3.1. *Ab initio* calculations are presented in section 4.3.2. A discussion of the results is given in section 4.4.

4.2. Experimental:

The HREELS spectra were recorded with electrons of 8 eV kinetic energy and in the specular ($\theta_i=\theta_f=45°$) and off specular ($\theta_i=45°$, $\theta_f=65°$) directions. The spectrometer (VSW-HIB 1000) was tuned to 40 cm^{-1} in the straight through position. Silicon samples were cut from single sided polished wafers (n-type, 500 Ωcm) and mounted on a sample carrier using Ta clips. Clean Si(100)-2x1 samples were prepared in a standard procedure by resistive heating to 900°C to remove the native oxide. In order to facilitate resistive heating for oxide removal, the rear of the samples were coated with a thin platinum layer. The cleanliness of Si(100)-2x1 was confirmed in HREELS, by the absence of Si-O or Si-C features. For temperature calibration, a thermocouple was attached to the front side of the sample with ceramic glue after the completion of the HREELS experiments. Sodium was deposited from a well-degassed SAES getter situated 3 cm from the sample. Excess Na was desorbed by heating the sample to 120° [6]. The glycine and d_5-glycine powders (Aldrich, 99+%) were contained in small glass vessels separated from the main chamber by a gate valve and pumped by a diffusion pump.

Before dosing into UHV, the polycrystalline solids were cleaned by several cycles of sublimation and pumping with the gate valve closed. While dosing the main chamber pressure rose from $2x10^{-10}$ mbar to $4x10^{-9}$ mbar. The HREEL spectra of both glycine and fully deuterated glycine were obtained at room temperature. The monolayers of glycine

on clean Si(100)-2x1 and on Na/Si(100)-2x1 were heated to increasing temperatures to probe the thermal stability of the deposited films.

4.3. Results:

4.3.1. HREELS

Following the adsorption of glycine and d_5-glycine either on clean Si(100)-2x1 or Na modified Si(100)-2x1, sharp 2x1 diffraction spots could be observed in LEED. These indicate the preservation of the surface reconstruction on the two substrates. Fig 1 shows the vibrational spectra of clean Si(100)-2x1 after exposure to (a) glycine and (c) d_5-glycine at room temperature. All the features observed in the vibrational spectra have been assigned by comparison with our *ab initio* calculations which will be described in detail in section 3.2. Table 1. shows the frequency assignments of the observed features.

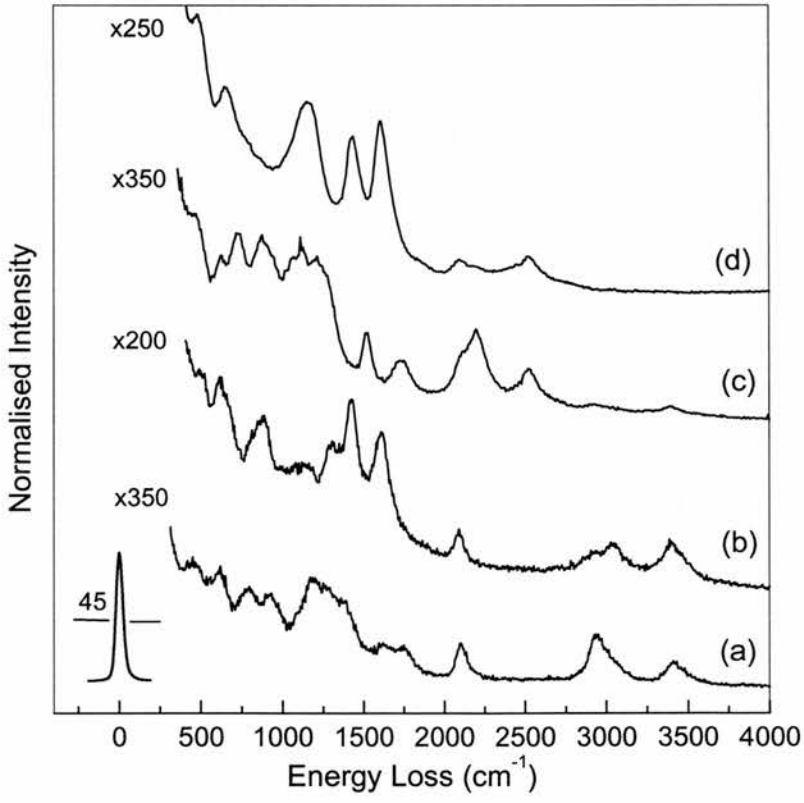

Figure 1. HREEL spectra of (a) glycine and (c) d_5-glycine adsorbed on clean Si(100)-2x1 and (b) and (d) on Na/Si(100)-2x1. The spectra were recorded in specular scattering geometry ($\theta_i=\theta_f=45°$) and an electron energy of $E_0=8$ eV.

In the HREEL spectrum of glycine adsorbed on clean Si(100)-2x1, carboxylate group peaks assigned to the ν(C=O) stretch, and the ν(C-O) stretch can be observed at 1750 cm^{-1} and 1170 cm^{-1} respectively. The loss features at 2940 cm^{-1} are assigned to ν(CH) stretching modes and those at 1260 cm^{-1} and 925 cm^{-1} to β(CH) bending and $\delta(CO_2)$ modes respectively. The band observed at 2115 cm^{-1} is assigned to Si-H species present at the surface. The loss peak at 1620 cm^{-1} is attributed to $\delta(NH_2)$ scissor vibrations. The feature observed at 620 cm^{-1}, is attributed to a $\beta(NH_2)$ mode. Other amino group related vibrations, $\nu_s(NH_2)$ and $\nu_{as}(NH_2)$, are present in a broad band observed at 3460 cm^{-1}.

In the deuterated form spectrum (c), the $\nu(ND_2)$ and $\nu(CD_2)$ vibrations give rise to the bands at 2584 cm^{-1} and 2200 cm^{-1} respectively. The carbonyl band, present at 1736 cm^{-1}, shifts very little compared with the non-deuterated glycine. The sharp feature at 1520 cm^{-1} is attributed to Si-D vibrations. The bands observed at 1216 cm^{-1} and 1120 cm^{-1} are assigned to $\beta(CD_2)$ and $\delta(ND_2)$ vibrations, respectively. The observation of the ν(SiO) feature at 780 cm^{-1} (736 cm^{-1}) shows clearly that the adsorption of glycine (d_5-glycine) on Si(100)-2x1 occurs through cleavage of the OH (OD) bond and the formation of a Si-O linkage.

Fig 1 shows the HREEL spectrum of Na/Si(100)-2x1 after exposure to (b) glycine and (d) d_5-glycine at room temperature. The deposition of the Na monolayer has induced a dramatic change in the spectrum relative to that of the unmodified surface. In the HREEL spectrum of glycine on Na/Si(100)-2x1, the strong loss at 1420 cm^{-1} can be identified as the symmetric ν_s(OCO) stretch of the carboxylate group in a bidentate coordination (see table 2 for the frequency assignments). Note that the carbonyl ν(C=O) mode at 1750 cm^{-1} is now entirely absent in the spectrum. This shows that glycinate species on Na/Si(100)-2x1 are exclusively present in a bidentate coordination. The band observed at 1620 cm^{-1} has contributions from both $\delta(NH_2)$ and ν_{as}(OCO) vibrations. Additional carboxylate group, $\delta(CO_2)$, vibrations give rise to the band observed at 890 cm^{-1}. The peaks observed at 1305 cm^{-1} and 1152 cm^{-1} are attributed to bending C-H modes. In the HREEL spectra of deuterated glycine adsorbed on Na/Si(100)-2x1, the bands observed at 2530 cm^{-1} and 2200 cm^{-1} are assigned to $\nu(ND_2)$ and $\nu(CD_2)$ vibrations

respectively. The strong intensity at 1608 cm^{-1} is now straightforwardly attributed to a ν_{as} (OCO) mode. The ν_s (OCO) vibration is clearly observed at 1430 cm^{-1}. The $\delta(ND_2)$ vibrations give rise to the broad band at 1088 cm^{-1} shifted from approximately 1590 cm^{-1} i.e. overlapping the ν_{as} (OCO) as suggested earlier. It should be noted that the expected vibration corresponding to Si-D species present at the surface is not observed in the vibrational spectra since it falls in the tail of the ν_{as} (OCO) band.

Fig 2 shows the HREEL spectra of glycine adsorbed on Na/Si(100)-2x1 recorded (a) on specular and (b) off-specular. In the off specular spectrum, the intensity of the ν_s(OCO) mode decreases compared with the on specular although no noticeable change occurs in the intensity of the band at 1620 cm^{-1}. Curves (c) and (d) show the HREEL spectra of Na/Si(100)2x1 exposed to deuterated glycine recorded on specular and off specular respectively.

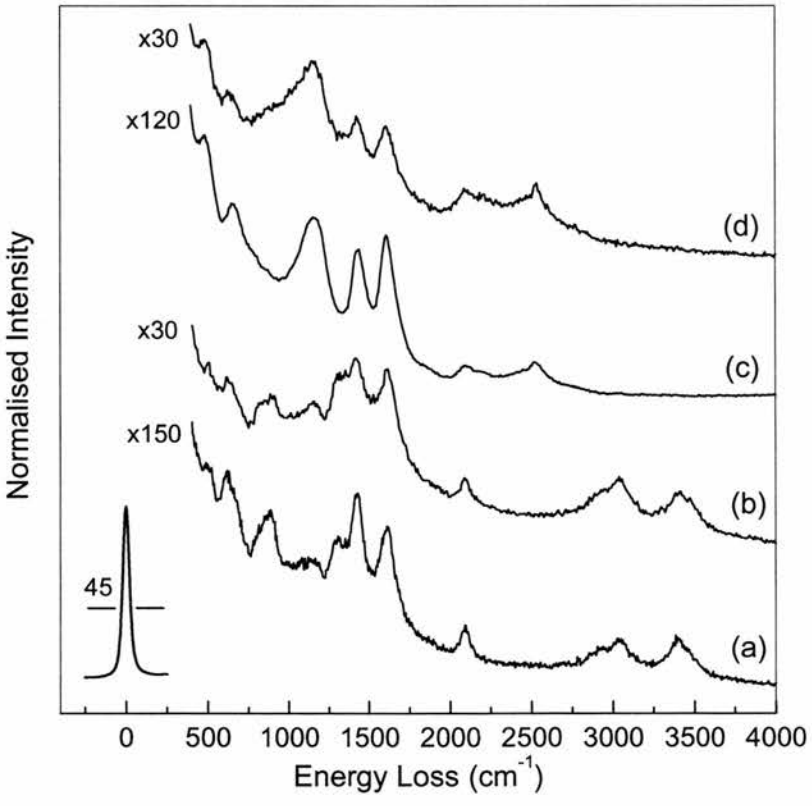

Figure 2. HREEL spectra of glycine (a) on specular, (b) off specular adsorbed on Na/Si(100)-2x1. The spectra for the deuterated glycine is shown in curves (c) and (d).

In this case, the off specular spectrum shows a reduction in the intensity of the modes at 1430 cm^{-1} and 1608 cm^{-1} assigned to $\nu_s(OCO)$ and $\nu_{as}(OCO)$ vibrations respectively. Additionally, the intensity of the band at 1160 cm^{-1}, attributed to $\delta(ND_2)$ vibrations, is unchanged in the off specular spectrum. Fig. 3 shows the HREEL spectra of glycine adsorbed on clean Si(100)-2x1 at room temperature and after heating to various temperatures.

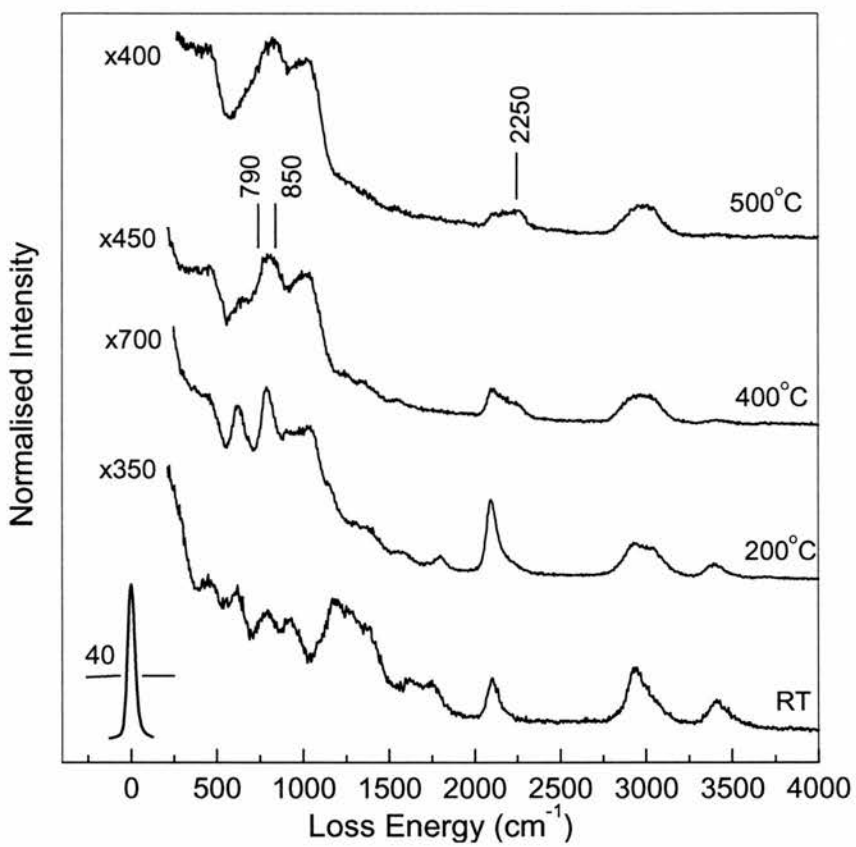

Fig 3. On-specular HREEL spectra of glycine on Si(100)-2x1 at room temperature and after annealing to the indicated temperatures.

Annealing to 200 °C results in the appearance of a small shoulder observed at 2250 cm^{-1}. Although the observed features show significant change in the intensity, suggesting a change in the orientation of the species, the loss vibrations can still be identified with the room temperature spectrum. The intensity of this mode increases when annealing the substrate to 400 °C. Additionally, at this temperature the overall shape of

the vibrational spectrum continues to evolve with loss of intensity above 1000 cm^{-1}. The band appearing at 850 cm^{-1} is characteristic of Si-N vibrations [1], and shows clearly that glycine species start to decompose at the surface. The amino related band at 3400 cm^{-1} although substantially reduced is not completely absent even after annealing to 400 °C. This shows most likely monodentate bonding of the amino group to the Si dimer.

Fig 4 shows the HREEL spectra of glycine adsorbed on Na/Si(100)-2x1 at room temperature and after heating the substrate for 1 min to the temperatures indicated.

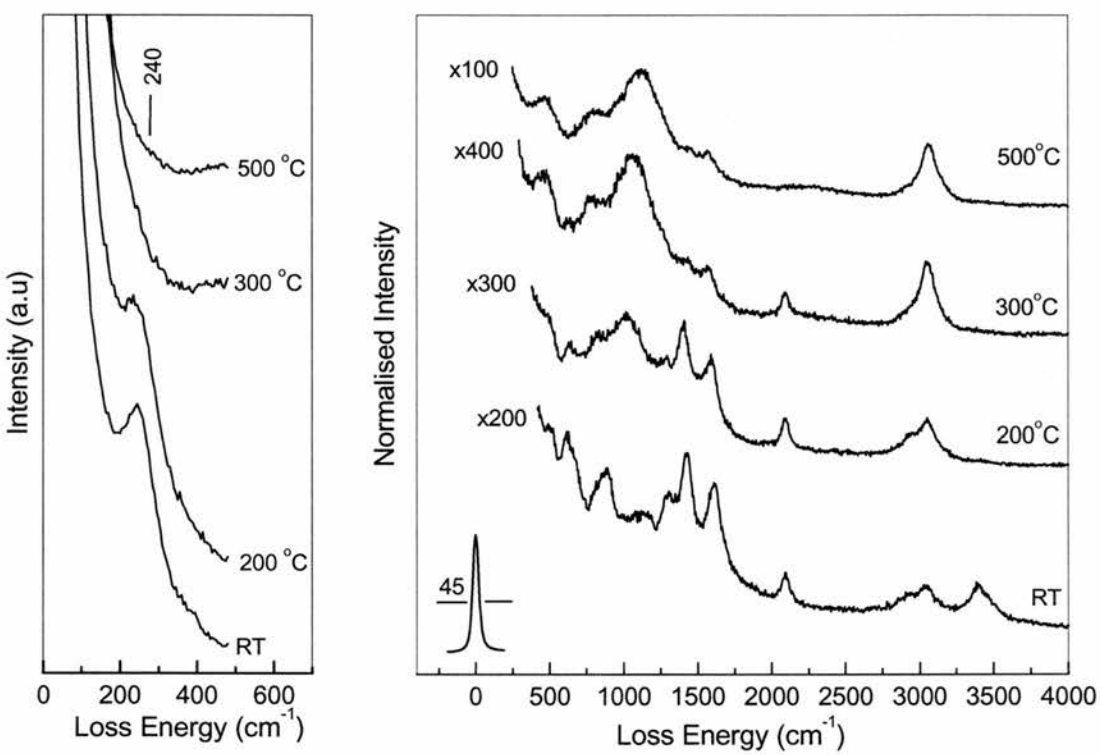

Fig 4. On-specular HREEL spectra of glycine on Na/Si(100)-2x1 at room temperature and after annealing to the indicated temperatures. The evolution of the Na related feature upon annealing can be observed in the graph on the left side. Note that the carboxylate group features are absent at 300 C which corresponds to the desorption of Na from Si(100)-2x1.

Heating the substrate to 200 °C results in the disappearance of the amino group related band at 3400 cm^{-1}. It should be noted that the carboxylate group peaks are still observed although the feature assigned to C-O vibrations starts to appear at 1200 cm^{-1} [7]. Annealing to 300 °C leads to a decrease of the intensity of the carboxylate group related

bands and an increase of a feature attributed to C-O vibrations. Further annealing to 500 °C results in removal of hydrogen from the surface as indicated by the disappearance of the Si-H feature at 2115 cm^{-1}. The evolution of the Na loss feature at 240 cm^{-1} in the annealing process is shown in fig 4. Note that this band is absent in the 300°C and 500°C spectra, which indicates the desorption of Na at these temperatures.

4.3.2. *Ab initio* calculations

Ab initio methods have been used to simulate the vibrational spectrum to assist the interpretation of the HREEL spectra. The cluster calculations have been performed using GAUSSIAN 98 [5] software under the *b3lyp* functional and 6-31G basis set. Initially, we have calculated the geometry and frequencies of an isolated glycine molecule in order to validate the approximations used. By comparison with previously published vibrational data of amino acids [8-9], all calculated frequencies have been scaled by a factor of 0.98.

Glycine adsorbed on clean Si(100)-2x1 has been modelled as one glycinate species interacting with a silicon cluster in two different interaction geometries. Fig 6 shows the glycinate molecule adsorbed on the dimer (a) through the amino group and (b) through the carboxylate group. In both models, the cleaved hydrogen atom saturates the adjacent dimer atom. The optimisation procedure was carried out in two steps. First, a silicon/hydrogen cluster consisting of eight silicon atoms with all bonds, except those of the dimer, saturated with hydrogens was fully optimised. Second, the glycinate molecule was adsorbed on one of the dimer atoms in one of the two adsorption geometries described above and the geometry of the silicon/hydrogen cluster was frozen during the optimisation of the adsorbate structural parameters. The model of glycine adsorbed on the Si cluster through the carboxylate group was used to assign the features observed in the vibrational spectrum of glycine on Si(100)-2x1 at room temperature. This is justified since in this case the vibrational spectrum shows no evidence for Si-OH vibrations expected in case the carboxylic group is undisturbed. The results from this optimisation give an adsorption geometry for glycine on the Si cluster on which the Si-O bond is tilted 15° relative to the surface normal. The C-C bond is almost perpendicular to the surface as shown in fig 6 (b). Since the HREELS data suggest thermal decomposition of glycine on

the substrate, resulting in the formation of Si-N species, we carried out calculations of glycine interacting with the silicon cluster through the amino group (fig 6 (a) in order to assign the vibrational features observed in the HREEL spectra of glycine/Si(100)-2x1 after annealing.

The cluster used for the adsorbed glycine on Na/Si(100)-2x1 consisted of a single molecule interacting with a Na atom via the carboxylate group (see fig 5 (c)). This approach is justified by the strong interaction between the carboxylate group and the Na atom indicated by the HREELS data.

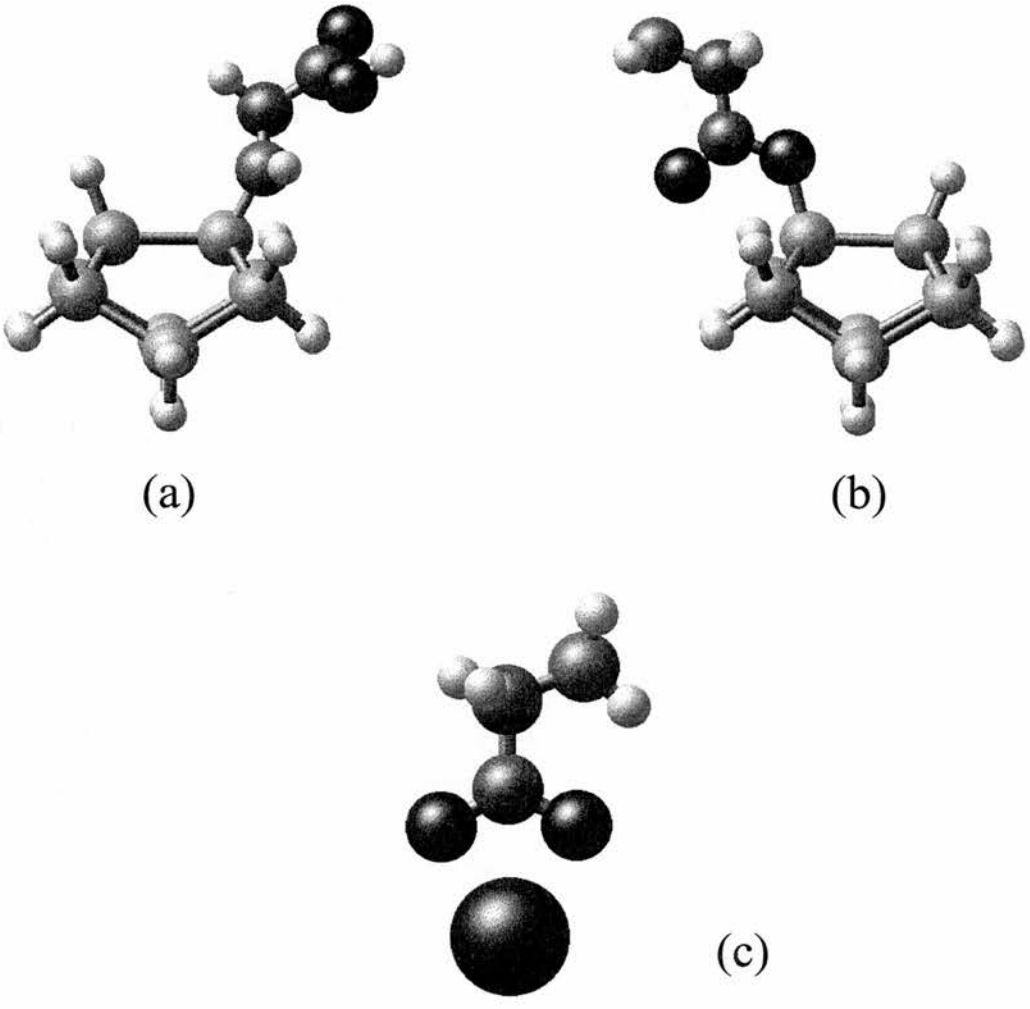

Fig 5. Optimized structures for glycine interacting with the silicon cluster through (a) the amino group, (b) the carboxylate group and (c) with the Na atom.

Following an optimisation of the geometry, the vibrational frequencies were calculated via computation of the force constants. Tables 1 and 2 show the calculated frequencies in comparison with those obtained from the vibrational spectra of glycine and d_5-glycine adsorbed on Si(100)-2x1 and Na/Si(100)-2x1 respectively.

GAUSSIAN 98 (cm^{-1})		HREELS (cm^{-1})		Assignment	
Glycine	d_5-glycine	Glycine	d_5-glycine	Glycine	d_5-glycine
3400	2689	3460	2584	$\nu_s(NH_2)$	$\nu_s(ND_2)$
3398	2544	3410	2520	$\nu_{as}(NH_2)$	$\nu_{as}(ND_2)$
3021	2311	3040	2200	$\nu_s(CH_2)$	$\nu_s(CD_2)$
2967	2098	2940	2112	$\nu_{as}(CH_2)$	$\nu_{as}(CD_2)$
2134	1655	2115	1520	ν(SiH)	ν(SiD)
1790	1800	1750	1736	ν(C=O)	ν(C=O)
1700	-	1620	-	δ (NH_2)	-
1348	-	1380	-	$\beta(CH_2)$	-
1100	1256	1260	1216	$\beta(CH_2)$	$\beta(CD_2)$
1097	1167	1170	1120	ν(C-O)	δ (ND_2)
989	988	925	936	$\delta(CO_2)$	$\delta(CO_2)$
-	894	-	880	-	$\beta(CD_2)$
790	805	780	736	ν(SiO)	ν(SiO)
654	620	630	615	ν(CN)	ν(CN)
453	453	475	472	Amin/carbox	Amin/carbox

Table 1. Assignment based on our ab initio calculations of the vibrational features of glycine and d_5-glycine on Si(100)-2x1

GAUSSIAN98 (cm^{-1})		HREELS (cm^{-1})		Assignment	
Glycine	d_5-Glycine	Glycine	d_5-Glycine	Glycine	d_5-Glycine
3500	2600	3472	2530	$\nu_s(NH_2)$	$\nu_s(ND_2)$
3458	2568	3408	2456	$\nu_{as}(NH_2)$	$\nu_{as}(ND_2)$
3098	2190	3040	2200	$\nu_s(CH_2)$	$\nu_s(CD_2)$
2987	2098	2944	2088	$\nu_{as}(CH_2)$	$\nu_{as}(CD_2)$
2085	-	2088	-	ν(SiH)	-
1654	1598	1620	1608	ν_{as}(OCO) δ (NH_2)	ν_{as}(OCO)
1489	1498	1420	1430	ν_s(OCO)	ν_s(OCO)
1190	1065	1290	1088	$\beta(CH_2)$	$\beta(CD_2)$
1054	1176	1152	1160	$\beta(CH_2)$	δ (ND_2)
876	-	890	-	$\delta(CO_2)$	-
676	610	650	640	ν(CN)	ν(CN)
566	500	500	480	Amin/carbox	Amin/carbox
-	-	241	238	Na related	

Table 2. Assignment based on our ab initio calculations of the vibrational features of glycine and d_5-glycine on Na/Si(100)-2x1

4.4. Discussion

The vibrational spectrum of glycine and its deuterated analogue d_5-glycine adsorbed on clean Si(100)-2x1 shows that the species bond to the surface, mainly through cleavage of the OH and OD bonds respectively, and the formation of a Si-O linkage. The cleaved hydrogen atom most likely saturates the adjacent dimer, giving rise to Si-H and Si-D species. The presence of the carbonyl bands ν(C=O) at 1750 cm^{-1} confirms that the species are bonded to Si(100)-2x1 in monodentate coordination.

The bonding of the species to the surface through the amino groups, as found in the case of aniline adsorbed on Si(100)-2x1 [1] would lead in this case to the observation of a band at 3600 cm^{-1} attributed to a retained ν(OH) stretching mode [10]. This is absent from the spectrum. Additionally the bands assigned to $\delta(NH_2)$ and $\delta(ND_2)$ vibrations

respectively, would be replaced by lower frequency N-H and N-D bending modes in case of reaction of the amino groups with silicon surface.

The adsorption geometry of alkali metals Na on Si(100)-2x1 has been described in detail elsewhere [6-11-13]. It is widely agreed that at saturation coverage Na atoms adsorb on Si(100)-2x1 on a cave site between two silicon dimers. In this adsorption geometry Na atoms form rows parallel to the dimer rows. The HREELS data show clearly that the bonding geometry of glycine to Si(100)-2x1 is dramatically modified by co-adsorbed Na atoms. The feature observed at 1420 cm^{-1} in the HREEL spectrum of glycine on Na/Si(100)-2x1, is assigned to ν_s(OCO) and indicates that bonding now occurs exclusively via the carboxylate group. The band at 1615 cm^{-1} can be assigned to the ν_{as}(OCO) but contributions from $\delta(NH_2)$ are also possible at this frequency. The observation of the ν_s(OCO) and the ν_{as}(OCO) modes in the vibrational spectrum of deuterated glycine on Na/Si(100)-2x1 clearly demonstrates that bidentate species are present at the surface. The complete absence of the carbonyl band at 1750 cm^{-1} in the glycine/Na/Si(100)-2x1 spectra supports this adsorption model.

According to the surface dipole selection rules, which are strictly applicable to IR and EELS spectroscopy at metal surfaces, dynamic electric dipole moments aligned parallel to the surface are completely screened. On the other hand, an enhancement is observed for vibrations with a dynamic dipole moment oriented perpendicular to the surface. Due to the sufficiently high dielectric constant of silicon this rule can be applied to the glycinate/Na/Si(100)-2x1 system. As can be seen in the fig 2 (spectra (c) and (d)) the ν_s(OCO) and ν_{as}(OCO) modes at 1430 cm^{-1} and 1608 cm^{-1}, respectively have a strong dipole character. The intensity of these bands is proportional to the square of the perpendicular component of the dynamic dipole associated with those vibration modes. The IR intensity ratio for ν_s(OCO) and ν_{as}(OCO) in glycine dispersed in a KBr matrix [14] is 0.96. In the case of deuterated glycine on Na/Si(100)-2x1, the intensity ratio obtained from fitting the two bands at 1430 cm^{-1} and 1608 cm^{-1}, respectively is 1.7. This ratio indicates that the molecule axis is tilted an angle of 50° relative to the surface normal with the CO_2 plane assumed to be perpendicular to the surface. Based on these

experimental results, we suggest a structural model in which the glycinate species adsorb through the carboxylate group standing on the Na atom.

The amino group is not involved directly in the adsorption process as demonstrated by the observation of the $\nu(NH_2)$ and $\nu(ND_2)$ bands at 3400 cm^{-1} and 2530 cm^{-1} respectively. The $\delta(ND_2)$ band observed at 1120 cm^{-1} in the deuterated glycine spectrum clearly indicates that the adsorption of these forms of glycine on Na/Si(100)-2x1 lead to an amino terminated surface with amino groups pointing into the vacuum. In case of glycine adsorbed on clean Si(100)0-2x1, the annealing process leads to oxidation of the substrate and decomposition of the adsorbed species. By comparison with IR data [15], the shoulder observed at 2250 cm^{-1} is identified as O-Si-H vibrations and indicates the diffusion of oxygen in the carboxylate group in the Si back bonds. Annealing to 200°C causes the oxygen atoms in the carboxylate group start to diffuse into the Si back bonds oxidising the substrate. It is important to note that in this case heating the substrate to 400 °C leads to the formation of Si-N-H species as seen by the observation of the Si-N band and the low intensity feature at 3400 cm^{-1}.

On the other hand in the case of glycine adsorbed on Na/Si(100) the thermally induced removal of the amino groups at 200 °C is confirmed by the complete absence of the band at 3400 cm^{-1}. In case the amino group would tilt and bond to the Si dimer, Si-N-H species would be expected at the surface, leading to an observed feature. The bidentate carboxylate group however, stays intact as confirmed by the observation of the $\nu_s(OCO)$ and the $\nu_{as}(OCO)$ modes. Note that the Na template is still unperturbed as seen from fig 5. Further annealing to 300 °C leads to the desorption of sodium atoms from the surface and consequent loss of the bidentate coordination of the carboxylate group. This is acknowledged in the spectrum of glycine on Na/Si(100)-2x1 heated to 300 °C. The observation of the band at 785 cm^{-1} indicates that glycine bonds to the Si dimer through a Si-O linkage. The strong band at 1200 cm^{-1} characteristic for C-O vibrations confirms this model.

4.5. Conclusion

The adsorption of glycine and deuterated glycine on Na/Si(100)-2x1 has been studied by HREELS. Glycine bonds to Na/Si(100)-2x1 through the carboxylate group in bidentate coordination. Thermally induced removal of the amino group is achieved by heating the substrate to 200 °C for 1 min. Further heating to 300 °C results in the desorption of the Na template and consequent loss of the bidentate coordination.

In contrast, we observe monodentate species after the exposure of Si(100)-2x1 to glycine. The vibrational spectra show a decomposition of the glycine species followed by a substrate oxidation when heating the sample to 500°C.

References

[1] T. Bitzer, T. Alkunshalie, N.V. Richardson. Surface Science 368 (1996) 202-207

[2] A. Lopez, T. Bitzer, T. Heller, N.V. Richardson. Surface Science In press

[3] T. Bitzer, N.V. Richardson, S. Reiss, M. Wuhn, C. Woll. Surface Science 458 (2000) 173-184

[4] T. Bitzer, N.V. Richardson. Surface Science 428 (1999) 369-373

[5] M.J. Frisch *et al.* GAUSSIAN 98, Gaussian, Inc., Pittsburgh, PA (1998)

[6] M. Tikhov, G. Boishin, L. Surnev. Surface Science 241 (1991) 103-110

[7] P. Mirone, P. Chiorboli. Spectrochimica Acta 18 (1962) 1425-1432

[8] S. Tanaka, M. Onchi, M. Nishijima. Surface Science 191 (1987) L756-L764

[9] S.M. Barlow, K.J. Kitching, S. Haq, N.V. Richardson. Surface Science 401 (1998) 322-335

[10] W. Ranke, D. Schmeisser. Surface Science 149 (1985) 485-499

[11] P.S. Mangat *et al.* Physical Review B 47 (1993) 16311-16321

[12] P. Soukiassian. Acta Physica Polonica a 81 (1992) 19-32

[13] P. Soukiassian, S.T. Kim, Z. Hurych, J.A. Kubby. Applied Surface Science 56-8 (1992) 394-401

[14] B. Liedberg, I. Lundstrom, C.R. Wu, W.R. Salaneck. Journal of Colloid and Interface Science 108 (1985) 123-132

[15] P. Gupta, A.C. Dillon, A.S. Bracker, S.M. George. Surface Science 245 (1991) 360-372

CHAPTER 5.

The influence of Na on the adsorption of 4-aminobenzoic acid on Si(100)-2x1

5.1. Introduction:

The interaction of the amino acid glycine with the clean and Na modified Si(100)-2x1 surfaces has been described in detail in the previous chapter. In the case of glycine adsorbed on clean Si(100)-2x1, glycinate species are bonded to the surface through the cleavage of the OH bond in the carboxylate group resulting in to a strong interaction between the oxygen atom and the silicon atom in the dimer. The cleaved hydrogen was found to saturate adjacent dimers. The deposition of a Na template dramatically modifies the chemistry at the Na/Si(100)-2x1 surface. In this case, after cleavage of the OH bond, HREELS showed that the glycinate species interact strongly with the Na atom through the carboxylate group, leading to the formation of a delocalized bond in which the two oxygen atoms are equivalent. This type of interaction has been described in previous studies of amino acids on copper and Na modified silicon surfaces [1-2].

In this study, we are now interested in the aromatic amino acid 4-aminobenzoic acid. Analogous to the case of glycine, we have used HREELS to determine which of the two functional groups is preferred in the adsorption process (C-O-Si or C-N-Si) and thereby which functionality is available for further reactive steps in film growth. Since we were particularly interested in possible long-range order and preferential molecular orientations, we used NEXAFS to determine the precise tilt of the molecules on the surface and obtain information about the molecular electronic structure. XPS experiments were particularly useful in the determination of the C and O core levels and, in conjunction with *ab initio* calculations, enabled us to assign the first NEXAFS π resonances. Additionally, it is important to note that all the bands observed in the HREELS spectra have been assigned according to the results from our *ab initio* calculations.

5.2. Experimental:

The experiments were carried out in three different UHV chambers each with a base pressure in the low 10^{-10} mbar. The NEXAFS experiments were performed at the HE-TGM2 beam line at BESSY I (Berlin, Germany). Multilayer formation was achieved by condensing amino benzoic acid on the sample, cooled by l-N_2. The monolayer spectra were recorded at 30^{o} and 90^{o} incidence angles. All spectra were recorded in partial electron yield detection mode (PEY). The voltage applied to the grid placed at the channeltron entrance was –150 V.

The HREELS spectra were recorded at 8 eV kinetic energy of incident electrons and in the specular direction ($\theta_i=\theta_f=45°$). The spectrometer (VSWHIB 1000) was tuned to 40 cm^{-1} in the straight through position. Clean Si(100)-2x1 (n-type, 500 Ωcm) samples were prepared in the standard procedure by resistive heating to 900°C for native oxide removal. The cleanliness of Si(100)-2x1 was confirmed in HREELS and NEXAFS, by the absence of oxide or contaminant related features. The sample temperature was measured with a thermocouple pressed to the back of the sample, which was coated with platinum for optimum conductivity. Sodium was deposited from a well-degassed SAES getter situated 3 cm from the sample. Excess Na was desorbed by heating the sample to 120° [3]. 4-aminobenzoic acid (Aldrich, 99+%), which was purified by several pump-sublimation cycles, was introduced into UHV through a stainless steel tube. All dosing experiments were carried out at room temperature.

XPS spectra of multilayers 4-aminobenzoic were recorded with a pass energy of 20 eV using a hemispherical analyser. Multilayers were achieved by cooling the copper manipulator to l-N_2 temperatures and dosing amino benzoic acid in UHV. The relative peak position was used to determine the relative energy of the C1s atomic levels.

5.3. Results

5.3.1 HREELS:

Following the adsorption of 4-aminobenzoic acid either on clean Si(100)-2x1 and Na modified Si(100)-2x1, sharp 2x1 diffraction spots could be observed in LEED. These indicate the preservation of the surface reconstruction on the two substrates. Fig 1 shows the vibrational spectra of 4-aminobenzoic acid adsorbed at room temperature on (a) Si(100)-2x1 and (b) Na/Si(100)-2x1, respectively. Table 1. shows the frequency assignment of the observed features by comparison with our *ab initio* calculations which will be described in detail in section 5.3.4.

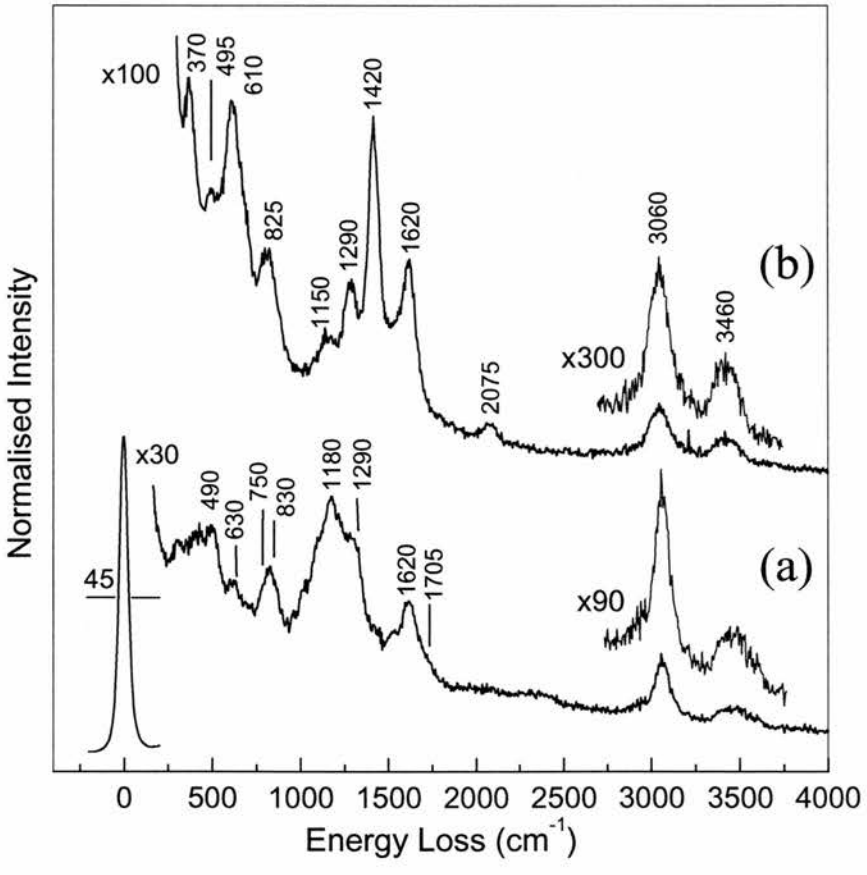

Fig 1. HREELS spectra of 4-aminobenzoic acid adsorbed on clean Si(100)-2x1 and Na modified Si(100)-2x1.

In the HREEL spectrum of 4-aminobenzoic acid adsorbed on clean Si(100)-2x1 carboxylate group peaks assigned to the ν(C=O), the ν(C-O) stretch and the $\delta(CO_2)$ bending mode can be observed at 1705 cm^{-1}, 1290 cm^{-1} and 830 cm^{-1} respectively. The loss feature at 3060 cm^{-1} is assigned to ν(CH) stretching modes and at 1180 cm^{-1} and 830 cm^{-1} to β(CH) bending modes. The loss peak at 1620 cm^{-1} is attributed to $\delta(NH_2)$ vibrations. The feature observed at 630 cm^{-1}, is attributed to a ring mode. Other amino group related vibrations, ν_s(NH) and ν_{as}(NH), are present in a broad band observed at 3460 cm^{-1}. The shoulder observed at 750 cm^{-1} is attributed to Si-O vibrations. The vibrational data show clearly that 4-aminobenzoic acid adsorbs on clean Si(100)-2x1 through the carboxylate group. The observation of the ν(C=O) stretch indicates species bonded to Si(100)-2x1 in monodentate coordination.

Fig 1 (b) shows the HREEL spectrum of 4-aminobenzoic acid adsorbed on the Na modified silicon surface. The dramatic change of the spectrum relative to that of the unmodified surface is clearly observed. The strong loss at 1420 cm^{-1} can be identified as the symmetric ν_s(OCO) stretch of the carboxylate group in a bidentate coordination (see table 1 for the frequency assignments). Note that the carbonyl ν(C=O) mode, found at 1705 cm^{-1} in the absence of Na, is entirely absent in the spectrum. This demonstrates that the 4-aminobenzoate species on Na-Si(100)-2x1 are exclusively present in a bidentate coordination. Note also the relative increase in the intensity of the peak at 1620 cm^{-1}, attributed to $\delta(NH_2)$ vibrations. These are a strong indication for an adsorption geometry on which the amino groups point out into the vacuum. The features observed at 610 cm^{-1}, 495 cm^{-1} and 370 cm^{-1} can be assigned, to a C-N stretching mode, an amino-carboxylate deformation mode and a NH_2 bending vibration respectively. The peaks observed at 1290 cm^{-1} and 1150 cm^{-1} are attributed to ν(C-O) and β(C-H) modes, respectively. Additionally the band observed at 825 cm^{-1} is assigned to $\delta(CO_2)$ vibrations.

Fig 2. shows the on-specular HREEL spectra of 4-aminobenzoate on Na/Si(100)-2x1 at room temperature and after heating to 200 °C and 300 °C. Heating to 200° C induces no significant changes in the vibrational spectrum compared with the room

temperature one. Further heating to 300 °C leads clearly to a broadening of the loss features. This line broadening is caused by an increase of the line width of the elastic peak and is interpreted as an increase of the surface disorder. However, the overall shape of the spectrum is retained after heating to 300° C, except for the decrease in the intensity of the NH_2 band at 3400 cm^{-1}which indicates the significant desorption of amino groups from the surface.

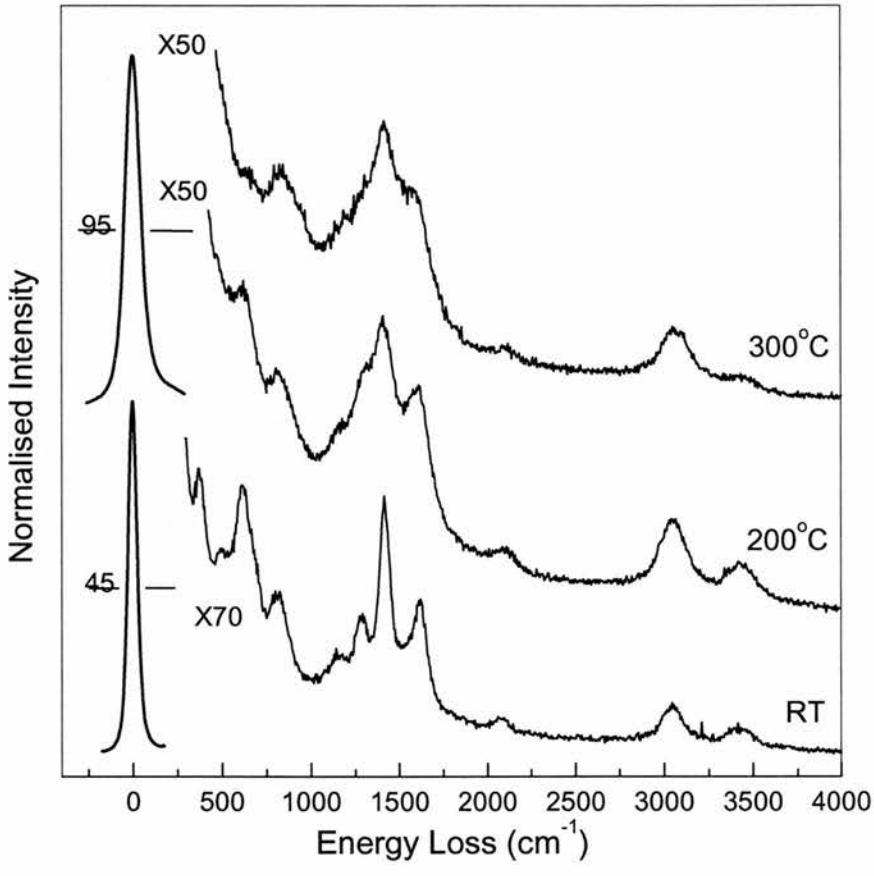

Fig 2. HREELS spectra of 4-aminobenzoic acid on Na/Si(100)-2x1 annealed up to 300 °C. Note that the vibrational features observed at room temperature are still visible after annealing although the line width has dramatically increased.

GAUSSIAN 98 (cm^{-1})		Observed in HREELS (cm^{-1})		Assignment
ABA/Na/Si	ABA/Si	ABA/Na/Si	ABA/Si	
3512	3540	3513	3513	$\nu_{as}(NH_2)$
3408	3490	3460	3460	$\nu_{s}(NH_2)$
3180	3110	3120	3120	$\nu_{as}(CH)$
3050	3000	3060	3060	$\nu_{s}(CH)$
-	2090	2075	-	$\nu(SiH)$
-	1780	-	1705	$\nu(C=O)$
1685	1690	1620	1620	$\delta(NH_2)$
1495	-	-	-	$\nu_{as}(OCO)$
1404	-	1420	-	$\nu_{s}(OCO)$
1213	1300	1290	1290	$\beta(CH)/\ \nu(CO)$
1156	1190	1150	1180	$\beta(CH)$
854	860	825	830	$\delta(CO_2)$
-	800	-	750	$\nu(SiO)$
-	620	-	630	Ring
643	-	610	-	$\nu(CN)$
429	480	495	490	Amin/carbox
364	-	370	-	o.p.(NH_2)

Table 1. Frequency assignments of the HREELS vibrational features according to the ab initio calculations.

5.3.2 NEXAFS:

Fig 3. shows the NEXAFS C K-edge spectrum of the 4-aminobenzoic acid/Na/Si(100)-2x1 surface recorded at normal incidence angle. Characteristic π^*-shape resonances are observed at 285.0 eV, 286.1 eV, 287.3 eV, 288.0 eV and 289.0 eV, respectively. At photon energies above 290 eV broader features with predominantly σ^* character are present in the absorption spectrum.

By comparison with our *ab initio* calculations (see fig 9), the first π^* resonance at 285.0 eV can be associated with an excitation from C1s levels of phenyl ring carbon atoms into the lowest unoccupied molecular orbital (LUMO). Transitions from the 1s levels of the carbon atom linked to the amino group give rise to the resonance observed at 286.1 eV. The resonance at 288.0 eV is attributed to excitations from C1s level of the carboxylate group carbon atom into the LUMO. The resonance observed at 286.1 eV, also has contributions from transitions from C1s levels of phenyl ring atoms into the

LUMO+1. It should be noted that excitations from C1s levels of carbon atoms in the carboxylate group or adjacent to the amino group into the LUMO+1 are not possible since the *ab initio* calculations show that there is no p_z contribution from these atoms to the molecular orbital (see fig 9). The shoulder observed at 287.3 eV is attributed to transitions from C1s levels of phenyl ring atoms into the LUMO+2. Additionally, excitations from the C1s levels of carbons bonded to the amino group into the LUMO+2 give rise to the low intensity feature at 289.0 eV.

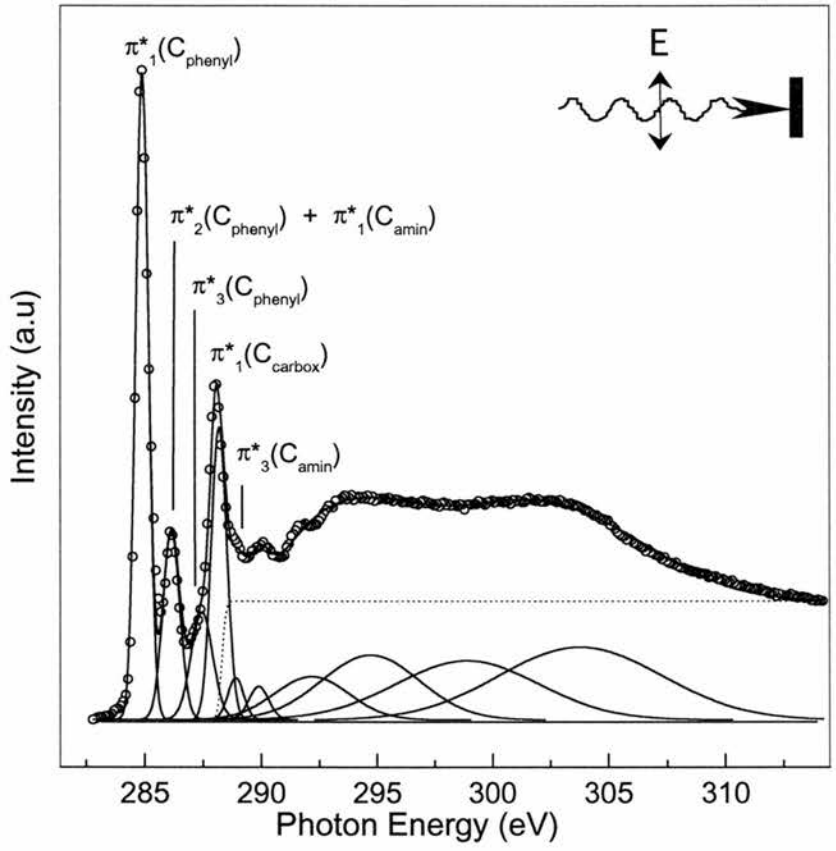

Fig 3. NEXAFS C 1s spectrum of 4-aminobenzoic acid on Na/Si(100)-2x1. The energy scale has been calibrated using the carbon contaminant peak adsorbed on the gold grid.

Fig 4. displays the NEXAFS C K-edge spectra of (a) multilayers 4-aminobenzoic acid and (b) monolayer 4-aminobenzoic acid adsorbed on Na/Si(100)-2x1 recorded at grazing and normal incidence angles respectively. The π^* resonances exhibit a strong angular dependence in both the monolayer and multilayer regimes. However, no remarkable differences are observed in the overall shape of the NEXAFS spectra. In the

multilayer regime, an analysis of the π^*_1 resonance gives a tilt angle of 24°±5° between the molecular plane and the surface plane. In the monolayer regime, the analysis of the intensities of the π^*_1 resonance at 285.0 eV gives an intensity ratio of 0.78 for normal to grazing incidence angles. From this ratio, we calculate a polar tilt angle α between the molecular plane and the surface plane of 61°±5°.

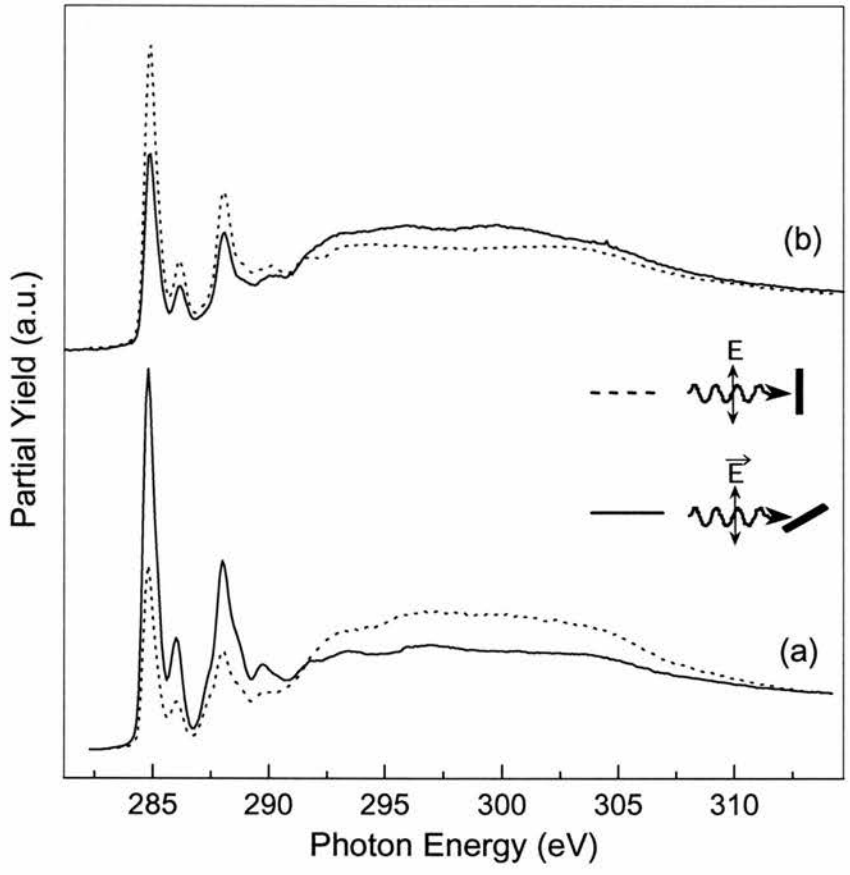

Fig 4. Comparative of NEXAFS C 1s spectra of (a) multilayers amino benzoic acid and (b) monolayer ABA on Na/Si(100)-2x1 recorded at normal and grazing incidence angles.

Fig 5 shows the O1s NEXAFS spectra of (a) multilayers 4-aminobenzoic acid and (b) 4-aminobenzoic acid on Na/Si(100)-2x1 recorded at grazing and normal incidence angles. The multilayer spectra show two characteristic π^* resonances at 534 eV and 536 eV respectively. These resonances correspond to excitations from O1s atomic levels into the first and second multilayer unoccupied molecular orbitals. The resonances

observed above 540 eV are due to excitations into unoccupied molecular orbitals with a strong σ* character.

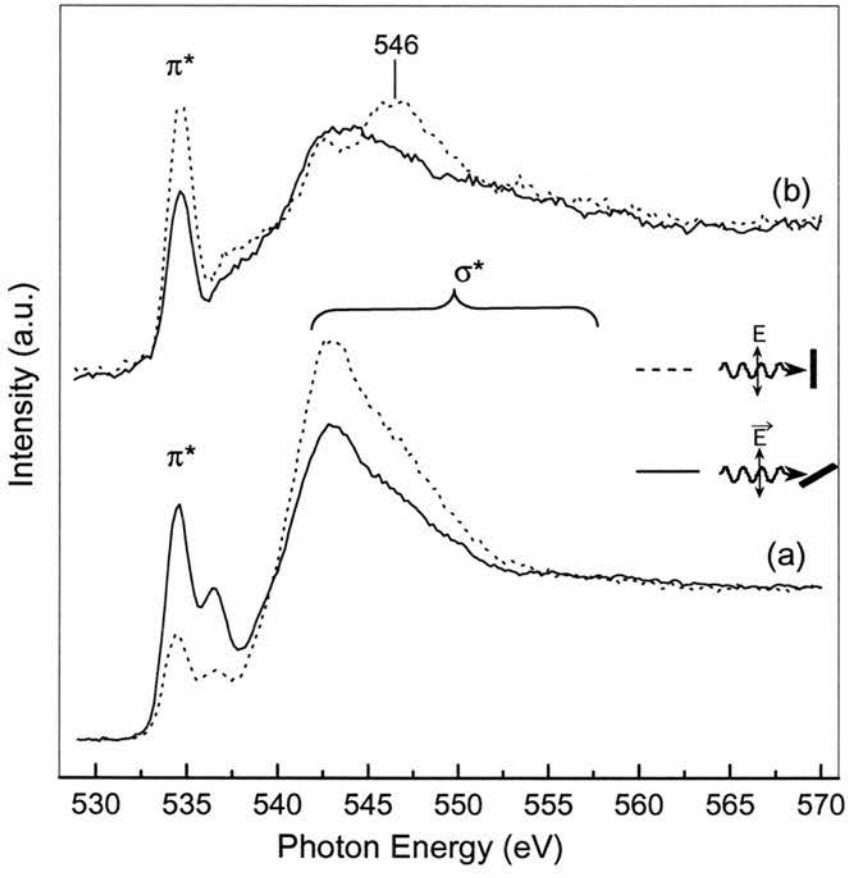

Fig 5. O1s NEXAFS spectra of (a) multilayers 4-aminobenzoic acid and (b) 4-aminobenzoic acid on Na/Si(100)-2x1 recorded at normal and grazing incidence angles.

All the resonances assigned above are visible in the monolayer regime except for a new feature appearing at 546 eV in the normal incidence spectrum. This peak cannot be straightforwardly assigned to a σ* resonance. The σ* resonances are expected to be less intense than π* resonances at normal incidence angles. However, on the normal incidence angle spectrum of 4-aminobenzoic acid on Na/Si(100)-2x1 the peak at 546 eV increases its intensity compared with the grazing incidence angle spectrum. Chapter 2 gave a detailed description of the different detection modes in NEXAFS and the experimental setups to avoid photoemission peaks appear in the X-ray absorption spectrum. The partial electron yield mode (PEY) used as grid, which was set to a

negative potential to stop photoemitted electrons entering the detector. In this case, the feature appearing at 546 eV photon energy, is originated from electrons coming from energy levels situated at: 546 eV-150 eV=396 eV (-150 V was the retarding voltage applied in our experimental setup). This clearly indicates that the voltage applied to the grid was not sufficient to avoid the N1s photoemission peak to enter the scanned energy region. The photoemission peak is only observed clearly in the monolayer spectrum, since in the multilayer case the stronger intensity of the adjacent σ^* resonance makes it impossible to distinguish from the background. The angular dependence of the π^* resonance in the monolayer regime confirms the orientation predicted from the analysis of the NEXAFS C1s edge. In the multilayer case, the stronger intensity of the π^* resonances in the grazing incidence angle spectrum, shows clearly that the molecules are oriented preferentially parallel to the surface.

The N1s NEXAFS spectrum of 4-aminobenzoic acid on Na/Si(100)-2x1 recorded at normal incidence angle is shown in fig 6.

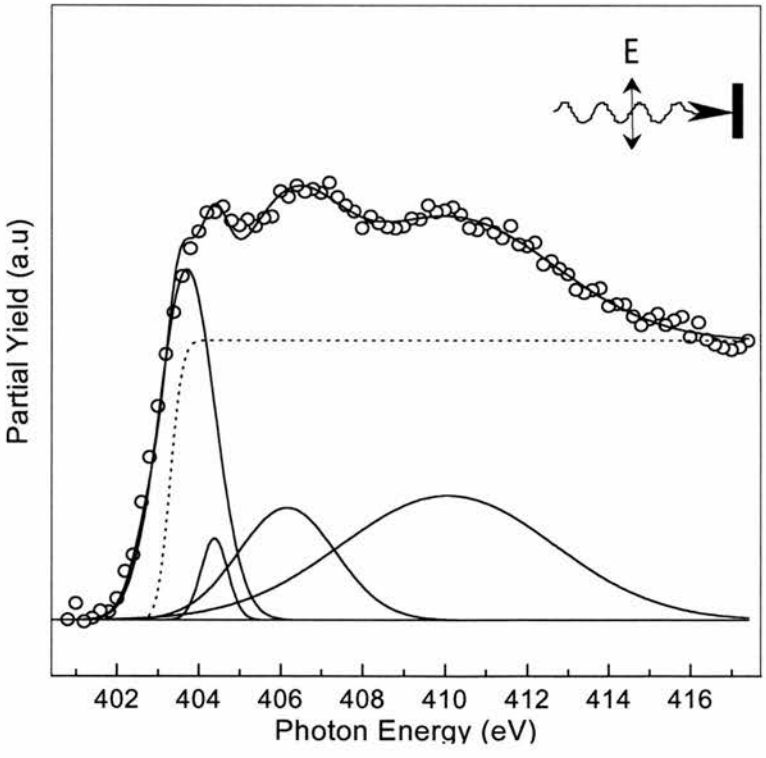

Fig 6. N1s NEXAFS spectrum of 4-aminobenzoic acid on Na/Si(100)-2x1.

By comparison with our ab initio calculations, we attribute the π^* resonances at 403.7 eV and 404.7 eV to transitions from N1s atomic levels into the LUMO and LUMO+1 of the adsorbed molecule.

Fig 7 shows the N1s NEXAFS spectra of (a) multilayers 4-aminobenzoic acid and (b) 4-aminobenzoic acid on Na/Si(100)-2x1 recorded at grazing and normal incidence angles. Note that the first π^* resonance observed in the multilayer spectra shifts by 1 eV in the monolayer spectra. Additionally, the angular dependence of the π^* and σ^* resonance show the expected behaviour.

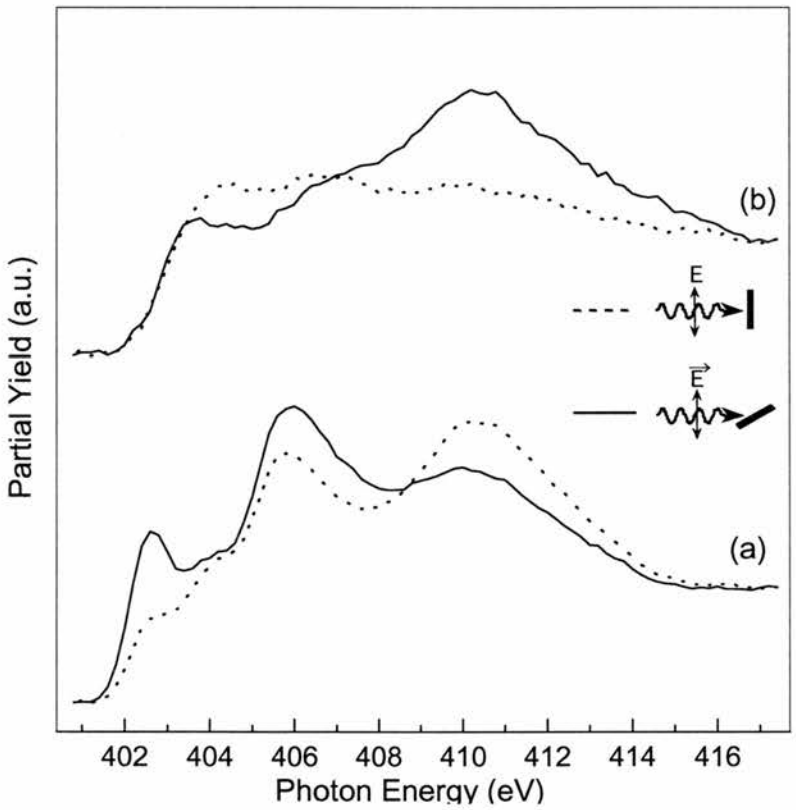

Fig 7. N1s NEXAFS spectra of (a) multilayers 4-aminobenzoic acid and (b) 4-aminobenzoic acid on Na/Si(100)-2x1 recorded at normal and grazing angles.

In the multilayer spectra the observed angular dependence of the π^* resonances points to a preferred orientation of the molecules parallel to the surface plane. In contrast, in the monolayer regime, the observed angular dependence shows that the 4-amino

benzoate species stand upright on the surface. This behaviour was also observed for the C1s and O1s edges and the precise orientation of the molecules was determined.

5.3.3 XPS:

The relative position of the C1s energy levels has been determined using XPS. Fig 8 shows the x-ray photoelectron spectrum (XPS) multilayers of 4-aminobenzoic acid. As it has been explained in previous chapters, the understanding of the core levels is essential for the analysis of the NEXAFS spectra since electrons are being excited from these atomic orbitals into the unoccupied molecular orbitals. In the case of the C1s edge, the splitting of the C1s atomic level is likely to occur in 4-aminobenzoic acid since three distinguishable type of carbon atoms are present in the molecular structure. The carbon atoms in the carboxylate group have a chemical environment different to that of the carbon atoms in the benzene ring and carbon atoms linked to the amino group.

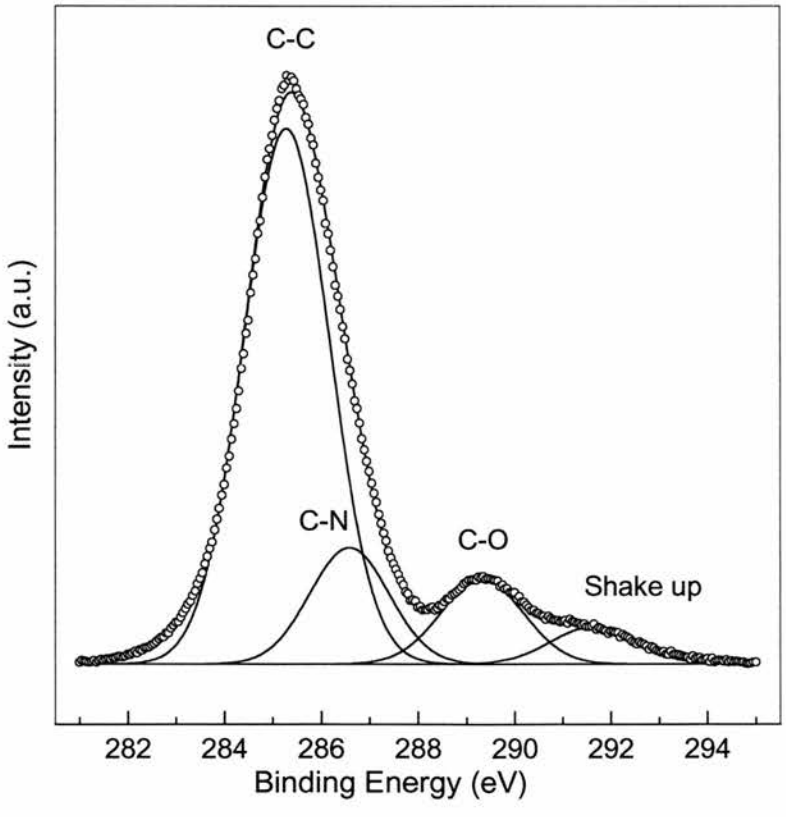

Fig 8. XPS of multilayers 4-aminobenzoic acid. Note the expected three photoemission peaks of the three different carbon atoms present in the molecule.

The splitting of 1s levels due to different chemical environments is reported in the literature as "chemical shift" and it has been widely studied for a large number of elements.

5.3.4. Ab initio study:

Ab initio methods have been used to model the unoccupied molecular orbitals and simulate the vibrational spectrum to assist the interpretation of the HREELS and NEXAFS data. The cluster calculations have been performed using the GAUSSIAN 98 [4] software under the *b3lyp* functional and 6-31G basis set. Initially, we have calculated the geometry and frequencies of undisturbed 4-aminobenzoic acid in order to validate the used approximations. The geometry optimisation predicts a molecular structure which is in good agreement with the reported by crystallographic data [5-6]. By comparison with previously published vibrational of amino acids [2] [7-10], all calculated frequencies have been scaled by a factor of 0.98. 4-aminobenzoic acid adsorbed on Si(100)-2x1 has been modelled as one 4-aminobenzoic acid molecule interacting with a silicon cluster. The optimisation procedure was carried out in two stages. Firstly, a Si_8H_{12} cluster consisting of eight-silicon atoms with all bonds saturated with hydrogens was fully optimised. Secondly, the 4-aminobenzoic acid molecule was adsorbed on the dimer and the geometry of the silicon/hydrogen cluster was frozen during the geometry optimisation. The cluster used for the adsorbed 4-aminobenzoate species on Na/Si(100)-2x1 consisted of a single 4-aminobenzoic acid molecule interacting with a Na atom via the carboxylate group. This approach is justified by the strong interaction between the carboxylate group and the Na atom indicated by the HREELS data.

The optimised structure of 4-aminobenzoic acid on the silicon cluster predicts a geometry in which the sum of the angles in the amino group is 354°. In the case of amino benzoic acid on Na the sum is 352°. Following an optimisation of the geometry, the vibrational frequencies were calculated via computation of the force constants. The calculated frequencies in comparison with those obtained from the vibrational spectra of Na/Si(100)-2x1 exposed to 4-aminobenzoic acid were shown in table 1. Fig 9 displays the empty π^* molecular orbitals and the contribution from p_z atomic orbitals for (a)

adsorbed amino benzoate and (b) undisturbed amino benzoic species. The expected transitions from C1s levels into those molecular orbitals are also shown for the monolayer regime. Note that some transitions are not allowed for carbons in the carboxylate and amino groups. The p_z contribution from nitrogen atoms to the LUMO of adsorbed amino benzoate species is reduced compared with the undisturbed molecule (see fig 4). Table 2 shows the energy differences between the π^* resonances observed in C1s NEXAFS compared with the expected transition energies obtained from our calculations. The energies are relative to the lowest transition.

The Mulliken charges analysis shows that in the case of 4-aminobenzoic acid adsorbed on Na, the carboxylate group and the benzene ring become more negative compared with the undisturbed molecule.

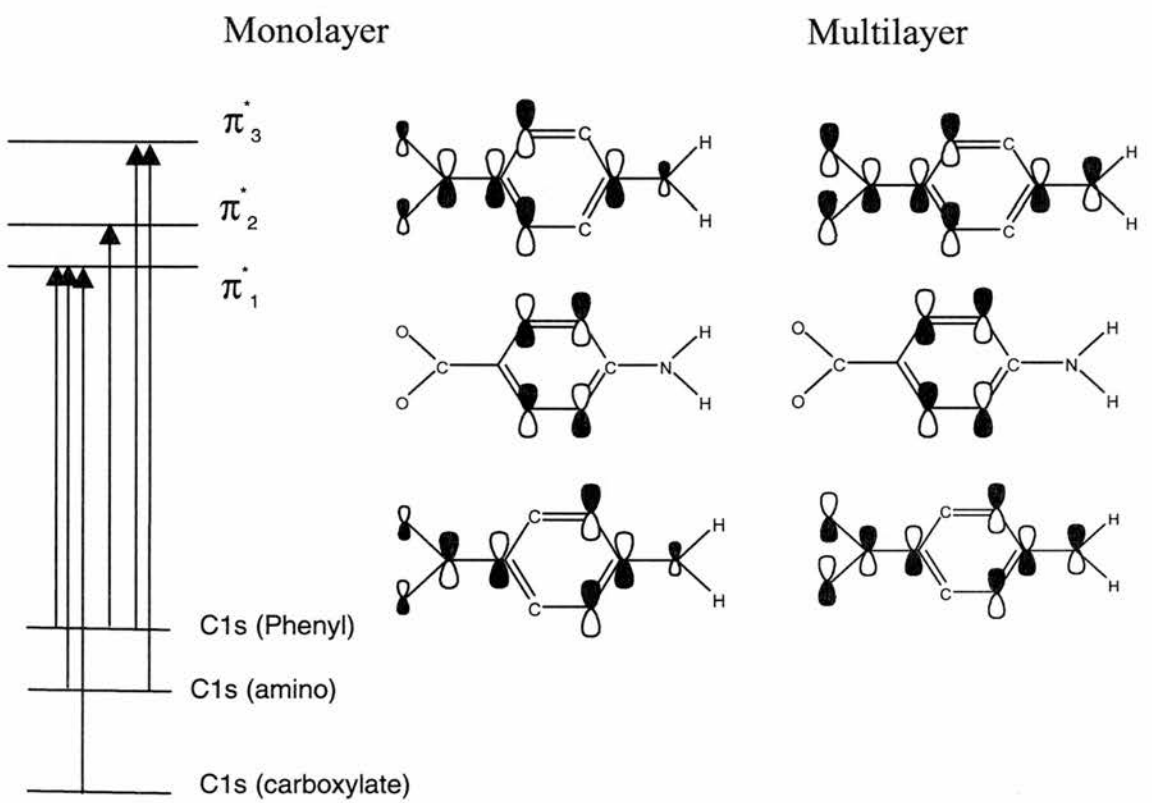

Fig. 9. Expected transitions for amino benzoic acid on Na obtained from the *ab initio* study. Additionally the contributions from the atoms in the molecule to the unoccupied molecular orbital are show for the monolayer and multilayer regimes. The splitting of the C1s atomic levels has been taken from XPS data.

Observed in NEXAFS	Using GAUSSIAN 98	Assignment
0.0	0.0	C1s(Phenyl)->π^*_1
1.1	0.97	C1s(Phenyl)->π^*_2
	1.15	C1s(Amino)->π^*_1
2.5	2.8	C1s(Phenyl)->π^*_3
3.2	3.9	C1s(Carbox)->π^*_1
3.9	4.0	C1s(Amin0)->π^*_3

Table 2. Assignments of the π^* resonances obserevd in NEXAFS by comparison with ab initio calculations.

5.4. Discussion:

The vibrational spectrum of 4-aminobenzoic acid adsorbed on clean Si(100)-2x1 shows that the species bond to the surface, mainly through cleavage of the OH bond and the formation of a Si-O linkage. The bonding of 4-aminobenzoic acid to the surface through the amino group would lead to the observation of a band at 3600 cm^{-1} , attributed to a ν(OH) [11] stretching mode that is absent in the spectrum (a). Additionally the band assigned to $\delta(NH_2)$ vibrations would not be visible in case of reaction of the amino group with the silicon surface. However, a minority of species bonded through the amino group can not be discarded from the vibrational spectrum.

The adsorption geometry of alkali metals Na on Si(100)-2x1 has been described in detail in chapter 1 and references there in. It has been shown that at saturation coverage Na atoms adsorb on Si(100)-2x1 on a cave site between two silicon dimers. In this adsorption geometry Na atoms form rows parallel to the dimer rows.

The HREELS data show clearly that the bonding geometry of 4-aminobenzoic acid to Si(100)-2x1 is dramatically modified by co-adsorbed Na atoms. The sharp feature observed at 1420 cm^{-1} in the HREEL spectrum of 4-aminobenzoic acid on Na-Si(100)-2x1, shows clearly that bonding occurs exclusively via the carboxylate group, leading to 4-aminobenzoate species in bidentate coordination. The absence of the carbonyl and

asymmetric bands at 1705 cm^{-1} and 1495 cm^{-1} supports this adsorption model. The amino group related bands observed at 3460 cm^{-1}, 1620 cm^{-1} and 370 cm^{-1} indicate that this adsorption geometry leads to an amino terminated surface with NH_2 groups pointing out into the vacuum. In Accordance with these experimental results, we suggest a structural model in which the 4-aminobenzoate species adsorb on Na/Si(1001)-2x1 through the formation of a delocalized bond between the deprotonated carboxylate group and the Na atom. Heating the sample to 300 °C, results in significant desorption of amino groups from the surface, while benzoate species are still present at the surface. The line width broadening is most likely attributed to an increase of the surface disorder [11].

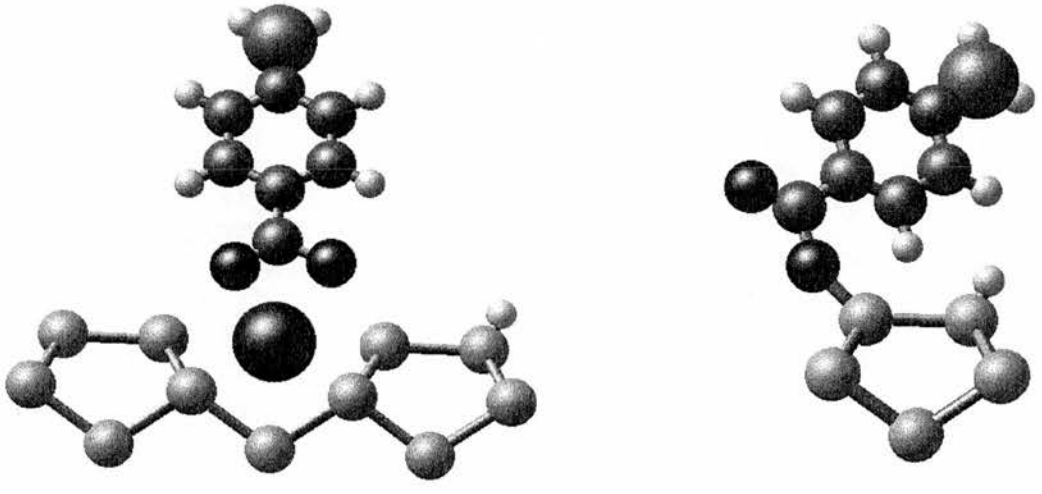

Fig 10. Adsorption geometries for amino benzoic acid on Na/Si(100)-2x1 and on Si(100)-2x1

The C1s NEXAFS spectra show a strong angular dependence of the π^* resonances. In the monolayer regime an analysis of the intensity gives a polar tilt angle between the phenyl ring and the surface plane of 61°±3°. This is consistent with the adsorption model proposed from the HREELS data. In the multilayer regime, the observed angular dependence is reversed. This indicates that condensing 4-aminobenzoic acid on the sample leads to the growth of a 4-aminobenzoic acid crystal in which the

molecules are preferentially oriented parallel to the surface plane. The O1s and N1s NEXAFS spectra of the monolayer and multilayer regimes support these hypotheses.

The π^* resonance observed at 402.5 eV in the N1s multilayer spectra, shifts by 1.2 eV in the monolayer spectra. Based in our calculation we have assigned this resonance to transitions from N1s levels into the LUMO. We attribute the shift in the position of the resonance to a disturbance originated from the extraction of a N1s electron that shifts all the energy levels downwards. The Mulliken charge analysis shows that the benzene ring becomes more negative in the presence of a Na atom attached to the carboxylate group. The perturbance originated after the extraction of the 1s electron is greater in the 4-aminobenzoic acid/Na system since there is less charge in the benzene ring to restore the equilibrium and therefore all the energy levels become more tightly bounded.

The calculations show a decrease on the p_z contribution of N1s atoms to the LUMO. This is consistent with the change in the molecular geometry of amino benzoic acid on Na compared with the undisturbed molecule. Since the calculations predict a geometry of amino benzoic acid/Na on which the hydrogens atoms in the amino group move towards the tetrahedral structure, the interaction between the amino group and the benzene ring becomes reduced.

5.5. Conclusions:

The deposition of the Na template on Si(100)-2x1 has clearly modified the adsorption geometry of this amino acid on the substrate. HREELS experiments have shown that the surface chemistry is radically different in the Na modified surface compared with the clean Si. The strong angular dependence of the NEXAFS resonances clearly demonstrate that long-range order is achieved and 4-aminobenzoate species adsorb on the surface via the carboxylate group leading to an amino terminated. The 3D model in fig 12 shows the rows of dimers with Na adsorbed on cave sites and 4-aminobenzoate species bonded to Na in bidentate coordination.

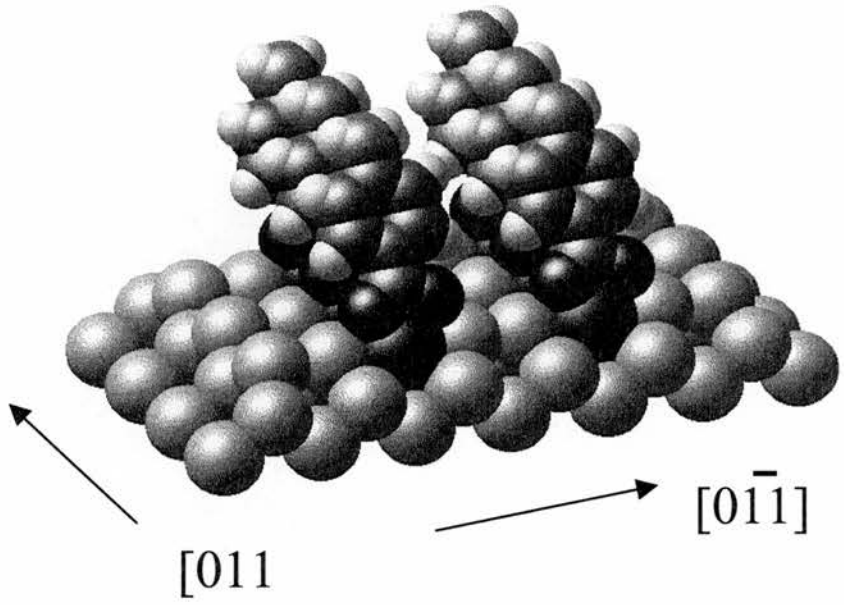

Fig 11. Model of Amino benzoic acid/Na/Si(100)-2x. Note that the amino groups are not involve in the chemisorption process and are available for further film growth.

5.6. References:

[1]S.M. Barlow, K.J. Kitching, S. Haq, N.V. Richardson. Surface Science 401 (1998) 322-335

[2] J.H.S. Green. Spectrochimica Acta 33A (1977) 575-581

[3] M. Tikhov, G. Boishin, L. Surnev. Surface Science 241 (1991) 103-110

[4] M.J. Frisch *et al.* GAUSSIAN 98, Gaussian, Inc., Pittsburgh, PA (1998)

[5] M. Tsuboi. Spectrochimica Acta 16 (1960) 505-512

[6] T.F. Lai, R.E. Marsh. Acta Crystallographica 22 (1967) 885-891

[7] J.H.S. Green, D.J. Harrison. Spectrochimica Acta 26A (1969) 1925-1937

[8] J.H.S. Green, W. Kynaston, A.S. Lindsey. Spectrochimica Acta 17 (1961) 486-502

[9] K. Machida, A. Kuwae, Y. Saito, T. Uno. Spectrochimica Acta 34A (1978) 793-800

[10] D. Hadzi, N. Sheppard. Journal of Chemical Physics 477 (1979) 236-256

[11] A. Lopez, T. Bitzer, T. Heller, N.V. Richardson. Surface Science 473 (2001) 108-116

CHAPTER 6

Adsorption of simple alcohols on Si surfaces

6.1. Introduction:

Organic additives to HF and KOH based systems for the etching of silicon wafers have been widely employed in microelectronics for a long time [1-3]. For anisotropic etching of silicon, aqueous potassium hydroxide-isopropanol (KOH-IPA) is typically used [2-4]. Although studies have shown that the addition of IPA ($(CH_3)_2CH\text{-}OH$) to the alkaline etching bath not only moderates the etching process but also improves the surface finish, the mode of action of the organic additive is still not known [4]. An improved surface finish, i.e. a surface roughness on the atomic scale, is highly desirable for the production of nanostructures for sensors and optoelectronic and micro-mechanical devices. In addition, a precise control of the etching process is essential to guarantee the 3-dimensional resolution required for the micromachined silicon surfaces.

In order to improve the understanding of the chemistry at the etchant/Si interface, we concentrate on the adsorption of ethanol (CH_3CH_2OH), isopropanol ($(CH_3)_2CHOH$) and tert-butanol ($(CH_3)_3CHOH$) on the Si(100)-2x1, Si(113)-3x1 and Si(115)-3x1 surfaces under ultra-high vacuum (UHV) conditions. The chemisorption of the alcohols such as ethanol, isopropanol and *tert*-butanol was found to occur through cleavage of the O-H bond and the formation of a Si-O-C linkage. Further exposure to water of these saturated substrates has been carried out, in order to understand the competitive adsorption of water and alcohols on Si(100)-2x1, Si(113)-3x1 and Si(115)-3x1. High resolution electron energy loss spectroscopy (HREELS) and low energy electron diffraction (LEED) have been employed to follow the adsorption of H_2O on alkoxy passivated Si(100), Si(113) and Si(115) surfaces. Additionally, *ab initio* calculations of the surface complexes were carried out in order to explain the reduction of the reactivity towards water molecules of Si(100)-2x1 after ethanol, *tert*-butanol and, specifically, isopropanol saturation.

On the other hand, we have carried out experiments of the adsorption of benzyl alcohol on clean and Na modified Si(100)-2x1 surfaces. In previous chapters it was shown that the deposition of a Na template dramatically modifies the chemistry at the Si(100)-2x1 surface. In the case of the adsorption of amino acids, we demonstrated that Na induces an ordering that is reflected in the angular dependence of the NEXAFS resonances. In the case of benzyl alcohol adsorbed on clean and Na modified Si(100)-2x1, we used HREELS to obtain information about the bonding between the molecules and the substrate and NEXAFS to determine the possible orientation of the species at the surface.

6.2. Experimental:

Samples sized 17 x 6 mm^2 have been cut from n-type Si (100) wafers with a resistivity of 2 – 10 Ωcm and mounted on a sample carrier with Ta clips. After a prolonged outgassing of the carrier and Si sample, the native oxide layer was thermally removed by resistive heating. We would like to emphasize that the clean sample HREELS spectrum showed no Si-C or Si-O related features. The technique is able to detect up 0.1% of a monolayer [10]. Prior to the admittance into UHV, the alcohols and distilled water were purified by several pump-freeze cycles. The alcohols and water were admitted into UHV through leak valves. While dosing, the pressure did not exceed the 10^{-6} mbar range. All experiments, including dosing, were carried out at room temperature.

The exposure to air (5 μm particle filter) at normal pressure was carried out in a glove box, which was directly attached to the fast entry lock chamber of the UHV system. For the treatment of the sample at normal pressure, the sample was first transferred into a load lock chamber under UHV, then this chamber slowly vented with dry nitrogen gas and finally the sample transferred into the glove box at normal pressure. After the conditioning in the glove box, the sample was returned into the fast entry lock chamber, which was first slowly evacuated by a l-N_2 sorption pump below 10^{-1} mbar and then pumped to the 10^{-7} mbar range with a turbo-molecular pump. For the vibrational analysis the samples were then transferred into the HREEL spectrometer (VSW Ltd., HIB

1000). All vibrational spectra were recorded at room temperature with a primary electron energy of 6 eV in specular scattering geometry ($\theta_i = \theta_s = 45°$). The LEED patterns were recorded at an electron energy of 100 eV. The NEXAFS experiments were carried out at HE-TGM2 beam line at BESSY I (Berlin, Germany). The NEXAFS data was normalised dividing the sample spectrum by the transmission function of clean Si(100)-2x1. Correction of the storage ring current has been performed using a gold grid monitor at the entrance of the UHV chamber. The photon energy was calibrated using the carbon K-edge on the peak at 284.7 eV of contaminant carbon adsorbed on the gold grid.

6.3. Results:

6.3.1. HREELS results.

Fig. 1 shows the HREEL spectra of Si(100), Si(113) and Si(115) exposed to 20 L (1L =1x10^{-6} Torr s) of ethanol at room temperature.

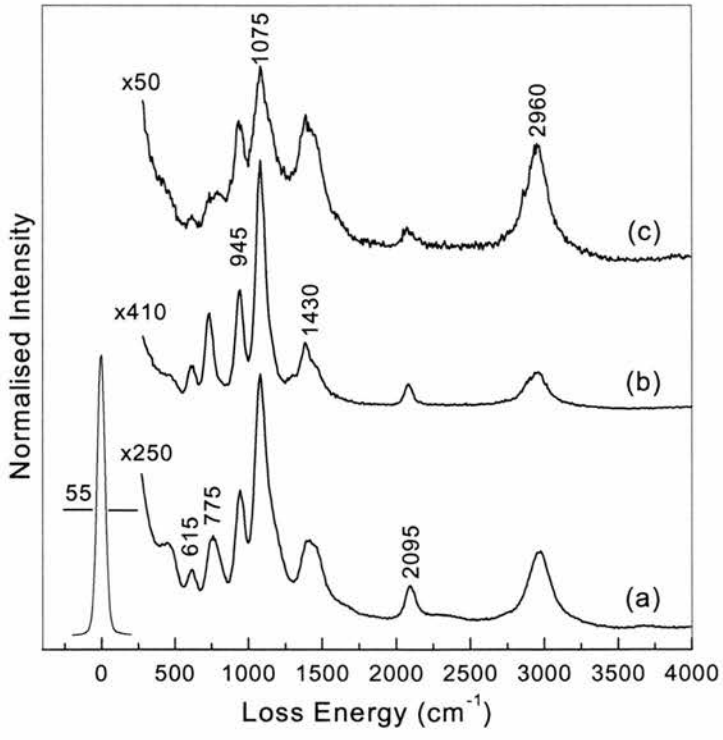

Fig 1. HREEL spectra of (a) Si(100), (b) Si(113) and (c) Si(115) exposed to 20 L ethanol at room temperature.

In the three spectra, external modes assigned to the β(SiH) bending, the ν(SiO) stretch and the ν(SiH) stretch can be observed at 615 cm^{-1}, 775 cm^{-1} and 2095 cm^{-1}, respectively [6,5]. The loss peaks at 945 cm^{-1}, 1075 cm^{-1} and 2960 cm^{-1} are related to the C-C skeleton, the ν(CO) and the ν(CH) stretching modes [7,8]. The symmetric and antisymmetric $\delta(CH_3)$ deformation modes give rise to the broad peaks at 1430 cm^{-1} [7]. In LEED, following ethanol adsorption, we observed sharp 2x1 diffraction spots for Si(100) and 3x1 spots for Si(113) and Si(115). These indicate that the surface reconstructions were not changed by the chemisorption of ethanol. Obviously, ethanol chemisorbs on the three surfaces via a cleavage of the OH bond and bonds to the Si substrate through a Si-O-C linkage. The dissociated hydrogen most likely saturates one of the nearest dangling Si bonds.

Following the exposure of the ethoxy saturated surfaces to 10 kL of H_2O, only a faint 1x1 LEED pattern on a bright, diffuse electron background could be seen. The corresponding vibrational spectra are shown in Fig. 2.

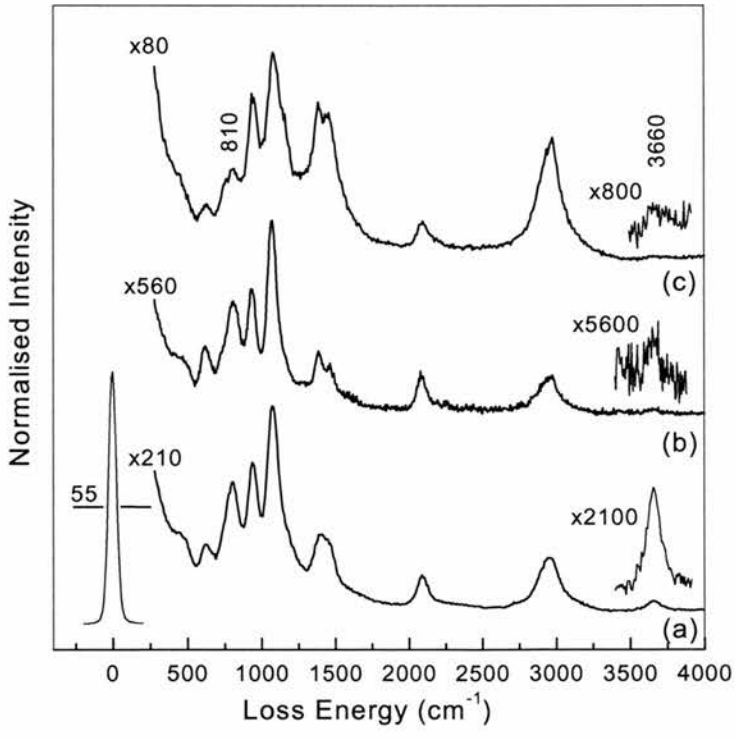

Fig 2. Vibrational EEL spectra of chemisorbed ethanol (20 L) on (a) Si(100), (b) Si(113) and (c) Si(115) at room temperature and after subsequent exposure to 10^4 L H_2O.

In comparison with the spectra in Fig. 1, the intensity of the ν(CO) stretching mode at 1075 cm^{-1} has in all cases decreased with respect to the other modes. The chemisorption of H_2O on the ethoxy modified Si(100), Si(113) and Si(115) surfaces is indicated by the loss peak at 3660 cm^{-1}, which can be assigned to the ν(SiO-H) stretching mode [9]. The δ(Si-OH) bending mode can be found at 810 cm^{-1} [9]. Some increase in intensity of the Si-H band at 2045 cm^{-1} is also observed. On the basis of the HREELS and LEED results, it is evident that the chemisorption of H_2O on the three surfaces occurs via a cleavage of the Si-Si bonds and loss of the 2x1 reconstruction.

The vibrational EELS data of *tert*-butanol chemisorbed on Si(100), Si(113) and Si(115) at room temperature are given in Fig. 3. In curves (a) and (b), the ν(CO) stretching mode gives rise to the intense peak at 1010 cm^{-1}[8]. In curve (a), the symmetric and antisymmetric ν(CCC) stretching vibrations at 1180 and 1240 cm^{-1} and the symmetric and antisymmetric $\delta(CH_3)$ deformation modes at 1380 and 1450 cm^{-1} are clearly resolved [8,7].

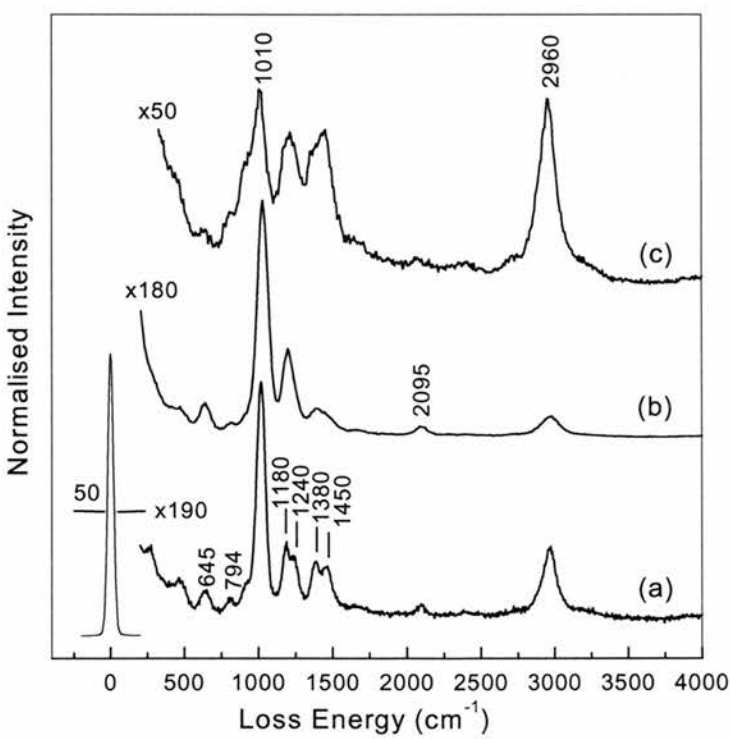

Fig 3. HREEL spectra of (a) Si(100), (b) Si(113) and (c) Si(115) exposed to 20 L *tert*-butanol at room temperature.

We attribute the weak features at 645, 795 and the 2095 cm^{-1} to the β(SiH) bending, ν(SiO) and ν(SiH) stretching modes. The ν(CH) stretch is present at 2960 cm^{-1}. In LEED, sharp spots could be observed indicating the 2x1 reconstruction for Si(100) and the 3x1 reconstruction for Si(113) and Si(115). As observed in the case of the chemisorption of ethanol on Si(100), Si(113) and Si(115), *tert*-butanol adsorbs on these surfaces through a deprotonation of the OH group and the formation of a Si-O-C linkage. Once again, following the exposure of these surfaces to 10 kL H_2O, a significant intensity for the ν(SiO-H) stretch at 3660 cm^{-1} is present in the HREELS spectra (Fig. 4) of *tert*-butoxy/Si(100), Si(113) and Si(115). The δ(Si-OH) bending vibration of chemisorbed water can be observed at 810 cm^{-1}. The *tert*-butoxy related loss peaks are virtually unaffected by the chemisorption of water which we suggest occurs by the cleavage of Si-Si bonds, as indicated by the loss of the reconstruction in LEED.

Figure 4 shows the HREEL spectra of the *tert*-butoxy saturated (a) Si(100), (b) Si(113) and (c) Si(115) surfaces after exposure to 10 kL of water.

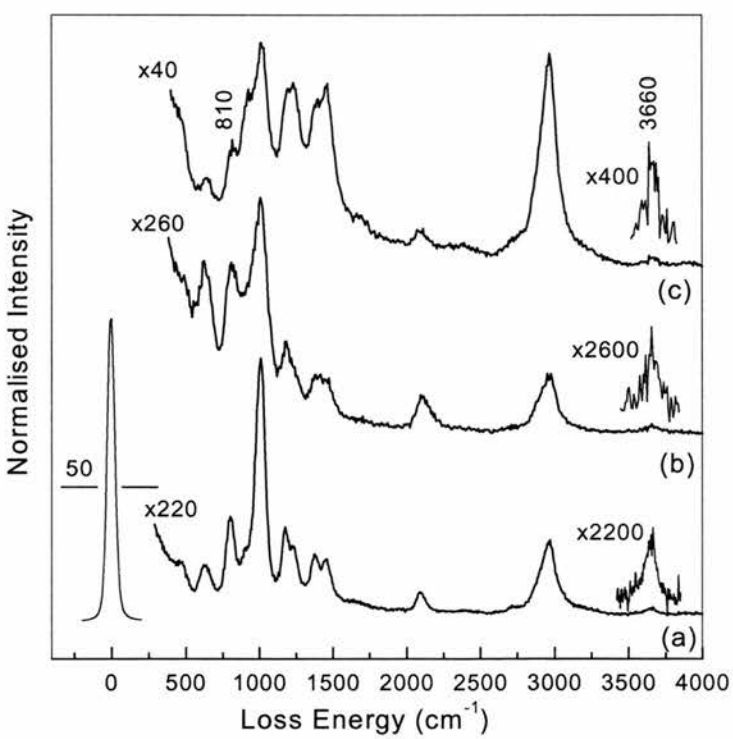

Fig 4. HREEL data of the chemisorption of water on the *tert*-butoxy saturated (a) Si(100), (b) Si(113) and (c) Si(115) surfaces.

Fig. 5 displays HREEL spectra of isopropanol chemisorbed on Si(100), Si(113) and Si(115). The loss peaks observed at 625, 730 and 2095 cm^{-1} can be attributed to the β(SiH) bending mode, the ν(SiO) and ν(SiH) stretching vibrations, respectively. The feature at 1015 cm^{-1} is the ν(CO) stretch mode. Features at 1165, 1380, 1450 and 2950 cm^{-1} can be assigned to the ν(CCC) stretch, symmetric and antisymmetric $\delta(CH_3)$ deformation modes and the ν(CH) stretching vibration, respectively [7]. At 2330 cm^{-1} a broad feature can be observed, which we assign tentatively to an overtone of the ν(CCC) stretching mode. Obviously, the isopropoxy species, as for the other alcohols, are bonded to the surfaces through a Si-O-C link.

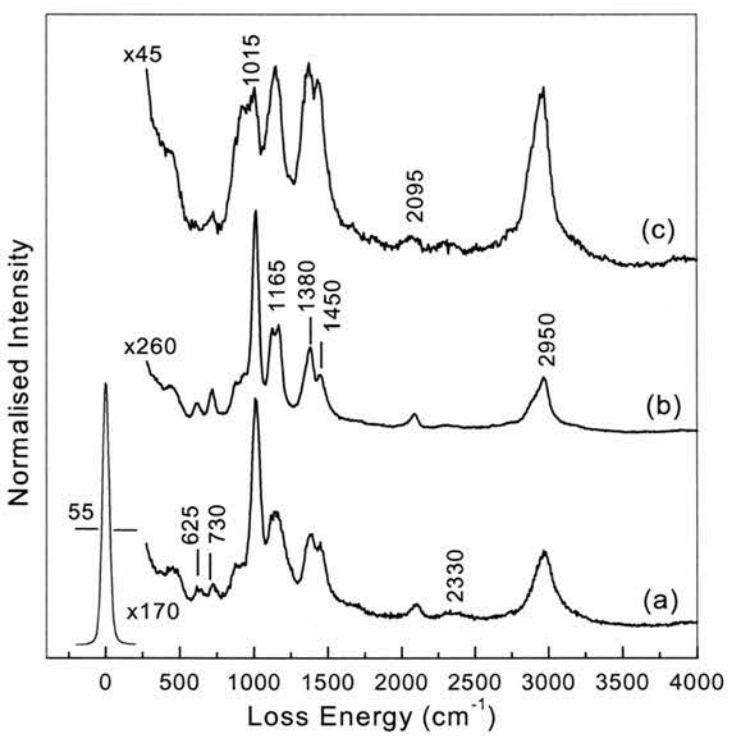

Fig 5. HREEL spectra of (a) Si(100), (b) Si(113) and (c) Si(115) exposed to 20L isopropanol at room temperature.

Figure 6 shows the HREEL spectra of the isopropoxy modified Si(100), Si(113) and Si(115) surfaces exposed to 10 kL H_2O. The features at 3660 cm^{-1} and 810 cm^{-1} observed in (b) and (c) clearly indicate that substantial water chemisorption occurs on the isopropanol modified Si(113) and Si(115) surfaces. In marked contrast, the HREEL

spectra of Si(100) shows no water related peaks which indicates that this substrate is more resistant to water adsorption after isopropanol modification. In order to understand the exceptional lack of reactivity of the isopropoxy saturated Si(100) surface towards water, further experiments involving exposure to air and rinsing with water have been carried out.

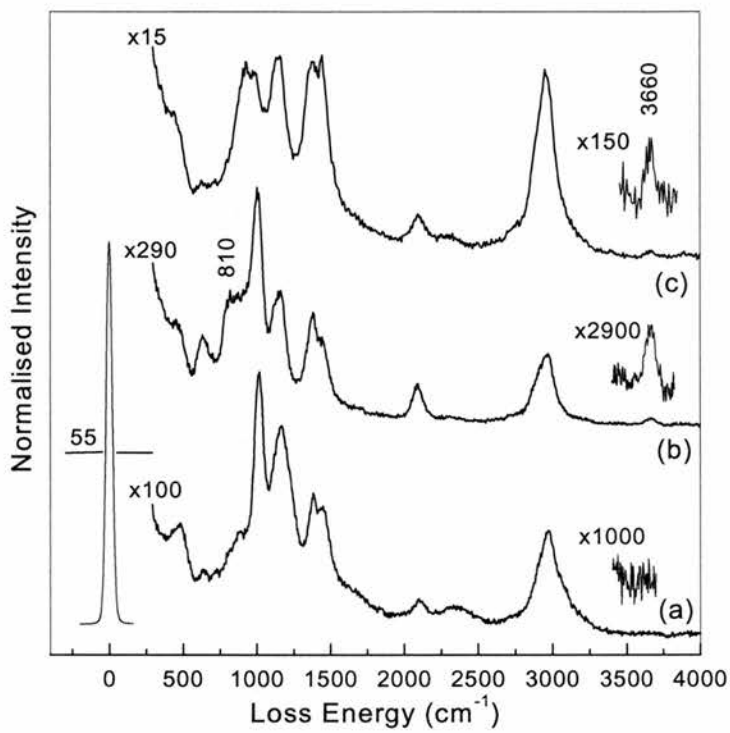

Fig 6. HREELS data of the adsorption of water on the isopropoxy modified (a) Si(100), (b) Si(113) and (c) Si(115) surfaces.

Fig. 7 displays the HREEL spectra of isopropanol chemisorbed on Si(100), following exposure of the sample to 10^4 H_2O, in air at normal pressure and after a 1 minute water rinse. In general, the overall shape of the vibrational spectrum is little affected by these treatments, although the relative intensity of the ν(CO) stretch to the skeleton stretch is considerably reduced after 10 kL water exposure. In spectrum (c), significant intensities for vibrational modes, at 810 cm^{-1} and 3660 cm^{-1} which would indicate the chemisorption of water, are not observed. We estimate an H_2O dosage during the exposure to air of > 10^9 L. A comparison with curve (b) in Fig. 7 shows that the relative intensity of the ν(CO) stretching mode at 1015 cm^{-1} with respect to the ν(CCC)

stretch at 1165 cm^{-1} has decreased. The LEED pattern following exposure of the isopropoxy/Si(100)-2x1 surface to air, is shown in Fig. 8 (b). Although the diffuse electron background has considerably intensified, a weak 2x1 pattern is clearly present. Finally, the isopropoxy/Si(100)-2x1 surface was rinsed with distilled water for 1 min. As can be seen in the top most curve in Fig. 7, the line width at half maximum of the elastic peak has increased to 80 cm^{-1}, which reduces considerably the resolution of the vibrational data. We ascribe the line broadening to the adsorption of contaminants, possibly metal ions [12] and organics during the water rinse. However, even the water rinse does not result in a significant presence in the spectrum of vibrational modes, which could be assigned to the presence of chemisorbed H_2O. Note that only a weak shoulder remains at 1015 cm^{-1}, which we attribute to the formerly intense ν(CO) stretching mode.

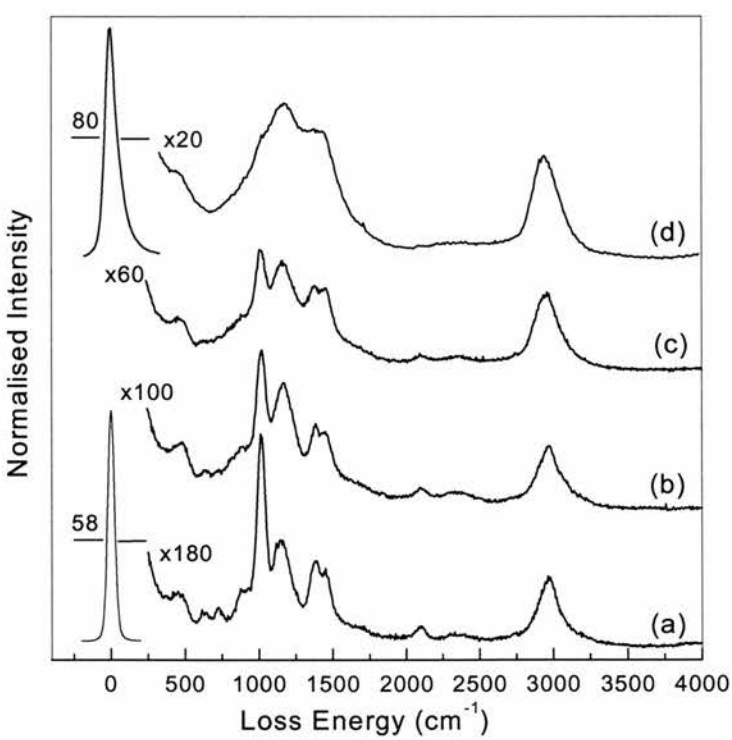

Fig 7. HREEL spectra of isopropanol passivated Si(100)-2x1 after exposures to H_2O and air. Curve (a) shows the spectrum of the Si(100)-2x1 surface, which has been exposed to 20 L isopropanol. Curve (b) was recorded after exposure of the sample to 10^4 L H_2O at room temperature. Curves (c) and (d) present the spectra of isopropoxy/Si(100)-2x1 exposed to air at normal pressure for 1 min and after a rinse with distilled water for 1 min, respectively.

The inert character of the isopropoxy passivated Si(100)-2x1 surface is also seen in LEED (see Fig. 8 (c)) in section 4.3.2. Even though the sample has been rinsed with water, weak 2x1 diffraction spots on a diffuse electron background are still visible, i.e. Si-Si dimer bonds remain intact. This observation demonstrates clearly that the chemisorption of isopropanol reduces dramatically the reactivity of H_2O on Si(100)-2x1 which was not observed for ethanol and *tert*-butanol chemisorbed on Si(100)-2x1.

6.3.2. LEED results:

The LEED images of Si(100) show a 2x1 reconstruction as observed in the figure below. Even after exposure to filtered air the 2x1 pattern is visible, indicating the preservation of the reconstruction.

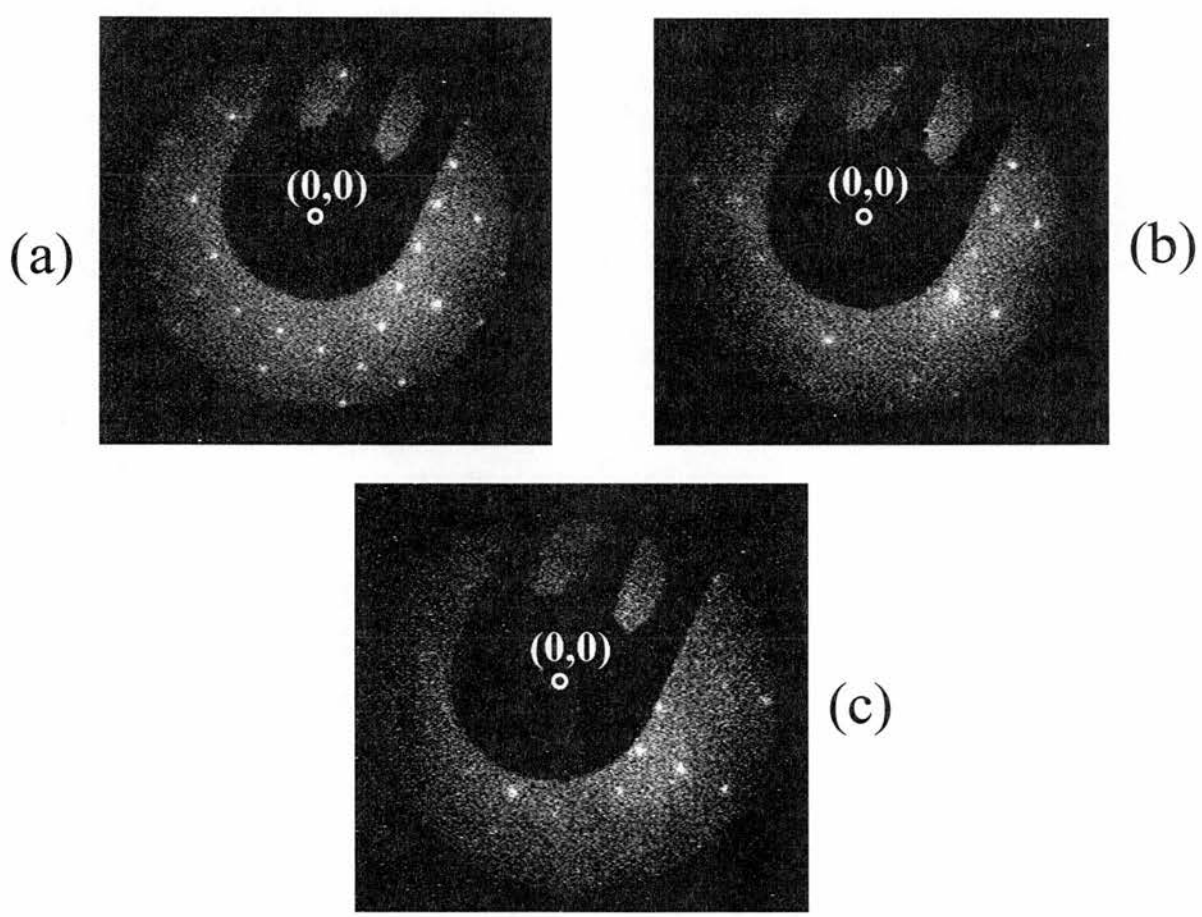

Fig 8. LEED patterns of isopropanol chemisorbed on Si(100) at room temperature (a), after exposure to air for 1 min (b) and following a water rinse (c). Part of the LEED pattern is blocked by the sample holder.

6.3.3. Cluster calculations:

In order to understand the exceptional stability of the isopropoxy modified Si(100) surface, theoretical studies have been carried out using the GAUSSIAN 98 [13] software under the *blyp/6-31* basis set. The cluster used for the adsorption geometry optimisation is shown in Fig. 9.

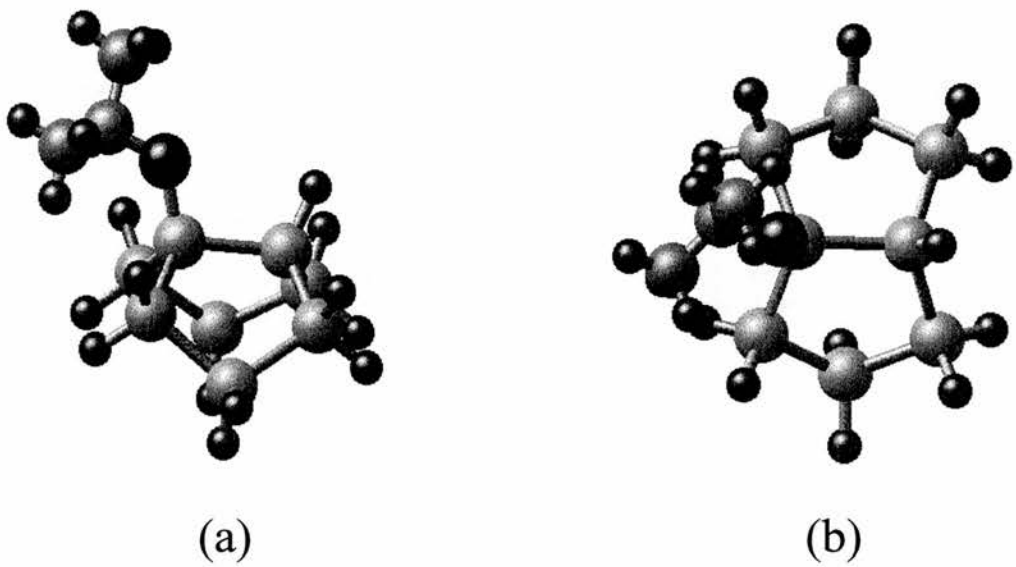

Fig 9. (a) Side and (b) top views of the optimised isopropoxy/Si(100)-2x1 cluster.

As observed, this consisted of eight silicon atoms with the alkoxy species adsorbed on one of the dimer atoms, and hydrogens saturating the rest of the silicon cluster atoms. The optimisation procedure was carried out in two stages. Firstly, a silicon cluster consisting of eight silicon atom with all bonds saturated with hydrogens was fully optimised. Secondly, the ethoxy, isopropoxy and *tert*-butoxy species were adsorbed on one of the dimer atoms and the geometry of the silicon cluster was frozen during the optimisation. For the alkoxy species, we performed several optimisations from different initial configurations in order to understand the potential surface of the adsorbed species on the substrate. The results for the ethoxy and isopropoxy species showed a very low energy barrier (<1 meV) for the free rotation of the molecule around the Si-O axis. It is important to note that some configurations are not possible for the *tert*-butoxy species,

since the methyl groups are obstructed by the silicon dimer. This imposes a restriction on the rotation of the adsorbed molecule around the Si-O axis.

Then, the optimised clusters have been used to model the alkoxy saturated surface as an array of silicon dimers on which the alcohol molecules were randomly adsorbed. The dissociated hydrogen atom was assumed to bond to the other silicon atom of the same dimer. Relaxation of the organic film was accomplished by maximisation of the molecule-molecule distances through the rotation of the alkoxy species around the Si-O axis. This approach is justifiable for the isopropoxy and ethoxy species, as pointed out by the single cluster optimisations. The cluster size has a strong influence in the computation of energy levels and frequencies. However, it should be noted that these calculations were carried out to model the adsorption geometry of the isopropoxy modified surface.

Figure 10 shows the optimised isopropanol/Si(100)-2x1 surface. All intermolecular methyl group distances are larger than 3.6 Å. From the model presented, it can be observed that the isopropoxy species are able to form a dense film on Si(100)-2x1, which may explain the inert character of this surface. Defects can occur in the surface, corresponding to dimers not saturated by isopropoxy species due to hindering by neighbouring molecules. However, approximately 95% of adsorption sites are occupied by isopropoxy species.

Fig. 11 shows the model for the relaxed ethanol/Si(100)-2x1 surface. Again, all intermolecular methyl group distances are greater that 3.5 Å. Ethanol does not form such a tightly packed structure as isopropanol, even though all silicon atoms in the dimer are saturated. This is a consequence of the smaller size of the alcohol due to the single methyl group. Finally, for the *tert*-butoxy modified silicon surface, the model presented in fig.12, clearly indicates that *tert*-butanol passivates significantly less than 50% of silicon dimers due to the size of the molecule.

Since a free rotation of the molecule around the Si-O axis is not possible due to sterical considerations, the adsorption of *tert*-butanol leads to a clearly open structure with many dangling bonds available for reaction with water molecules.

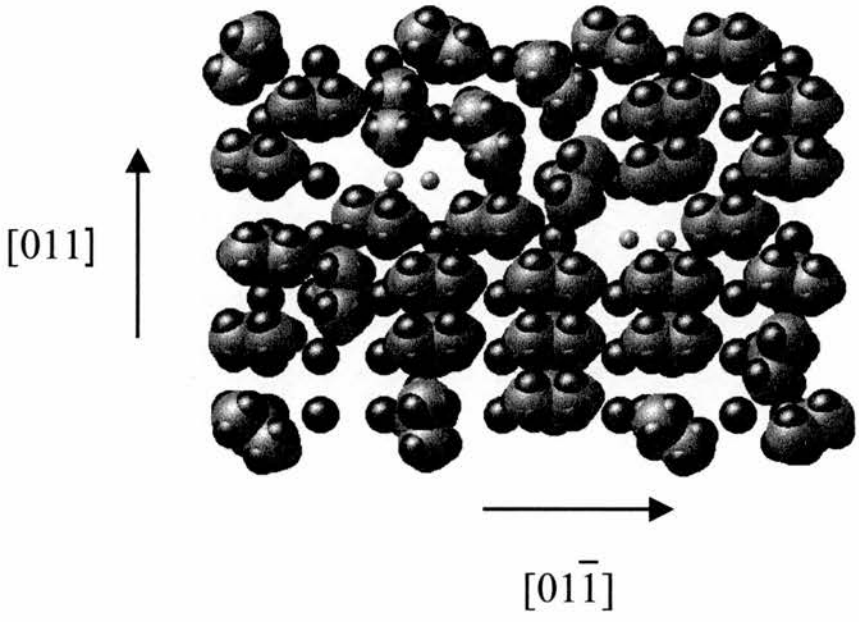

Fig 10. Model of isopropoxy saturated Si(100)-2x1. Van Deer Waals radii shown for all atoms except the Si surface. Note that two vacancies are present where dimers are not saturated with isopropoxy species due to steric restrictions arising from the size of the adsorbed species.

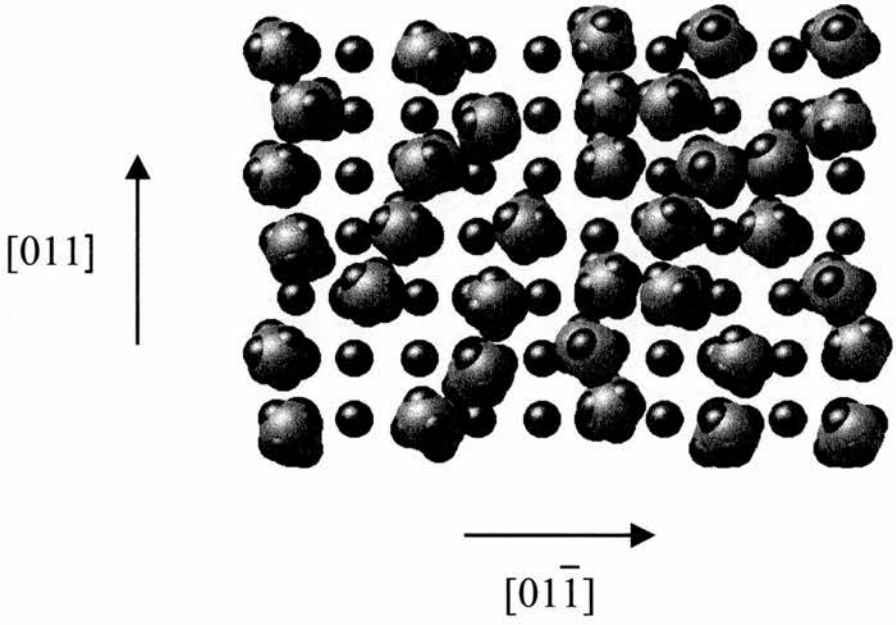

Fig 11. Model of ethanol saturated Si(100)-2x1 surface. Note that although all silicon dangling bonds are saturated, the small size of the alcohol results in a more open structure compared to isopropanol.

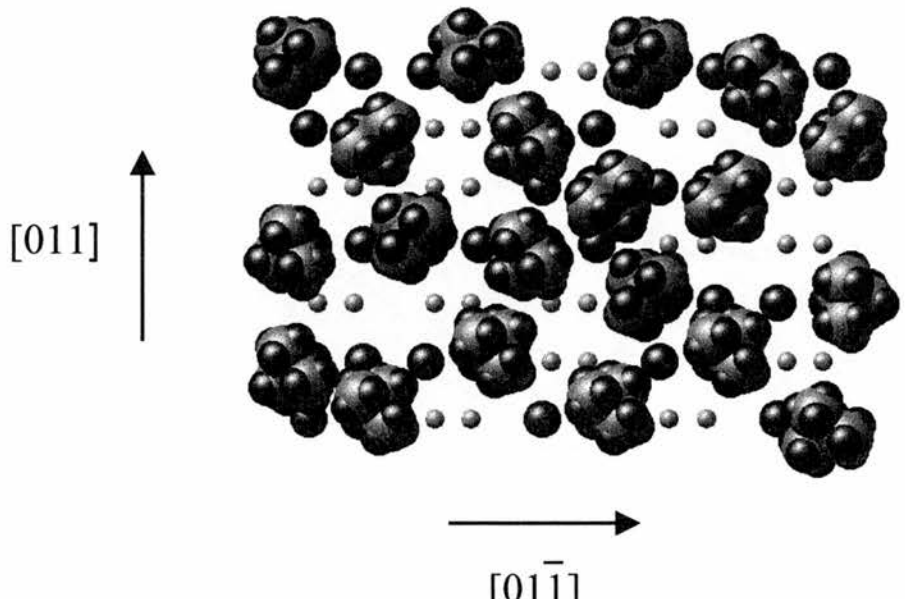

Fig 12. Model for the relaxed *tert*-butoxy/Si(100)-2x1 surface. Note that due to sterical considerations the adsorption of *tert*-butanol on Si(100)-2x1 leads to a clearly open structure.

6.4. Discussion:

The HREEL spectra clearly demonstrate that chemisorption of water is able to occur after saturation with any of the three alcohols on the Si(113) and Si(115) substrates. These surfaces can be regarded as a highly stepped Si(111)-1x1 surfaces with a high number of dangling bonds [14-15]. In this case, we presume that the adsorbed alkoxy species are not able to form a dense film, which inhibits the water adsorption. On the other hand, water chemisorbs on Si(100)-2x1 after saturation with ethanol and *tert*-butanol but the reactivity towards water molecules is significantly reduced after exposure to isopropanol (Fig. 6). The model calculations show that saturation of Si(100)-2x1 with ethanol and *tert*-butanol leads to open structures in which the Si dimers are not shielded and water adsorption is more likely to occur. On the other hand, the isopropoxy species are able to form a packed structure shielding the Si dimers, which reduces the reactivity towards water molecules. However, the exposure of the isopropanol saturated surface to H_2O and to air has induced a disordering of the isopropoxy/Si(100)-2x1 system as the increased electron background in LEED indicates (Fig. 8). This disordering of the organic/Si(100) system is also seen in the HREEL spectra. On ordered surfaces, the

angular distribution of dipole scattered electrons forms a narrow lobe close to the specular direction and higher order diffraction beams [10]. In contrast, on disordered films dipole scattered electrons are found in a larger range of scattering directions. As a result, with a finite acceptance angle of the analyser of the HREEL spectrometer, fewer dipole-scattered electrons are collected in specular direction in the case of a poorly ordered surface in comparison with a well ordered adsorbate structure. Thus, we attribute the decrease of the ν(CO) stretching mode to the disordering of the isopropoxy/Si(100) structure. The precise nature of this disordering process is not yet clear although adsorption of significant quantities of water can be discounted.

6.5. Adsorption of alcohols on Na modified silicon surfaces.

The deposition of a Na template dramatically modifies the chemistry at the Si(100)-2x1 surface in the case of adsorption of amino acids. We have observed a strong interaction of the carboxylate group with the coadsorbed Na atom that modifies completely the adsorption geometry compared with that in the absence of Na. Additionally we have observed a strong angular dependence in NEXAFS that shows clearly a long range order in the adsorbates. We are now interested in the adsorption of alcohols on Na modified Si(100)-2x1. We have used benzyl alcohol to probe the influence of the deposited Na template in the adsorption of alcohols on Si(100)-2x1.

In order to understand the chemical bonds present at the surface, we carried out HREELS experiments of benzyl alcohol adsorbed on the two substrates. Fig 13 shows the on-specular vibrational spectra of benzyl alcohol adsorbed (a) on clean Si(100)-2x1 and (b) on Na/Si(100)-2X1. In the spectrum of benzyl alcohol adsorbed on clean Si(100)-2x1, the band at 750 cm^{-1} is attributed to Si-O vibrations. Benzyl alcohol adsorbs on clean Si(100)-2x1 through cleavage of the OH bond and the formation of a Si-O-C linkage. The cleaved hydrogen atom adsorbs on the adjacent dimer, giving rise to the Si-H band present at 2085 cm^{-1}. The observation of the symmetric and asymmetric C-H bands at 2914 cm^{-1} and 3040 cm^{-1} respectively clearly shows that the benzene ring is not involved in the adsorption process. The bands observed at 1064 cm^{-1} and 1200 cm^{-1} are assigned

to CH bending vibrations. The feature observed at 2340 cm^{-1} corresponds to an overtone of the modes mentioned above. In the case of benzyl alcohol adsorbed on Na/Si(100)-2x1 (fig 3. (b)) the Si-O feature is still observed at 780 cm^{-1}. Additionally, the symmetric C-H band is observed at 3040 cm^{-1}. Note that the overall shape of the spectrum is not changed compared to that of the unmodified surface. This shows clearly that the deposition of a Na template does not alter substantially the chemistry at the Si(100)-2x1 surface. This is in contrast to the case of amino acids adsorbed on Na modified Si(100)-2x1, on which the vibrational spectra showed a dramatic change in the bonding geometry after deposition of the Na template.

Fig 13. HREEL spectra of benzyl alcohol adsorbed on (a) clean Si(100)-2x1 and (b) Na/Si(100)-2x1.

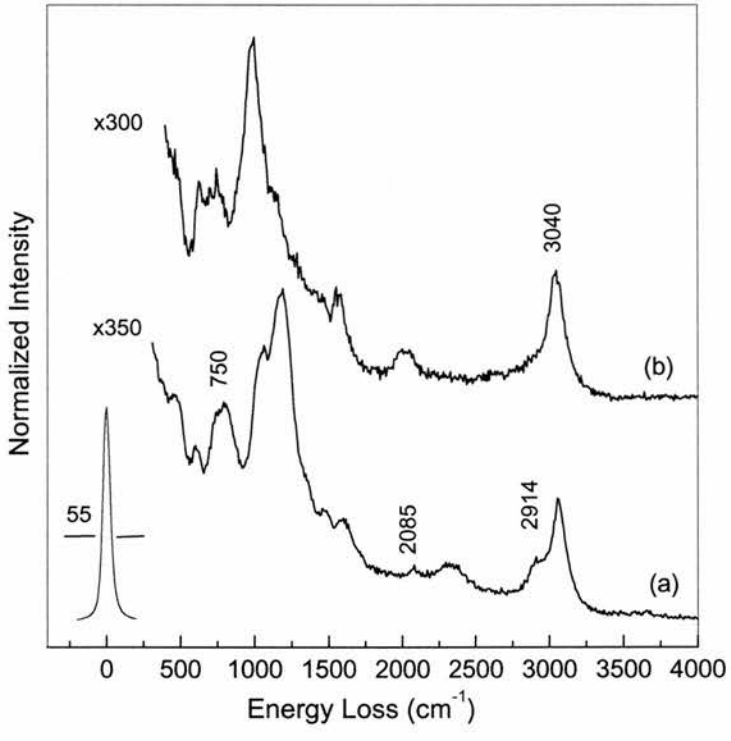

HREELS results show that the benzene ring in the alcohol does not play a role in the adsorption process. We are now interested in probing the orientation of the ring relative to the substrate in both the Na modified and clean Si(100)-2x1 surfaces. Fig 14 and 15 show the C1s NEXAFS spectra recorded at normal and grazing incidence angles of benzyl alcohol adsorbed on clean Si(100)-2x1 and Na/Si(100)-2x1 respectively, recorded at various temperatures. The spectra are dominated by the π^* resonance at 286

eV which corresponds to excitations from C1s levels into the first unoccupied molecular orbitals. The spectra show clearly no angular dependence of the resonance, neither in the clean or Na modified surfaces which clearly indicates the lack of surface order on both systems.

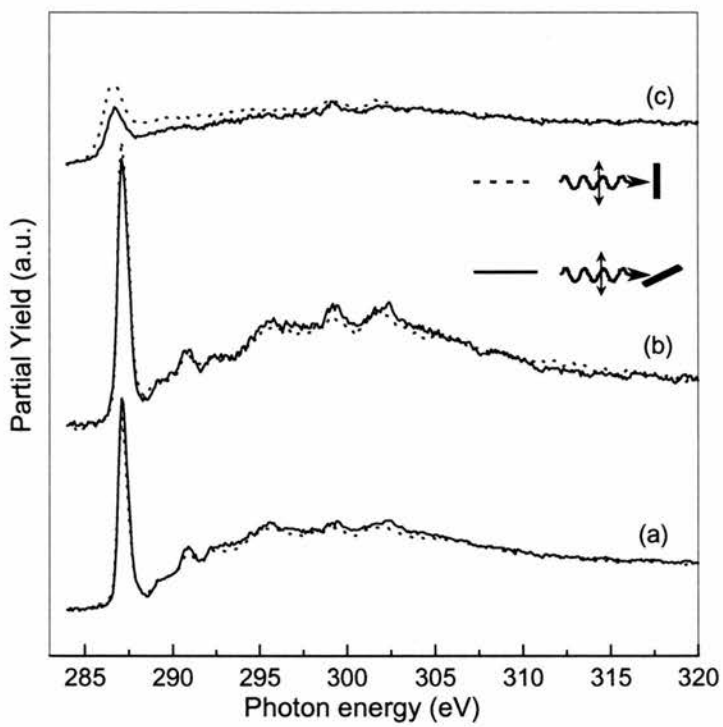

Fig 14. C1s NEXAFS spectra of benzyl alcohol adsorbed on Si(100)-2x1 recorded at (a) room temperature, (b) 150 °C and (c) 300 ° C

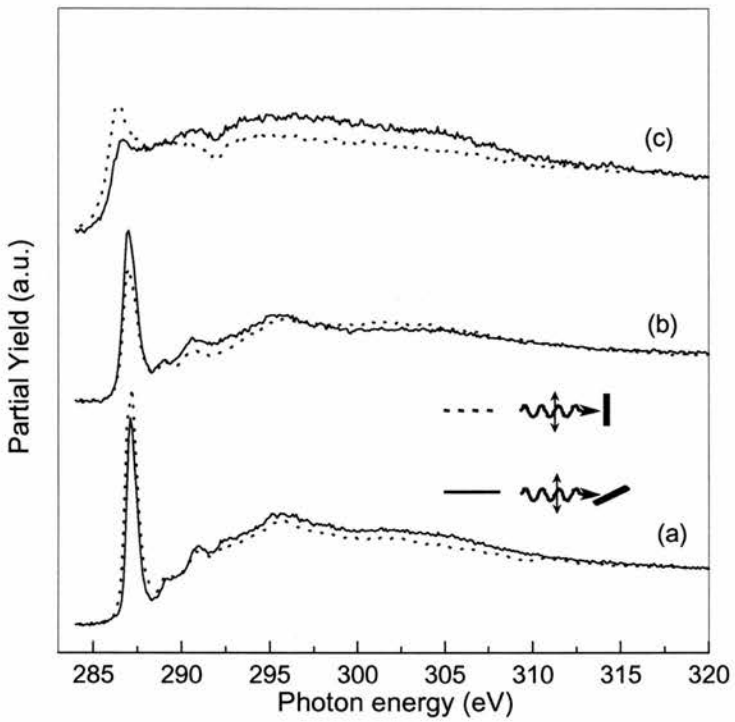

Fig 15. C1s NEXAFS spectra of benzyl alcohol adsorbed on Na/Si(100)-2x1 recorded at (a) room temperature, (b) 150 °C and (c) 300 °C.

6.6. Conclusion:

In conclusion, the alcohols ethanol, isopropanol and *tert*-butanol chemisorb dissociatively on Si(100), Si(113) and Si(115) through a Si-O-C linkage. We observe a considerable uptake of water on the high index surfaces after alcohol saturation. Similarly, ethanol and *tert*-butanol are not able to passivate Si(100). From the disappearance of the 2x1 LEED pattern, it can be concluded that H_2O is inserted into the Si-Si dimer bond at the ethoxy and *tert*-butoxy/Si(100)-2x1 surfaces. In contrast, the isopropoxy species reduces dramatically the reactivity of water molecules on Si(100)-2x1. Even after extreme exposures to H_2O, Si-Si dimer bonds are present at the isopropoxy/Si(100)-2x1 surface. A model based on *ab initio* calculations is given to explain the observed behaviour.

The experiments of benzyl alcohol adsorbed on clean and Na modified Si(100)-2x1 indicate the alcohol bonds through the formation of a Si-O bond. In this case the coadsorbed Na atoms cannot decouple the molecules from the substrate and long range order is not achieved in any of the surfaces.

References:

[1] H. Robbins, B. Schwartz, J. Electrochem. Soc. 107 (1960) 108

[2] D. B. J. Lee, Appl. Phys. 40 (1969) 4569

[3] H. Seidel, L. Csepregi, A. Heuberger, H.J. Baumgärtel, Electroch. Soc. 137 (1990) 3612

[4] S. A. Campbell, K. Cooper, L. Dixon, R. Earwaker, S.N. Port, D. J. Schiffrin, J. of Micromech. and Microeng. 5 (1995) 209.

[5] T. Bitzer, N.V. Richardson, D.J. Schiffrin, Surf. Sci. Lett. 382 (1997) L686.

[6] Froitzheim, H.; Köhler, U.; Lammering, H. Surf. Sci. 149 (1985) 537.

[7] G. Blyholder, M.C. Allen, Inorg. Chem. 9 (1970) 302.

[8] A. Marchand, M. T. Forel, F. Metras, J. Valade, J. Chim. Phys. 61 (1964) 343.

[9] H. Ibach, H. Wagner, D. Bruchmann, Sol. State Comm. 42 (1982) 457.

[10] H. Ibach, D. L. Mills, Electron Energy Loss Spectroscopy and Surface Vibrations; (Academic Press: New York, 1982).

[11] B.S. Swartzentruber, Y.W. Mo, M. B. Webb, M.G. Lagally, J. Vac. Sci. Technol. A 7 (1989) 2901.

[12] L.M. Loewenstein, P.W. Mertens, Solid State Phenomena 65-6 (1999) 1.

[13] M.J. Frisch et al. *GAUSSIAN 98*, Gaussian Inc., Pittsburgh, PA (1998)

[14] W. Ranke Phys. Rev. B 8 (1990) 5243

[15] U. Myler, K. Jacobi, Surf. Sci. 220 (1989) 353-367

CHAPTER 7.

Adsorption of the nucleic acid base Uracil on Si(100)-2x1

7.1. Introduction:

The 2,4-dioxypyrimidine, uracil, molecule has biological functions as a component of the linear polymeric chain ribose nucleic acid (RNA). Molecular recognition between complementary sub-units within these polymers is involved in the process of heredity recognition as well as protein synthesis. The recognition process observed in these systems involves complementary base pairing between uracil and other base components in the same or other polymers through hydrogen bond mechanisms. The self-interaction between uracil molecules through hydrogen bonding has been observed previously [1]. An important aspect of uracil is related to the role this molecule plays in the process of mutation. It has been proposed that mutations occur when minor tautomers of the nucleic acid base form non-standard base pairs, that if left uncorrected might lead to changes in the genetic code [2-3].

The nucleic acid bases have been well characterised by spectroscopic and *ab initio* investigations in non-interacting environments [4-6]. However, little is known about structural changes and vibrational frequency shifts of these molecules when interacting with solid surfaces. The study of the interaction of uracil with single crystal surfaces can help to clarify the role of this molecule in more complex systems. Recently, STM studies of the adsorption of uracil on molybdenum disulphide and graphite surfaces have shown an influence of the substrate in the adsorbate structure [7]. In the case of uracil adsorbed on graphite the influence of the underlying substrate is less than for MoS_2 although the monolayer configuration is almost identical on both surfaces. It is interesting to note that while a rectangular lattice is observed after adsorption of uracil on graphite, an oblique structure is formed on MoS_2.

In this chapter we present a study of the adsorption of uracil on the clean Si(100)-2x1 surface using high resolution electron energy loss spectroscopy (HREELS), scanning tunneling microscopy (STM) and *ab initio* calculations. The combined STM, vibrational spectroscopy and *ab initio* analysis enabled us to identify the ordered structures of uracil on Si(100)-2x1 and obtain structural information about its bonding geometry. Fig 1 shows all possible adsorption geometries of uracil in its keto and enol forms on the Si(100)-2x1 surface.

Structures (a), (b) and (c), (d) correspond each to the possible adsorption geometries of uracil molecules which *both* C=O carbonyl bonds are in the ketoic and enolic forms respectively. In this case the adsorption occurs through cleavage of N-H and O-H bonds and the formation of Si-N and Si-O linkages respectively. Note that in structures (a) and (b) the carbonyl bonds (C=O) and the N-H bond are still intact after the adsorption process. On the other hand in structures (c) and (d), the carbonyl bonds have been replaced by OH groups and the N-H bonds are absent.

Structures (e), (f) and (g), (h) show the adsorption geometries of uracil molecules with *one* C=O carbonyl bond it is enolic form. Adsorption can occur through cleavage of OH or NH bonds as seen in the structures (e), (g) and (f), (h) respectively. In the first case, the adsorption geometries indicate an orientation of the remaining carbonyl bonds (C=O) almost parallel to the surface and a preservation of the N-H bonds in the adsorbed species. On the other hand structures (f) and (h) lead to an orientation of the carbonyl bonds almost perpendicular to the surface, and the absence of N-H bonds.

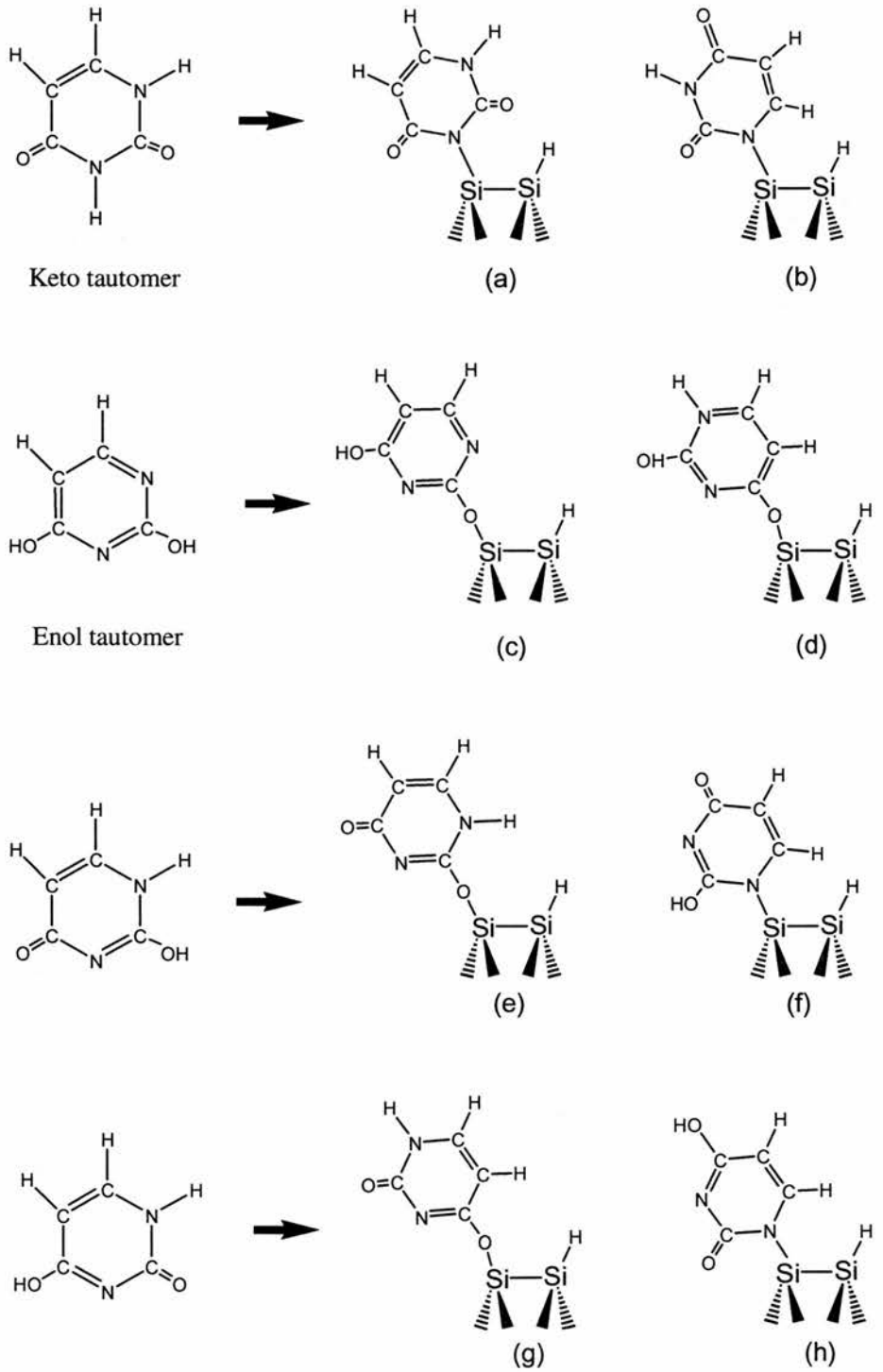

Fig 1. Possible adsorption geometries of uracil on Si(100)-2x1. Note that in all cases the chemisorption occurs through hydrogen cleavage. The C=O bonds are preserved in all structures except for (c) and (d) in which they are replaced by SiO bonds and OH groups respectively.

7.2. Experimental

The experiments were carried out in two separate UHV systems with a base pressure of $5x10^{-11}$ mbar. Each system was equipped with a preparation chamber in which the silicon native oxide was removed and the dosing experiments were carried out. The STM images were obtained using an Omicron STM with a tungsten tip prepared by an electrochemical etching technique. The samples sized 1x5 mm were cut from one side polished wafers with a resistivity of 1-3 Ω cm and mounted on the sample carrier equipped with heating capabilities. The vibrational spectroscopy analysis was carried out using a HREEL spectrometer (HIB 1000, VSW) which was tuned to 35 cm^{-1} in the straight through position. The electron energy loss spectra were taken at room temperature with a primary electron energy of 5 eV. Prior to oxide removal the samples were degassed intensively in the preparation chambers at 170 K. The silicon native oxide removal was achieved by heating the samples to 1500K while maintaining the pressure below $2x10^{-10}$ mbar. Uracil (Aldrich 99%) mounted on a glass vessel, which was separated from the main chamber by a gate valve, was cleaned through several cycles of sublimation and pumping. Mass spectroscopy confirmed the absence of significant contaminants during the dosing at room temperature.

7.3. Results

7.3.1. STM

The STM image of Si(100)-2x1 exposed to uracil at room temperature is shown in fig 2. The image clearly shows three silicon terraces which are separated by a single height atomic step and labelled as A, B and C respectively. The surface consists of rows of dimers, which are rotated by 90° in adjacent terraces. Uracil molecules appear as bright white features aligned preferentially along the dimer rows. The image shows ordering of uracil on the silicon substrate, with rows of up to six molecules parallel to the dimer rows. However, defects (appearing as darker regions in zone B) are present in this overlayer structure where the underlying dimer rows are still visible.

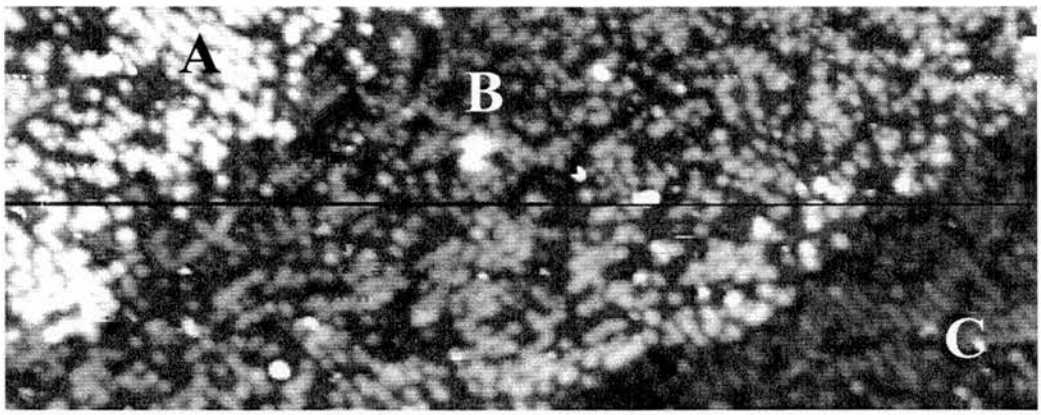

Fig 2. STM image of uracil adsorbed on Si(100)-2x1. The image is 54x21nm. The image was obtained at a gap voltage of –2.0V and a tunneling current of 0.51nA. The three regions labelled correspond to silicon terraces separated single atomic steps. The image size is 55x22 nm.

More details of the STM image above can be seen in fig 3. Uracil molecules seem to form an ordered layer except for defects in the structure that are related to the existence of defects in the surface prior to adsorption.

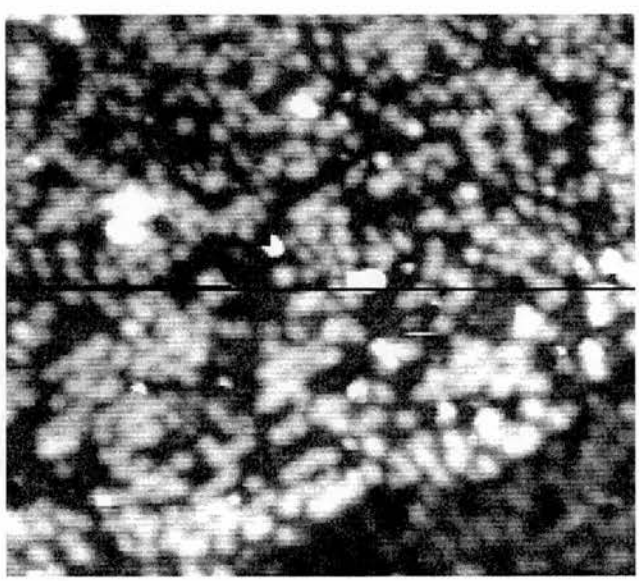

Fig 3. STM image of uracil on Si(100)-2x1. The image size is 23x23 nm.

7.3.2. HREELS

Following the exposure of Si(100)-2x1 to uracil at room temperature, sharp 2x1 spots could still be seen in the LEED pattern. This indicates the preservation of the surface reconstruction after the adsorption of the nucleic acid base. The vibrational spectroscopy is a good technique to differentiate between the adsorption geometries proposed in fig 1. Fig 4 shows the HREEL spectra of uracil adsorbed on Si(100)-2x1 at room temperature and after heating the substrate to the temperatures indicated.

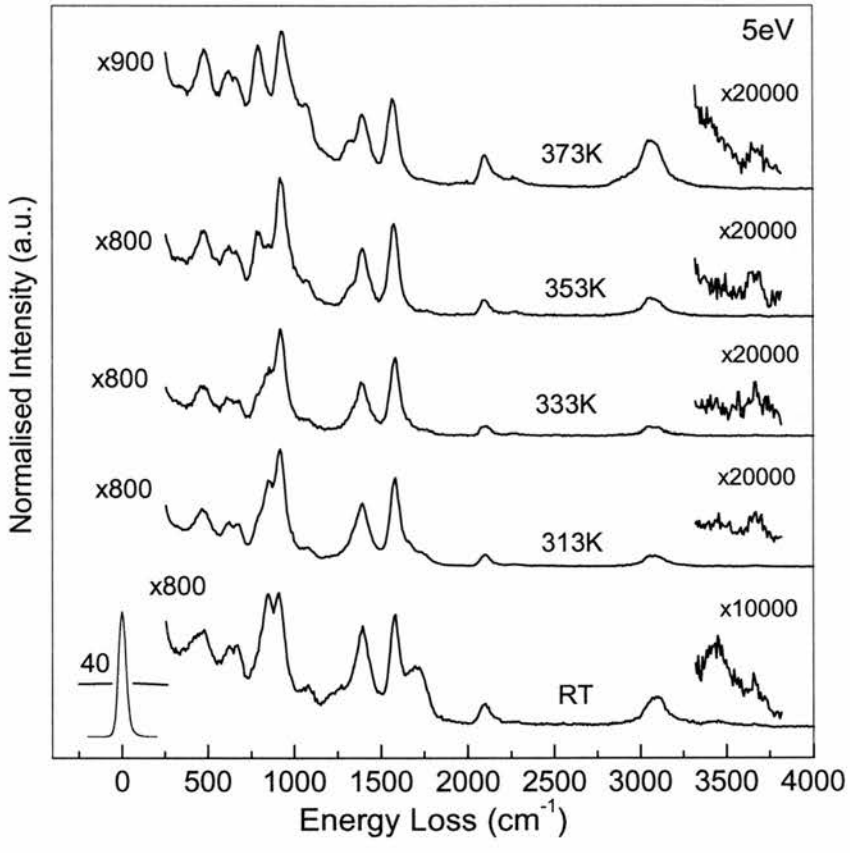

Fig 4. HREELS of uracil adsorbed on Si(100)-2x1 at room temperature and after annealing the substrate to the temperatures indicated.

The room temperature spectrum shows characteristic ν(N-H), ν(C-H) and ν(Si-H) stretching modes at 3480 cm^{-1}, 3090 cm^{-1} and 2105 cm^{-1} respectively. The characteristic carbonyl vibrational mode ν(C=O) can be seen at 1720 cm^{-1}. The two sharp features at 1585 cm^{-1} and 1390 cm^{-1} are assigned to in-plane β(N-H) and β(C-H) bending modes

respectively. The band observed at 1080 cm^{-1} is attributed to a mixture of in-plane and out-of-plane β(N-H) and β(C-H) modes. In the lower energy range of the spectrum the out-of-plane vibrations become predominant. The low intensity features observed at 480 cm^{-1} and 664 cm^{-1} correspond to β(C-H) and β(N-H) out-of-plane modes respectively. The band present at 848 cm^{-1} is a combination of β(C-H) and β(N-H) out of plane modes. It is important to note that the above frequency assignment has been carried out by comparison with *ab initio* calculations of an isolated uracil molecule in its keto form. This approach will be justified in section 7.4. The detailed assignment is shown in table 1. However, based on these calculations it is not possible to assign the bands observed at 3670 cm^{-1} and 912 cm^{-1}. In order to obtain more information about these vibrational features, we performed *ab initio* calculations of uracil adsorbed on a silicon cluster in the adsorption geometry shown in fig 1 (c). According to this optimisations, followed by vibrational frequency computation, the bands at 3670 cm^{-1} and 912 cm^{-1} can be attributed to ν(OH) stretching and β(CH) out-of-plane vibrations of uracil molecules in its enol form adsorbed on the silicon cluster.

Annealing the substrate to 313 K results in a significant loss of intensity of the N-H stretching and carbonyl bands at 3480 cm^{-1} 1720 cm^{-1} respectively, and a reduction of the C-H/N-H out of plane band at 848 cm^{-1}. Further annealing to 333 K and 353 K respectively, leads to the disappearance of this band while a new feature at 780 cm^{-1}, initially attributed to a ν(Si-O) stretching mode, can be observed in the vibrational spectra. This becomes more noticeable in the spectrum of Si(100)-2x1 exposed to uracil and annealed to 373 K. The vibrational feature seen at 3670 cm^{-1} is still observed after annealing at this temperature and indicates the presence of OH groups on the surface. Additionally, the band observed at 1585 cm^{-1}, initially attributed to a β(N-H) vibration is still observed, even after the disappereance of the ν(N-H) band at 3480 cm^{-1}. This suggests that the initial assignment of the band at 1585 cm^{-1} must be revised in the annealed sample spectra. According to our *ab initio* calculations of the uracil/silicon cluster system (fig 1(c)), the vibrational feature observed at 1585 cm^{-1} in the annealed sample spectra is now attributed to an in-plane β(C-OH) vibration.

Fig 5. shows the HREEL spectra Si(100)-2x1 exposed to uracil after heating the substrate to 373K recorded (a) on specular and (b) off specular. In the on specular spectrum the observation of the ν(Si-O) and ν(Si-H) stretches at 780 cm^{-1} and 2105 cm^{-1} respectively indicate that uracil adsorbs on the surface through cleavage of OH bonds and formation of Si-O bonds. The off specular spectrum shows a decrease of the intensity of the dipole active modes (ν(Si-O)) and the increase of the bands related to impact scattering processes (ν(CH) and ν(OH)). Additionally, the vibrational features at 3670 cm^{-1} and 1072 cm^{-1}, attributed to a ν(OH) stretching and a mixture of in-plane and out-of-plane β(N-H) and β(O-H) modes respectively, become now clearly visible in the vibrational spectrum. Note that the off-specular spectrum shows clearly no intensity in the 1700 cm^{-1} and 3400 cm^{-1} ranges, indicating the absence of carbonyl or N-H bonds at the surface.

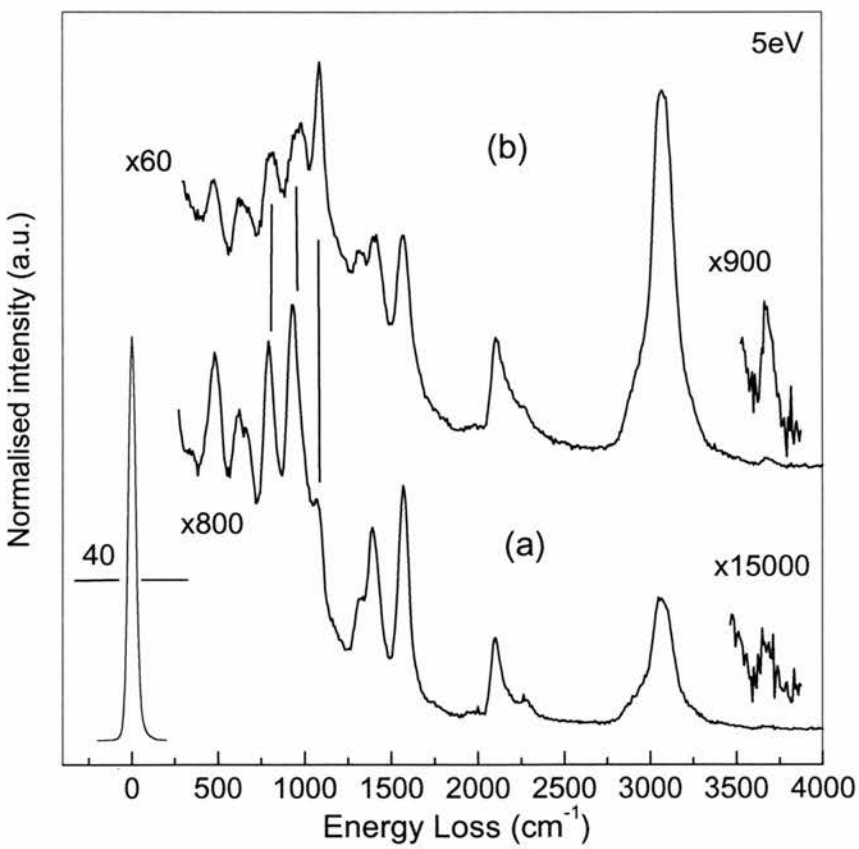

Fig 5. HREEL spectra of Si(100)-2x1 exposed to uracil and annealed to 373 K, recorded (a) on specular and (b) off specular. In spectrum (b) the band at 3670 cm^{-1} indicates clearly the presence of OH groups on the surface.

7.3.3. Ab initio calculations

Ab initio calculations of undisturbed uracil and uracil adsorbed on the silicon cluster have been performed following the same procedure and similar basis set as described in the previous chapters. For the uracil/silicon cluster, this involved the pre-optimisation of a hydrogen saturated silicon cluster followed by geometry optimisation, total energy calculation of uracil in the adsorption geometries shown in fig 1 (c) and (d). The aim was to try to distinguish between these two adsorption geometries from first principles. The calculations predict no apparent energy difference between the two structures, which can be attributed to the inaccuracy of the model due to the small size of the cluster. We have used the optimised structure from model (c) in fig 1 to carry out the vibrational frequency computation.

The results from this optimisation give an angle between the dimer and oxygen atoms of 125°. Additionally, the uracil molecule is tilted an angle of 20° relative to the surface normal and rotated an angle of 50° relative to the dimer row. Note that in this adsorption geometry the OH bond lies almost parallel to the surface. The adsorption geometries in which cleavage on N-H bonds occurs (fig 1 (a), (b), (f) and (e)), have not been optimised since the presence of the C=O bond almost perpendicular to the surface would lead to strong intensities in the 1700 cm^{-1} range, not observed in the vibrational spectra.

The comparison between calculated frequencies and obtained values in HREELS is shown in table 1. Fig 6 shows the (a) front and (b) side views of the optimised uracil/silicon cluster.

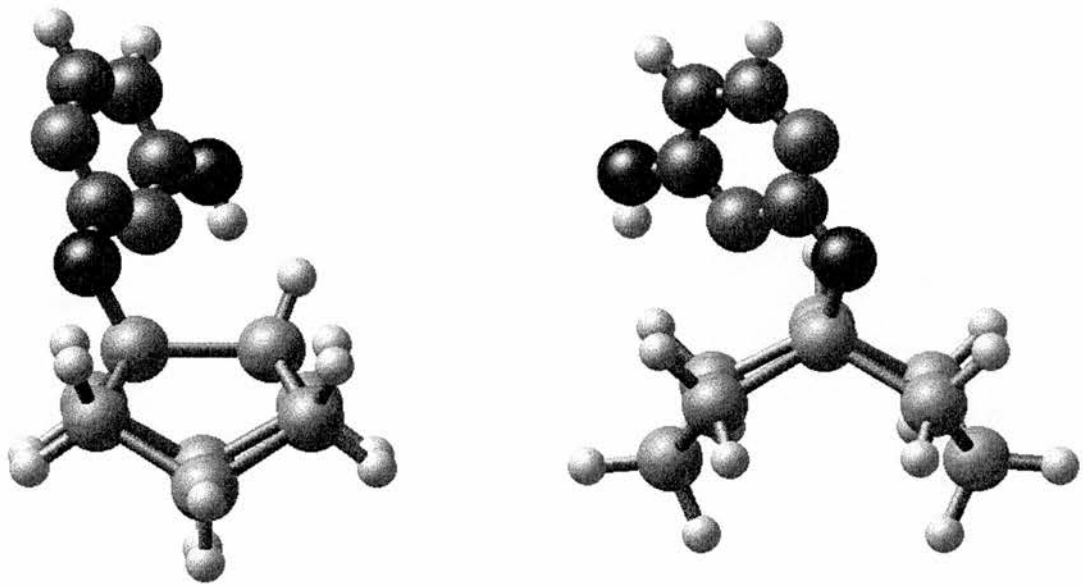

Fig 6. Side views of the optimised uracil/Si(100)-2x1 cluster. Note the orientation of the carbonyl bond almost parallel to the surface in this adsorption geometry.

HREELS (cm^{-1})		Ab initio (cm^{-1})		Assignment
RT spec	373 K spec	Undisturbed	Si cluster*	
3670	3680	3600	3590	ν(O-H)
3480	-	3580	3560	ν(N-H)
3090	3064	3120	3080	ν(C-H)
-	2264	-	-	-
2105	2105	2090	2095	ν(Si-H)
1720	-	1790	-	ν(C=O)
1585	1580	1590	1523	β(N-H) in plane
				*β(C-OH) in plane
1390	1390	1267	1200	β(C-H) in plane
1080	1072	990	1020	β(N-H)/ β(C-H)
				*β(C-H)/ γ(O-H)
912	936	-	980	β(C-H) out of plane
848	-	890	-	β(N-H)/ β(C-H)
-	790	-	810	*ν(Si-O)
664	625	690	700	Ring mode
480	480	356	390	β(C-H) out of plane

Table 1. Vibrational frequency assignment of undisturbed and adsorbed uracil, based on ab initio calculations.

7.4. Discussion

The STM images of uracil adsorbed on Si(100)-2x1 clearly demonstrate that short range order is achieved on this surface. The uracil molecules are oriented parallel to the dimer rows of each silicon terrace. The origin of this process can be attributed to interaction between uracil molecules through hydrogen bonding.

The HREEL spectra show a stronger intensity of the in-plane modes compared with out-of-plane vibrations. This indicates that the orientation of the molecular plane is more upright. The observation of the carbonyl, N-H and O-H modes at 1720 cm^{-1}, 3480 cm^{-1} and 3670 cm^{-1} respectively, indicate that preserved C=O, N-H and O-H bonds are present at the surface at this temperature. The observation of the Si-H stretch shows clearly that hydrogen coming from cleaved N-H or O-H bonds saturates the adjacent dimers. Note that the carbonyl and N-H bands disappear in the annealed sample spectra although the band attributed to OH vibrations is still observed. The presence of OH and absence of the carbonyl bands in those spectra show that only the enol uracil tautomer interacts with the surface through cleavage of OH bonds. This corresponds to the adsorption geometries (c) and (d) in fig 1. Assuming that uracil molecules adsorb on the substrate through cleavage of N-H bonds, (adsorption geometries described in fig 1 (a), (b), (f) and (h)), a strong C=O intensity, arising from the almost perpendicular orientation of the carbonyl dynamic dipole, would be expected in the vibrational spectra. On the other hand, in case uracil interacts with the surface according to structures (e) and (g), ν(N-H) and ν(C=O) bands should be visible in the off-specular spectrum in fig 5, even though the orientation of the dynamic dipoles parallel to the surface. The impact scattering mechanism becomes predominant in the off specular scattering geometry and the intensity of the vibrational features is independent of the orientation of the surface dipoles.

The room temperature spectrum in fig 4 corresponds to a monolayer of uracil bonded to the surface through the formation of a Si-O bond according to structure (c) in fig 1. However, at this temperature, some additional molecules are attached to the

chemisorbed uracil, probably through hydrogen bonding. This justifies the observation of the carbonyl and N-H bands at 1720 cm^{-1} and 3500 cm^{-1} respectively, in the room temperature spectrum. Annealing the substrate to higher temperatures results in the desorption of these weakly bonded molecules and the observation of distinctive monolayer bands in the HREEL spectra. This becomes particularly noticeable in the low frequency range of the spectra where the out-of-plane vibrations overlap with the Si-O band. The continuous observation of the band at 1585 cm^{-1}, even in the absence of the ν(N-H) stretching vibration at 3400 cm^{-1} suggests a different origin of this band in the annealed sample spectra. Based in our cluster calculations (fig 1 (c)) we assign this band to an in plane β(C-OH) mode.

Thermal programmed desorption (TPD) experiments of uracil on copper substrates have shown recently that desorption of uracil multilayers starts to occur at 320K which is in agreement with these results [8]. This interpretation is consistent with the assignment of the room temperature spectrum vibrational features using an undisturbed uracil molecule model while using the uracil/silicon cluster for the 373K annealed spectrum.

7.5. Conclusion

The interaction of uracil with the Si(100)-2x1 surface has been studied using STM, HREELS and ab initio calculations. We demonstrate that uracil, in contrast to previous organic molecules studied, is able to form ordered structures on the surface. The vibrational spectroscopy analysis indicates that only the enol tautomer is capable of adsorption on the surface.

7.5. References

[1] W. Saenger. Principles of nucleic acid structure, Springer Verlag, New York. (1984)

[2] M.D. Topal, J.R. Fresco. Nature 263 (1976) 289

[3] M.D. Topal, J.R. Fresco. Nature 263 (1976) 285

[4] P. Colarusso, K.Q. Zhang, B.J. Guo, P.F. Bernath. Chemical Physics Letters 269 (1997) 39-48

[5] M.K. Shukla, P.C. Mishra. Chemical Physics 240 (1999) 319-329

[6] A. Les, L. Adamowicz, M.J. Nowak, L. Lapinski. Spectrochimica Acta Part a-Molecular and Biomolecular Spectroscopy 48 (1992) 1385-1395

[7] S.J. Sowerby, M. Edelwirth, W.M. Heckl. Applied Physics a-Materials Science & Processing 66 (1998) S649-S653

[8] D.J. Frankel. Unpublished work